XANTHENE-BASED ARTIFICIAL ENZYMES AND A DIMERIC CALIXPYRROLE AS A CHROMOGENIC CHEMOSENSOR

A THESIS SUBMITTED TO
THE GRADUATE SCHOOL OF NATURAL AND APPLIED SCIENCES
OF
MIDDLE EAST TECHNICAL UNIVERSITY

BY

NESLİHAN ŞAKİ

IN PARTIAL FULFILLMENT OF THE REQUIREMENTS
FOR
THE DEGREE OF DOCTOR OF PHILOSOPHY
IN
BIOCHEMISTRY

SEPTEMBER 2004

Approval of the Graduate School of Natural and Applied Sciences.

_____

Prof. Dr. Canan Özgen

Director

I certify that this thesis satisfies all the requirements as a thesis for the degree of Doctor of Philosophy.

_____

Prof. Dr. Orhan Adalı

Head of Department

This is to certify that we have read this thesis and that in our opinion it is fully adequate, in scope and quality, as a thesis for the degree Doctor of Philosophy

_____

Prof. Dr. Engin U. Akkaya

Supervisor

Examining Committee Members

Prof. Dr. Faruk T. Bozoğlu (METU, FDE) _____

Prof. Dr. Engin U. Akkaya (METU, CHEM) _____

Prof. Dr. Mesude İşcan (METU, BIOL) _____

Prof. Dr. Akgül Yeşilada (Hacettepe Unv.) _____

Assoc. Prof. Dr. Özdemir Doğan (METU, CHEM) _____

I hereby declare that all information in this document has been obtained and presented in accordance with academic rules and ethical conduct. I also declare that, as required by these rules and conduct, I have fully cited and referenced all material and results that are not original to this work.

Neslihan Şaki

ABSTRACT

XANTHENE-BASED ARTIFICIAL ENZYMES AND A DIMERIC CALIXPYRROLE AS A CHROMOGENIC CHEMOSENSOR

Şaki, Neslihan
Ph.D., Department of Biochemistry
Supervisor: Prof. Dr. Engin U. Akkaya

September, 2004, 172 pages

This thesis covers the combination of two seperate work accomplished during the throughout the study. In the first part of the study, xanthene based artificial enzymes were synthesized, and kinetic hydrolysis studies done.

Artificial enzyme design is an active field of supramolecular chemistry and metalloenzymes are attractive targets in such studies. Enzymatic catalysis is essentially a 'multifuctional' catalysis.

As part of our work, we designed and synthesized three novel xanthene derivatives. All three model contain Zn(II) in their active sites. Using the model substrate *p*-nitrophenyl acetate, we showed that the bifunctional model is at least an order of magnitude more active in catalyzing the hydrolysis of the substrate.

Compared to the uncatalyzed hydrolysis reaction of the p-nitrophenyl ester at pH 7.0, the bifunctional model complex showed a 5714-fold rate acceleration.

The second part of the thesis involves the design of a dimeric calixpyrrole as a chromogenic chemosensor.

Anions are involved in a large number of biological processes and there is an interest in developing molecular sensors for these charged species. The calixpyrroles are a class of old but new heterocalixarene analogues that show considerable promise in the area of anion sensing.

In this work, we have designed, synthesized and characterized a calixpyrrole-dimer anion sensor for its anion binding strength. The dimer forms stable complexes with *p*-nitrophenolate ion. This formed complex is used as a colorimetric sensor by displacing the chromogenic anion with the addition of various anions. like fluoride and acetate. The receptor shows strong affinity and high selectivity for fluoride anion, and also show reasonable affinity toward acetate. Thus, effective optical sensing of biochemically relevant these anions is accomplished using the calixpyrrole dimer.

Keywords: Supramolecular chemistry, artificial enzymes, anion recognition, chemosensor, calixpyrrole-dimer, colorimetric sensor.

ÖZ

KSANTEN TÜREVİ YAPAY ENZİMLER VE KROMOJENİK RESEPTÖR OLARAK DİMERİK KALİKSPİROL

Şaki, Neslihan
Doktora, Biyokimya Bölümü
Tez Yöneticisi: Prof. Dr. Engin U. Akkaya

Eylül, 2004, 172 sayfa

Bu tez, çalışmamız süresince gerçekleştirilen iki ayrı projenin bir bileşimidir. Çalışmanın ilk bölümünde, ksantene dayalı yapay enzimler sentezlenmiş ve kinetik çalışmaları yapılmıştır.

Yapay enzim tasarımı supramoleküler kimyanın önemli hedeflerinden biridir ve bu çalışmalar içinde, metaloenzimler özellikle önemlidirler. Enzimatik kataliz genel olarak multifonksiyonel kataliz olarak adlandırılabilir.

Çalışmamızın bir parçası olarak, üç yeni ksanten türevi tasarlayarak sentezledik. Her üç molekül de aktif bölgelerinde Zn(II) metal iyonu bulundurmaktadır. Örnek substrat olarak p-nitrofenil asetat kullanarak, bifonksiyonel model bileşiğin bu substratın hidrolizinde en etkin yapay enzim

olduğunu gösterdik. p-nitrofenil esterinin pH 7.0'da katalizörsüz hidroliz reaksiyonuyla karşılaştırıldığında, bifonksiyonel modelin 5714 kat bir hız artışına neden olduğu görülmüştür.

Tezin ikinci bölümü kromojenik bir moleküler algılayıcı olarak dimerik kalikspirol bileşiğinin tasarımını içermektedir.

Anyonların çok sayıda biyolojik süreçte rol almalarına rağmen, seçici olarak algılanmaları zor bir hedef oluşturmaktadır. Kalikspiroller, hetero-kaliksaren derivativleri olarak, anyon seçiciliğinde dikkat çekmektedirler.

Bu çalışmada, bir kalikspirol-dimer anyon reseptörü tasarlayarak sentezledik. Bu dimer p-nitrofenolat iyonu ile kararlı kompleksler oluşturmaktadır. Sonuçta, elde edilen bu komplekse bağlı kromojenik nitrofenolat iyonunun florür veya asetat gibi çeşitli anyonların ilavesiyle yer değiştirerek kolorimetrik bir moleküler algılayıcı olarak kullanılabileceği gösterildi. Reseptörümüz, florür anyonuna oldukça yüksek bir seçicilik gösterirken asetat iyonuna karşı da bir seçicilik gözlenmiştir. Bu nedenle, kaliks-dimer molekülünün çalışmada kullanılan ve biyokimyasal önem taşıyan anyonlar için etkili bir optik sensör olduğu belirlenmiştir.

Anahtar kelimeler: Süpramoleküler kimya, yapay enzimler, anyon seçiciliği, moleküler algılayıcı, kalikspirol-dimer, kolorimetrik algılayıcı.

To my sweet little brother

ACKNOWLEDGEMENTS

I would like to express my sincere thanks to my advisor Prof. Dr. Engin U. Akkaya for his guidance, understanding, and patience during the course of this research as well as his unlimited knowledge and experience which I have benefited from greatly.

I would like to thank to my family for their moral support, endless love and encouragement.

Thanks go to all my labmates, Nalan, Ali, Orkun, Serdar, Tarık and Funda for their supports and sincere friendships.

I would also like to thank to my great friends Güvenç and Çiğdem for their continous patience and love.

Finally, my special thanks go to my dear friend Süleyman Gürsoy who has been in my life for years and be there whenever I need. I am very lucky to have him.

TABLE OF CONTENTS

ABSTRACT.....iv
ÖZ.....vi
ACKNOWLEDGEMENTS.....ix
TABLE OF CONTENTS.....x
LIST OF TABLES.....xiv
LIST OF FIGURES.....xv
LIST OF SCHEMES.....xxii

PART I
CHAPTER
1. INTRODUCTION.....1
1.1 Supramolecular Chemistry.....1
1.2 The Supramolecular Chemistry of Life.....5
1.3 Host-Guest Chemistry.....5
1.4 Supramolecular Chemistry of Xanthene-based Molecular Complexes.....9
1.5 Enzymes.....15
1.6 General Hydrolytic Enzymes.....17
1.7 Artificial Enzymes.....21
1.8 Acid-base Catalysıs.....26
1.9 Metal ions in Biochemistry and Metalloenzymes.....28
1.10 Zinc Enzymes.....33
1.11 Aim of the Study.....38

2. MATERIALS AND METHODS.....40
2.1 Materials.....40
2.2 Synthesis of 2,7-Di-*tert*-butyl-4,5-bis-chloromethyl-9,9-dimethyl-9*H*-xanthene **(2.2)**…….....41
2.3 Synthesis of 1,4,7 Tris (tert-butyloxycarbonyl)-1,4,7,10-tetraazacyclododecane (3-Boc-cyclen) **(2.4)**…….....42
2.4 Synthesis of and isolation of the dicyclen derivative **(2.5)** and the mono-substitution product **(2.6)**……...…..43
2.5 Deprotection of **(2.5)**…….44
2.6 The reaction of compound (2.6) with imidazole to yield compound **(2.8)**……45
2.7 Deprotection of **(2.8)**……..…46
2.8 The reduction of 2,7-di-*tert*-butyl-9,9-dimethyl-4,5-xanthenedicarboxylic acid **(2.10)**……..48
2.9 Synthesis of the monochlorinated compound **(2.12)**……49
2.10 Synthesis of compound **(2.13)**……..49
2.11 Deprotection of compound **(2.13)**…….....51
2.12 Kinetics…….52

3. RESULTS AND DISCUSSION.....56
3.1 Hydrolysis of PNPA by di-cyclen derivative-$[Zn^{2+}]_2$ ($DC[Zn^{2+}]_2$) **(2.16)**.....57
3.2 Hydrolysis of PNPA by mono-cyclen-imidazole derivative-$[Zn^{2+}]$ ($MC\text{-}Im[Zn^{2+}]$) **(2.17)**.....66
3.3 Hydrolysis of PNPA by monocyclen derivative-$[Zn^{2+}]$ ($MC[Zn^{2+}]$) **(2.18)**.....75

4. CONCLUSION.....87

PART II

CHAPTER

5. INTRODUCTION.....89
5.1 Chemosensors.....89
5.2 The Anion Coordination Chemistry.....92
5.2.1 Hydrogen bonds.....94
5.2.2 Electrostatic Interactions.....97
5.2.3 The Hydrophobic effect.....98
5.2.4 Metal Ion Coordination.....99
5.2.5 Electrostatic Interactions and Hydrogen Bonds.....100
5.3 Fluorisis.....101
5.4 Chloride Channels and Cystic Fibrosis.....102
5.5 Calixpyrroles.....104
5.6 Higher ordered calix[4]pyrroles.....111
5.7 Calixpyrrole Based Optical Sensors.....113
5.8 Aim of the Study.....117

6. MATERIALS AND METHODS.....118
6.1 Materials.....118
6.2 Synthesis of *m*-nitroacetophenone **(6.2)**.....119
6.3 Synthesis of m-aminoacetophenone **(6.3)**.....120
6.4 Synthesis of cbz-protected *m*-aminoacetophenone **(6.4)**.....120
6.5 Synthesis of Calix[4]pyrrole derivative **(6.5)**.....121
6.6 Synthesis of deprotected Calix[4]pyrrole **(6. 6)**.....123
6.7 Synthesis of Calix-dimer derivative **(6. 7)**.....124
6.8 UV-Vis Measurements.....125

7. RESULTS AND DISCUSSION.....127
8. CONCLUSION.....135

REFERENCES.....137

APPENDIX.....146

VITA.....171

LIST OF TABLES

TABLE

1.1 Classification of Phosphatases and the Reactions They Catalyze.....20

3.1 Kinetic data for hydrolysis of PNPA$^{(a,b,c)}$ by complexes 2.16, 2.17 and 2.18.....84

LIST OF FIGURES

FIGURE

1.1 From molecular to supramolecular chemistry.....3

1.2 Fischer's 'lock and key' hypothesis.....6

1.3 Structures of cyclodextrin (1.1), crown ether (1.2a) and calix[4]arene (1.2b).....8

1.4 The structure of Kemp's triacid.....10

1.5 Molecules featuring molecular clefts.....10

1.6 The catalytic effect of a molecule with divergent groups (1.8).....11

1.7 Examples of host-guest chemistry of molecules having convergent functional groups.....12

1.8 Xanthene-4,5-dicarboxylic acid derivatives.....13

1.9 A new porphyrin based molecular cleft.....14

1.10 A new family of molecular clefts.....14

1.11 The first compound called "artificial enzyme".....22

1.12 Structures of cyclodextrin based artifical enzymes.....24

1.13 Imidazole appended β-CD dimer as an artificial hydrolase.....25

1.14 Di-nuclear Zn(II)cryptate(Zn_2L).....26

1.15. A) General acid catalysis B) General base catalysis.....27

1.16 Bifunctional catalysis in the ketosteroid isomerase.....28

1.17 Model reaction for the first step of the hydrolysis of RNA. B=base.....31

1.18 The dinuclear Co^{3+} complex.....32

1.19 Postulated mechanisms for the hydrolysis of phosphoric acid esters (1.21 and 1.22).....32

1.20 Structures of di- (1.23) and mono-nuclear (1.24) calix[4]arene Zn(II) complexes.....36
1.21 An example of zinc containing enzyme.....36
1.22 Structures of ligands.....37
2.1 Synthesis of 2,7-Di-*tert*-butyl-4,5-bis-chloromethyl-9,9-dimethyl-9*H*-xanthene (2.2)……..….....41
2.2 Synthesis of 1,4,7 tris(tert-butyloxycarbonyl)-1,4,7,10-tetraazacyclododecane (2.4)……...…....42
2.3 Synthesis of and isolation of the dicyclen derivative (2.5 and the mono-substitution product (2.6)…….....44
2.4 Deprotection of (2.5)……..45
2.5 Synthesis of 10-(2,7-Di-*tert*-butyl-5-imidazol-1-ylmethyl-9,9-dimethyl-9*H*-xanthen-4-ylmethyl)-1,4,7,10tetraaza-cyclododecane-1,4,7-tricarboxylic acid tri-*tert*-butyl ester (2.8)…..…..46
2.6 Synthesis of 1-(2,7-Di-*tert*-butyl-5-imidazol-1-ylmethyl-9,9-dimethyl-9*H*-xanthen-4-ylmethyl)-1,4,7,10tetraaza-cyclododecane (2.9)……...47
2.7 Synthesis of 2,7-Di-*tert*-butyl-5-hydroxymethyl-9,9-dimethyl-9*H*-xanthen-4-yl)-methanol (2. 11)…….…….48
2.8 .Synthesis of (2,7-Di-*tert*-butyl-5-chloromethyl-9,9-dimethyl-9*H*-xanthen-4-yl)-methanol; compound with methane (2.12)……..…...…49
2.9 Synthesis of 10-(2,7-Di-*tert*-butyl-5-hydroxymethyl-9,9-dimethyl-9*H*-xanthen-4-ylm ethyl)-1,4,7,10-tetraaza-cyclododecane-1,4,7-tricarboxylic acid tri-*tert*-butyl ester (2.13)…….....50
2.10 Synthesis of [2,7-Di-*tert*-butyl-9,9-dimethyl-5-(1,4,7,10-tetraaza-cyclododec-1-ylm ethyl)-9*H*-xanthen-4-yl] methanol (2.14)……...51
2.11 Structure of p-nitrophenylacetate…….…..52
2.12 Illustrations of dinucleating (2.16) and mononucleating (2.17 and 2.18) complexes…….…53

3.1 Absorbance of p-nitrophenolate ion at 400 nm as a function of time, in the hydrolysis of PNPA catalyzed by $2x10^{-3}$ M of the compound 2.7 and $4x10^{-3}$ M Zn^{2+} ions in $12.6x10^{-2}$ M MOPS buffer at pH 7.0 and 25°C.....58

3.2 The plot of $\ln[(A_\infty-A)/A_\infty]$ as a function of time for $2x10^{-3}$ M compound 2.7 and $4x10^{-3}$ M Zn^{2+} ions in $12.6x10^{-2}$ M MOPS buffer at pH 7.0 at 25°C, yielding a pseudo-first order rate constant ($k_{cat}=0.9x10^{-3}$ s^{-1}) and $R^2=0.995$.....59

3.3 Absorbance of p-nitrophenolate ion at 400 nm as a function of time, in the hydrolysis of PNPA catalyzed by $2x10^{-3}$ M of the compound 2.7 and $4x10^{-3}$ M Zn^{2+} ions in $12.6x10^{-2}$ M MOPS buffer at pH 7.5 and 25°C.....60

3.4 The plot of $\ln[(A_\infty-A)/A_\infty]$ as a function of time for $2x10^{-3}$ M compound 2.7 and $4x10^{-3}$ M Zn^{2+} ions in $12.6x10^{-2}$ M MOPS buffer at pH 7.5 and 25°C, yielding a pseudo-first order rate constant ($k_{cat}=1.6x10^{-3}$ s^{-1}) and $R^2=0.9964$.....61

3.5 Absorbance of p-nitrophenolate ion at 400 nm as a function of time, in the hydrolysis of PNPA catalyzed by $2x10^{-3}$ M of the compound 2.7 and $4x10^{-3}$ M Zn^{2+} ions in $12.6x10^{-2}$ M TRIS .buffer at pH 8.0 and 25°C.....62

3.6 The plot of $\ln[(A_\infty-A)/A_\infty]$ as a function of time for $2x10^{-3}$ M compound 2.7 and $4x10^{-3}$ M Zn^{2+} ions in $12.6x10^{-2}$ M TRIS buffer at pH 8.0 and 25°C, yielding a pseudo-first order rate constant ($k_{cat}=4.5x10^{-3}$ s^{-1}) and $R^2=0.9978$.....63

3.7 Absorbance at 400 nm as a function of time, in the hydrolysis of PNPA catalyzed by $2x10^{-3}$ M of the compound 2.7 and $4x10^{-3}$ M Zn^{2+} ions in $12.6x10^{-2}$ M TRIS buffer at pH 8.5 and 25°C.....64

3.8 The plot of $\ln[(A_\infty-A)/A_\infty]$ as a function of time for $2x10^{-3}$ M compound 2.7 and $4x10^{-3}$ M Zn^{2+} ions in $12.6x10^{-2}$ M TRIS buffer at pH 8.5 and 25°C, yielding a pseudo-first order rate constant ($k_{cat}=12x10^{-3}$ s^{-1}) and $R^2=0.9998$.....65

3.9 Absorbance at 400 nm as a function of time, in the hydrolysis of PNPA catalyzed by $2x10^{-3}$ M of the compound 2.9 and $2x10^{-3}$ M Zn^{2+} ions in $13.3x10^{-2}$ M MOPS buffer at pH 7.0 and 25°C.....67

3.10 The plot of $\ln[(A_\infty-A)/A_\infty]$ as a function of time for $2x10^{-3}$ M compound 2.9 and $2x10^{-3}$ M Zn^{2+} in $13.3x10^{-2}$ M MOPS buffer at pH 7.0 and 25°C, yielding a pseudo-first order rate constant ($k_{cat}=12x10^{-3}$ s^{-1}) and $R^2=0.999$.....68

3.11 Absorbance at 400 nm as a function of time, in the hydrolysis of PNPA catalyzed by $2x10^{-3}$ M of the compound 2.9 and $2x10^{-3}$ M Zn^{2+} ions in $13.3x10^{-2}$ M MOPS buffer at pH 7.5 and 25°C.....69

3.12 The plot of $\ln[(A_\infty-A)/A_\infty]$ as a function of time for $2x10^{-3}$ M compound 2.9 and $2x10^{-3}$ M Zn^{2+} in $13.3x10^{-2}$ M MOPS buffer at pH 7.5 and 25°C, yielding a pseudo-first order rate constant ($k_{cat}=2.5x10^{-3}$ s^{-1}) and $R^2=0.9967$.....70

3.13 Absorbance of p-nitrophenolate ion at 400 nm as a function of time, in the hydrolysis of PNPA catalyzed by $2x10^{-3}$ M of the compound 2.9 and $2x10^{-3}$ M Zn^{2+} ions in $13.3x10^{-2}$ M TRIS buffer at pH 8.0 and 25°C.....71

3.14 The plot of $\ln[(A_\infty-A)/A_\infty]$ as a function of time for $2x10^{-3}$ M compound 2.9 and $2x10^{-3}$ M Zn^{2+} in $13.3x10^{-2}$ M TRIS buffer at pH 8.0 and 25°C, yielding a pseudo-first order rate constant ($k_{cat}=4.8x10^{-3}$ s^{-1}) and $R^2=0.9975$.....72

3.15 Absorbance of p-nitrophenolate ion at 400 nm as a function of time, in the hydrolysis of PNPA catalyzed by $2x10^{-3}$ M of the compound 2.9 and $2x10^{-3}$ M Zn^{2+} ions in $13.3x10^{-2}$ M TRIS buffer at pH 8.5 at 25°C.....73

3.16 The plot of $\ln[(A_\infty-A)/A_\infty]$ as a function of time for $2x10^{-3}$ M compound 2.9 and $2x10^{-3}$ M Zn^{2+} in $13.3x10^{-2}$ M TRIS buffer at pH 8.5 and 25°C, yielding a pseudo-first order rate constant ($k_{cat}=7.5x10^{-3}$ s^{-1}) and $R^2=0.9987$.....74

3.17 Absorbance at 400 nm as a function of time, in the hydrolysis of PNPA catalyzed by $2x10^{-3}$ M of the compound 2.14 and $2x10^{-3}$ M Zn^{2+} ions in $13.3x10^{-2}$ M MOPS buffer at pH 7.0 and 25°C.....76

3.18 The plot of $\ln[(A_\infty-A)/A_\infty]$ as a function of time for $2x10^{-3}$ M compound 2.14 and $2x10^{-3}$ M Zn^{2+} in $13.3x10^{-2}$ M MOPS buffer at pH 7.0 and 25°C, yielding a pseudo-first order rate constant ($k_{cat}=1.5x10^{-3}$ s^{-1}) and $R^2=0.996$.....77

3.19 Absorbance of p-nitrophenolate ion at 400 nm as a function of time, in the hydrolysis of PNPA catalyzed by $2x10^{-3}$ M of the compound 2.14 and $2x10^{-3}$ M Zn^{2+} ions in $13.3x10^{-2}$ M MOPS buffer at pH 7.5 and 25°C.....78

3.20 The plot of $\ln[(A_\infty-A)/A_\infty]$ as a function of time for $2x10^{-3}$ M compound 2.14 and $2x10^{-3}$ M Zn^{2+} in $13.3x10^{-2}$ M MOPS buffer at pH 7.5 and 25°C, yielding a pseudo-first order rate constant ($k_{cat}=1.6x10^{-3}$ s^{-1}) and $R^2=0.994$.....79

3.21 Absorbance of p-nitrophenolate ion at 400 nm as a function of time, in the hydrolysis of PNPA catalyzed by $2x10^{-3}$ M of the compound 2.14 and $2x10^{-3}$ M Zn^{2+} ions in $13.3x10^{-2}$ M TRIS buffer at pH 8.0 and 25°C.....80

3.22 The plot of $\ln[(A_\infty-A)/A_\infty]$ as a function of time for $2x10^{-3}$ M compound 2.14 and $2x10^{-3}$ M Zn^{2+} in $13.3x10^{-2}$ M TRIS buffer at pH 8.0 and 25°C, yielding a pseudo-first order rate constant ($k_{cat}=3.6x10^{-3}$ s^{-1}) and $R^2=0.9922$.....81

3.23 Absorbance at 400 nm as a function of time, in the hydrolysis of PNPA catalyzed by $2x10^{-3}$ M of the compound 2.14 and $2x10^{-3}$ M Zn^{2+} ions in $13.3x10^{-2}$ M TRIS buffer at pH 8.5 and 25°C.....82

3.24 The plot of $\ln[(A_\infty-A)/A_\infty]$ as a function of time for $2x10^{-3}$ M compound 2.14 and $2x10^{-3}$ M Zn^{2+} in $13.3x10^{-2}$ M TRIS buffer at pH 8.5 and 25°C, yielding a pseudo-first order rate constant ($k_{cat}=5.1x10^{-3}$ s^{-1}) and $R^2=0.9972$.....83
3.25 The mechanism of p-nitrophenylacetate hydrolysis with the enzyme model 2.17.....86
5.1 Demonstration of intrinsic and extinsic chemosensors.....90
5.2 The first purely amide-based anion receptor.....95
5.3 Another example for amide based anion receptor.....95
5.4 A urea-based anion receptor.....96
5.5 The azaphenol-thiourea based chromophore anion sensor.....96
5.6 Schematic representation of a positively charged tripodal receptor.....97
5.7 Molecules designed by Schmidtchen et al.....98
5.8 A series of examples for tin-based macrocycles.....99
5.9 The silicon- and germanium-based receptors.....99
5.10 Macrocyclic anion receptors represented by Park and Simmons.....100
5.11 An example of electrostatic and hydrogen-bonding interactions.....101
5.12 The structure of *meso*-octamethylcalix[4]pyrrole.....104
5.13 Tetraspirocyclohexyl[calix]pyrrole structure.....105
5.14 Viev of the molecular structures of 5.17 and 5.18.....106
5.15 X-ray crystal structure of 5.17-DMF complex.....108
5.16 A couple of novel calix(4)pyrrole molecules.....109
5.17 Ferrocene-appended calixpyrrole and proposed CH-anion. interaction in complex.....110
5.18 The acetylene-linked calix[4]pyrrole dimer.....111
5.19 The structure of well characterized calix[6]pyrrole.....111
5.20 Higher ordered calixpyrrole derivatives synthesized by Sessler et al.....113
5.21 Structures of calix[4]pyrrole based optical sensors.....115
5.22 Calix[4]pyrrole derivative complexes.....116
6.1 Synthesis of *m*-nitroacetophenone (6.2)…….....119

6.2 Synthesis of *m*-aminoacetophenone (6.3)……120
6.3 Synthesis of cbz-protected *m*-aminoacetophenone (6.4)……121
6.4 Synthesis of Calix[4]pyrrole derivative (6.5)…….....122
6.5 Synthesis of deprotected Calix[4]pyrrole (6.6)…….....123
6.6 Synthesis of calix-dimer derivative (6.7)…….....125
7.1 Decreasing absorbance of the p-nitrophenolate anion ($3.65x10^{-5}$ M) upon addition of calix[4]pyrrole dimer (0, $3.8x10^{-5}$, $7.6x10^{-5}$, $1.1x10^{-4}$, $1.5x10^{-4}$, $1.9 x10^{-4}$, $2.3x10^{-4}$, $2.6x10^{-4}$, $3.0x10^{-4}$, $3.4 x10^{-4}$, $3.8 x10^{-4}$, $4.2 x10^{-4}$, $4.5 x10^{-4}$, $4.9 x10^{-4}$, $5.3 x10^{-4}$, $5.7 x10^{-4}$ M) in CH_2Cl_2.....128
7.2 Benesi-Hildebrand plot for binding constant determination.....129
7.3 Absorption spectra of the calix[4]pyrrole dimer ($5x10^{-4}$ M) and p-nitrophenolate anion ($6x10^{-6}$ M) with $\mathbf{Cl^-}$ (0, $2x10^{-4}$, $4x10^{-4}$, $8x10^{-4}$, $3.2x10^{-3}$ M) in CH_3CN.....131
7.4 Absorption spectra of the calix[4]pyrrole dimer ($5x10^{-4}$ M) and p-nitrophenolate anion ($6x10^{-6}$ M) with $\mathbf{Br^-}$ (0, $4x10^{-4}$, $8x10^{-4}$, $3.2x10^{-3}$ M) in CH_3CN.....131
7.5 Absorption spectra of the calix[4]pyrrole dimer ($5x10^{-4}$ M) and p-nitrophenolate anion ($6x10^{-6}$ M) with $\mathbf{I^-}$ (0, $4x10^{-4}$, $8x10^{-4}$, $2.4 x10^{-3}$, $3.2x10^{-3}$ M) in CH_3CN.....132
7.6 Absorption spectra of the calix[4]pyrrole dimer ($5x10^{-4}$ M) and p-nitrophenolate anion ($6x10^{-6}$ M) with $\mathbf{HSO_4^-}$ (0, $2x10^{-4}$, $4x10^{-4}$, $8x10^{-4}$, $1.4x10^{-3}$, $3.2x10^{-3}$ M) in CH_3CN.....132
7.7 Absorption spectra of the calix[4]pyrrole dimer ($5x10^{-4}$ M) and p-nitrophenolate anion ($6x10^{-6}$ M) with $\mathbf{F^-}$ (0, $2x10^{-4}$, $4x10^{-4}$, $8x10^{-4}$, $1.4x10^{-3}$, $2.4 x10^{-3}$, $3.2x10^{-3}$ M) in CH_3CN.....133
7.8 Absorption spectra of the calix[4]pyrrole dimer ($5x10^{-4}$ M) and p-nitrophenolate anion ($6x10^{-6}$ M) with $\mathbf{AcO^-}$ (0, $2x10^{-4}$, $4x10^{-4}$, $8x10^{-4}$, $1.4x10^{-3}$, $2.4 x10^{-3}$, $3.2x10^{-3}$ M) in CH_3CN.....133
7.9 Normalized absorbance values for p-nitrophenolate displaced by the anions indicated at 3.2 mM concentration.....134

LIST OF SCHEMES

SCHEME

5.1 Section through the cell membrane of an epithelial cell.....103

5.2 An illustration for calix[4]pyrrole conformation.....107

5.3 Two approaches used to get calix[4]pyrrole based optical sensors.....114

5.4 F^- dependent equilibrium between the *meso*-octamethyl calixpyrrole-4-nitrophenolate and *meso*-octamethyl calixpyrrole-fluoride.....116

CHAPTER I

INTRODUCTION

1.1. Supramolecular Chemistry

Since Cram, Lehn and Pedersen shared the 1987 Nobel Prize for chemistry, supramolecular chemistry has evolved into one of the most active areas of contemporary chemical research, (Gokel, 1999).

Supramolecular chemistry was defined in words, “Just as there is a field of molecular chemistry based on the covalent bond, there is a field of supramolecular chemistry, the chemistry of molecular assemblies and of the intermolecular bond” (Lehn, 1995).

The term intermolecular bond includes ion pairing (electrostatic), hydrophobic and hydrophillic interactions, hydrogen-bonding, host-guest interactions, and Van der Walls interactions.

Supramolecular interactions are the foundation for highly specific biological processes, such as the substrate binding by enzymes or receptors, the formation of protein complexes, the decoding of the genetic code, neurotransmission processes and cellular recognition (immunology).

The exact knowledge of the energetic and stereochemical characteristics of these non-covalent, multiple intermolecular interactions within defined structural areas should allow the design of artificial receptor molecules, which bind the substrate strongly and selectively by forming supramolecular structures, (Vögtle, 1991).

Even the present-day synthetic chemist can not hope to fabricate complicated nanosystems using only the currently available covalent bond**,** (Whitesides, 1990). In order for the synthetic chemist to be able to build nanosystems, the intermolecular, non-covalent bond must be learned to control.

The current literatures clearly show that chemical researchs are rapidly moving from molecular to supramolecular level. Four reasons for this trend are:

1. the high degree of knowledge reached on molecular species
2. the extraordinary progress made by synthetic methods
3. the continuous search for new chemical functions
4. the need to fill the gap which seperates chemistry from biology.

Molecular recognition; with transformation, and translocation represent the basic functions of supramolecular chemistry, as described in Figure 1.1.

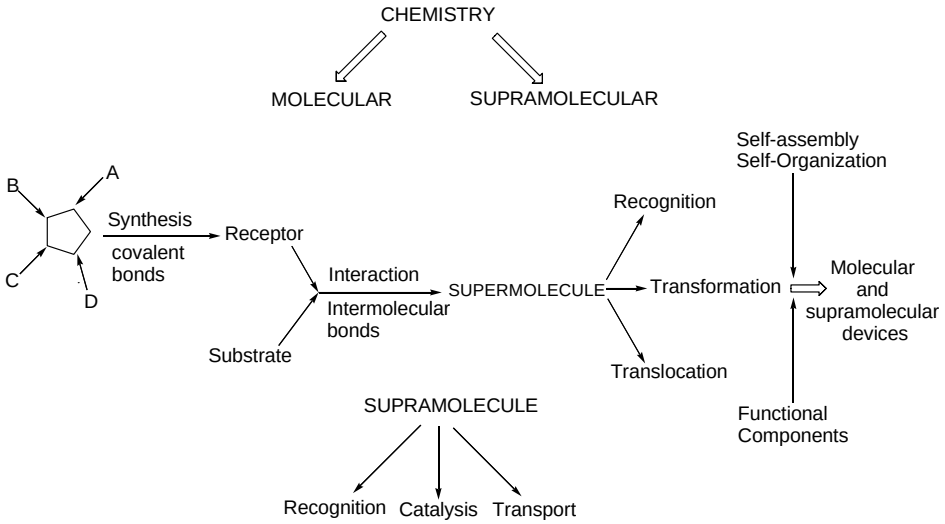

Figure 1.1. From molecular to supramolecular chemistry.

Molecular receptor (ρ) and substrate(s) (σ) are the partners of a supramolecular species, (Lehn et al, 1973). Selective binding of a specific substrate σ to its receptor p yields the supermolecule pσ and involves a molecular recognition process. The substrate is usually the smaller component whose binding is being sought. This terminology conveys the relation to biological receptors and substrates for which Paul Ehrlich stated that molecules do not act if they are not bound.

Substantial progress has been made toward the development of synthetic receptors that utilize hydrogen binding as a force in complexation, (Zimmerman & Wu, 1989).

Molecular recognition is one of the corner stones because of its implications in many field such as chemistry, biology, medicine (clinical biochemistry), enviroment, etc. In particular, selective detection of metal cations involved in biological processes, inclinical diagnosis, or in pollution

has recieved considerable attention, (Valeur, 1993). Also, molecular recognition of relevant biological targets constitutes a dynamic branch of organic chemistry and the work with model systems has led to a number of receptors for amino acids, nucleic acid heterocyclic bases, nucleotides, and carbohydrates, (Galan, et. al., 1992).

Molecular recognition is a question of information storage and read out at the supramolecular level. It requires the design of receptors possessing steric and electronic features complementary to those of the substrate to be bound and a balance between rigitidy and flexibility suitable for the function to be performed, (Lehn, 1988).

Information in here is the key and in this respect, supramolecular chemistry can be considered as a chemical information science or molecular "informatics".

Recognition implies geometrical and interactional complementarity which refers to size, shape, functionality and the weak intermolecular forces between the associating partners. In order to achieve high recognition, a well-defined three dimensional architecture with the correct arrangment of binding sites is needed, (Matthews, 1993). The use of hydrogen bonding with its modest directionality and easily recognized patterns has been quite successful in this regard, (Rebek et al., 1992).

Molecular recognition in the design of a receptor involves the understanding of many interactions at the molecular level, which are; (Dugas, 1980).

* Structural information
* Functional information

* The energetic of the process
* The three dimensional complementarity of molecular shapes
* Organic and inorganic adaptation and recognition of intermolecular chemical bonds
* The concept of molecular cavity as an architectural principle.

1.2. The Supramolecular Chemistry of Life

The chemistry found in living biological systems forms much of the inspiration and origins of supramolecular chemistry**.** Sometimes incredibly complex, or elegantly simple, nature has evolved highly specific, selective and cooperative chemistry that enables living systems to maintain themselves in their enviroment.

In biological chemistry, the supramolecular hosts are the receptor sites of enzymes, genes, antibodies of immune system and ionophores. The guests are substrates, inhibitors, cofactors drugs or antigens. All of these components exibit supramolecular properties such as molecular recognition, self-assembly, self-organisation and kinetic and thermodynamic complementarity, (Steed & Atwood, 2000).

1.3. Host-Guest Chemistry

When a molecule (a 'host') binds another molecule (a 'guest') a 'host-guest' complex or supramolecule is produced. A highly structured molecular complex is composed of at least one host and one guest component.

Three historical concepts which built host-guest chemistry are;

1. The recognition by Paul Erlich (in 1906) that molecules do not act if they do not bind. That way the concept of biological receptor is introduced.

2. The recognition by Emil Fischer (in 1894) that binding must be selective. It is described by a 'lock and key' image of steric fit in which the guest has a geometric size or shape complementarity to the host. This concept forms the basis for molecular recognition (Figure 1.2).

3. The fact that selective binding must involve attraction or mutual affinity between host and guest, (Steed & Atwood, 2000).

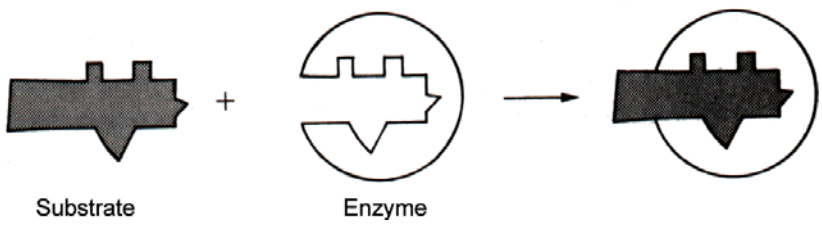

Figure 1.2. Fischer's 'lock and key' hypothesis.

Beginning with crown ethers, the field of host-guest, chemistry focused initially on complexation of cations. Although hydrogen bonds between neutral molecules are generally weaker than charge/dipole attraction and polar hydrogen bonds, several recent reports indicate that networks of hydrogen bonds may be used to form neutral complexes that are stable in solution, (Bell & Liu, 1988).

Host-guest chemistry to date has focused primarily on binding interactions which involve at least one charge-bearing partner (e.g., metal and alkylammonium ions). With rare exceptions, those relatively few systems which

consist of only neutral components and operate in nonaqueous solvents do not impose upon the guest a specific orientation once it is positioned within the binding site of the receptor. The control of such alignment would appear central to the development of efficient synthetic enzymes, (Kelly & Maguire, 1987).

Usually the host is a large molecule like an enzyme or synthetic cyclic compound with a sizeable, central hole or cavity. The guest may be a monatomic cation, a simple inorganic anion etc. More formally, the host is defined as the molecular entity possessing convergent binding sites, and the guest possesses divergent binding sites, (Steed & Atwood, 2000).

The inclusion of guest molecules into the cavities of supramolecular hosts with molecular container properties has the potential to allow novel chemical transformations, to mimic enzymatic activity, to isolate reactive species, and to promote uncommon spectroscopic effects. Many molecular-container-type hosts such as cyclodextrins (1.1), crown ethers (1.2a) and calixarenes (1.2b) allow a fast exchange of the guest, due to their unobstructed openings (Figure 1.3) (Marquez et al., 2004).

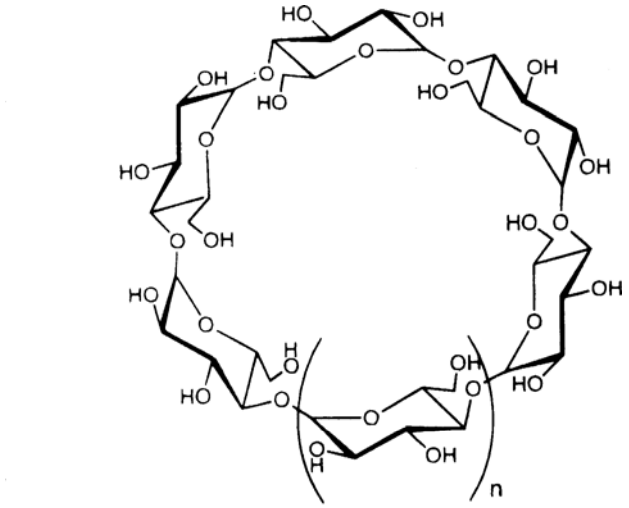

n = 1 α-CD
n = 2 β-CD
n = 3 γ-CD

1.1

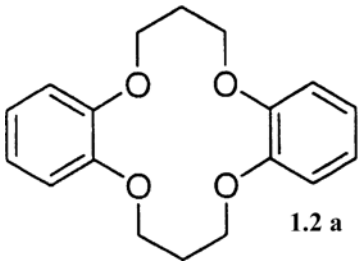

1.2 a

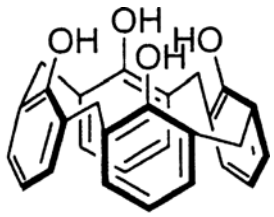

1.2 b

Figure 1.3. Structures of cyclodextrin (1.1), crown ether (1.2a) and calix[4]arene (1.2b).

1.4. Supramolecular Chemistry of Xanthene-based Molecular Complexes

Macrocyclic compounds are the dominant structures of bioorganic chemistry, therefore; this type of molecules have also influenced the trend in molecular recognition. Cyclodextrins, cyclophanes, and crown ethers are the examples of this type and they share the advantage that their interactions with smaller structures are easily conceptualized; recognition involves the filling of pockets or holes. However; the disadvantage common to macrocyclic molecules is that their structure causes problems in producing favorable interactions between functional groups on the substrate and macrocycle once the complex is formed. Functional groups attached to macrocycles tend to diverge or become away from the cavity and from the substrates that are held inside. In contrast, functional groups on receptors such as enzymes or antibodies tend to converge and act as an integral part of the active site. This focusing of functional groups leads to the recognition of molecules that bear complementary functionality. The general shape of these naturally occurring receptors often features a molecular cleft. The characteristics of convergent functional groups has been incorporated into synthetic structures. This aspect is the key to their success in molecular recognition, (Breslow, 1982).

In 1984 Rebek introduced molecules of a cleftlike shape to bioorganic chemistry. They used the Kemp's triacid (1.5) shown in Figure 1.4 to form the unique shapes of the molecules (1.3 and 1.4). One significant advantage of that work was the convergence of useful functional groups, particularly carboxylic acids. It permitted the use of hydrogen-bonding interactions rather than the ion-dipole interactions that are the principal forces offered by crown ethers or the hydrophobic interactions of cyclodextrins and cyclophanes. Directioanality in binding was the result, and structures bearing basic sites could be considered targets for recognition studies (Figure 1.5).

Later on, Rebek was also demonstrated their utility as a probe in molecular recognition studies, (Rebek, 1987).

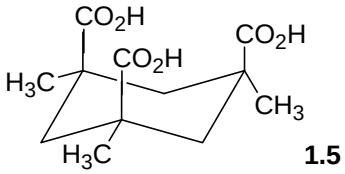

1.5

Figure 1.4. The structure of Kemp's triacid.

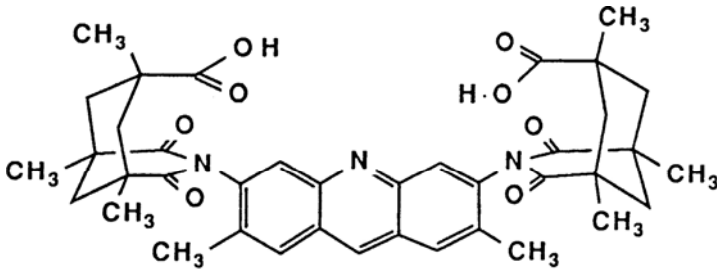

1.3

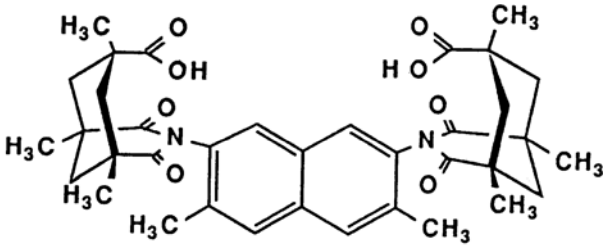

1.4

Figure 1.5. Molecules featuring molecular clefts.

In 1988, Rebek and co-workers underlined the importance of having the correct orientation of functional groups in the substrate-catalyst complex. In this regard, they focused on the dissociation of glycoaldehyde dimer (1.6) to the monomer (1.7) This reaction had been studied by a number of workers in various media, and was very slow in the absence of catalysts. They showed that the convergent diacid (1.3) is a remarkably effective catalyst for this reaction, while the divergent diacid (1.8) shows poor efficiency, (Figure 1.6). The structure bears all of the functional groups of (1.3), but its divergent structure does not permit these functional groups to act in a concerted manner.

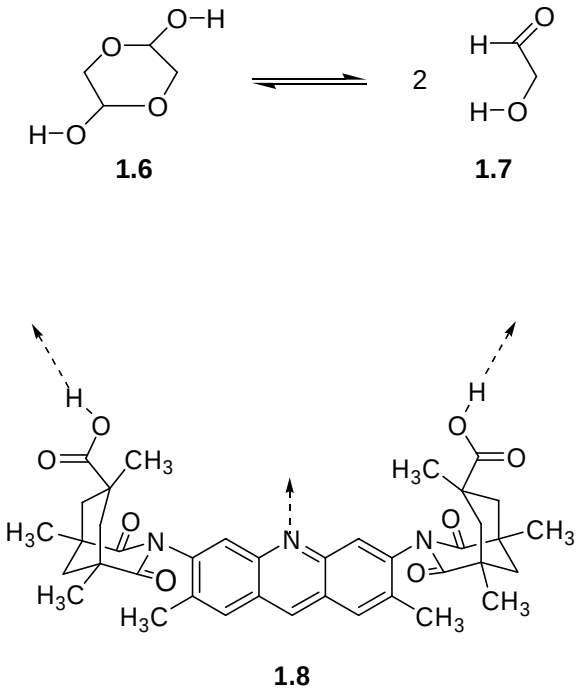

Figure 1.6. The catalytic effect of a molecule with divergent groups (1.8).

A year later, another group proposed a set of host molecules (1.9 and 1.10), in which the functional groups are well-arranged for binding to several guests, including adenine (1.11) and biotin (1.12) derivatives, through formation of four hydrogen bonds (Figure 1.7). The importance of this result was, it could be easily modified to afford a new hosts in which various functional groups are brought into opposition or other orderly configurations, (Adrian & Wilcox, 1989).

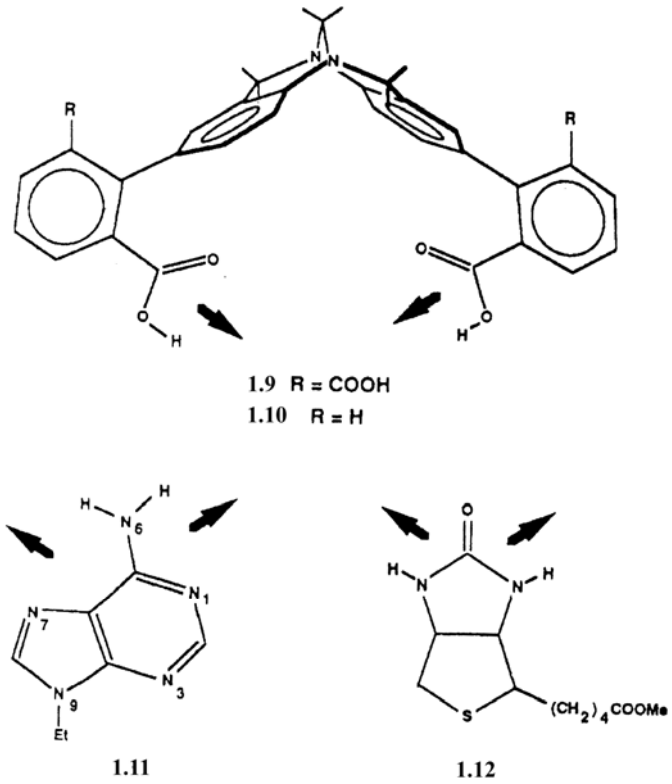

Figure 1.7. Examples of host-guest chemistry of molecules having convergent functional groups.

Later on, the structures having convergent functional groups in cleftlike shapes have emerged as useful receptors for small molecules**.** In such an attempt, Nowick et al. (1990) explored new modular units based upon xanthene-4,5-dicarboxylic acid derivatives (1.13a and 1.13b) shown in Figure 1.8. and report their advantages for complexation of larger target structures.

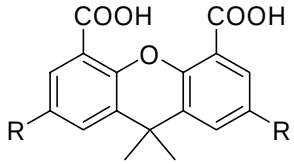

1.13a R= $C(CH_3)_3$

1.13b R= $C(CH3)_2CH_2CH_3$

Figure 1.8. Xanthene-4,5-dicarboxylic acid derivatives.

In 1994, Shipps and Rebek reported the synthesis of the first porphyrin based molecular cleft (1.14). The new structure takes advantage of xanthene skeleton fixed rigidly on a tetraaryl porphyrin platform showing high affinity for appropriate guests. The convergent functional groups attached to the porphyrin spacer are used to bind several guests (Figure 1.9).

In the same year, Rebek et al., introduced a new family of molecular clefts, (1.15a and 1.15b). Like the previous ones, they present functional groups on their inner, concave surfaces that converge on and are complementary to smaller, convex guest molecules. Unlike the diacid (1.3), the new molecules provide a deeper, roomier cavity and easier derivatization (Figure 1.10).

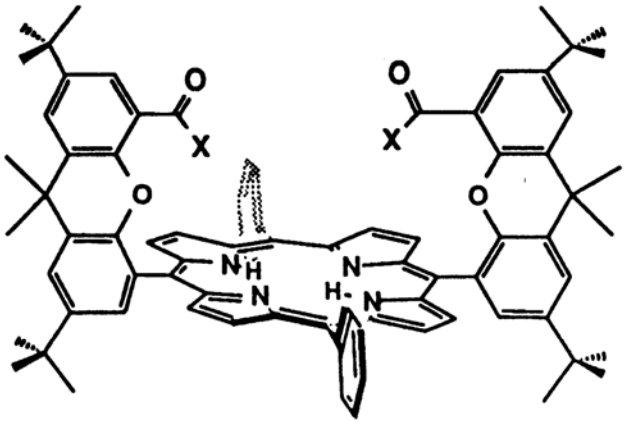

1.14

Figure 1.9. A new porphyrin based molecular cleft.

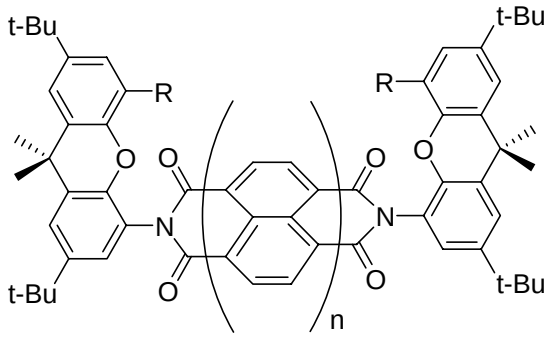

1.15a R = CO_2H , n =1

1.15b R = CO_2H , n =2

Figure 1.10. A new family of molecular clefts.

1.5. Enzymes

The enzymes are important and essential components of biological systems and their function is to catalyze the chemical reactions that are essential to life. Without the efficient aid of the enzymes these chemical processes would occur at greatly diminished rates, or not at all, (Laidler, 1958).

In 1835 J.J. Berzelius developed the theory of chemical catalysis. The specifity of enzymes impressed Emil Fischer, who in 1894 proposed the famous 'lock and key' hypothesis to explain enzyme action and specifity, (Robyt, 1987). According to this model, the molecule undergoing catalysis fits exactly into a site on the enzyme at which the catalysis occurs (Figure 1.2). The kinetic and catalytic properties of enzymes were studied in the early part of the twentieth century. In 1913 L. Michaelis and M. L. Menten published their classic study of the substrate concentration dependence of enzyme reactions and postulated the formation of an enzyme-substrate complex to explain their kinetic data, (Robyt, 1987).

J. B. Summer crystallized the first enzyme, jack bean urease, in 1926. Shortly therafter J. H. Northrup and M. Kunitz (1932) reported the crystallization of pepsin, trypsin, and chymotrypsin. Analysis of these crystalline compounds, which were shown to be proteins with enzymatic activitiy, established the protein nature of enzymes.

Enzymes generally bind their substrates and then use the action of two or more well-placed functional groups to achieve catalysis. This scheme leads to substrate selectivity, reaction selectivity, and stereoselectivity. Binding can be achieved by metal coordination, ion pairing, Lewis acid-base coordination, or hydrogen bonding in nonaqueous solvents, etc., (Breslow, 1995).

The essential characteristic of a catalyst is that it influences the rate of chemical reaction but is not itself used up during the process and can ideal cases be recovered at the end of the reaction. In other words; in all types of catalysis the catalyst forms some kind of complex with the substrate and that this complex finally breaks downn into the products of reaction and the catalyst, (Laidler, 1958).

Enzymes cannot catalyze reactions that are impossible without the enzyme. They can, however, provide for specifity of substrates and products that cannot be easily achieved in any other way. Enzymes, by providing favorable micro-enviroments and proper orientation of substrates in these micro-enviroments, accomplish a lowering of the activation energy of the reaction. The result is an increase in reaction rate, (Matthews, 1993).

Since there are very many different enzymes it is convenient to discuss them with reference to some type of classification. Various methods of classification are possible and none is completely satisfactory. For example; in terms of the types of reaction that the enzymes catalyse, they may be classified as the hydrolytic enzymes, proteolytic enzymes, carbohydrases, esterases, etc., (Laidler, 1958).

Enzymes also have found use as chemotherapeutic agents, especially in the treatment of hereditary diseases, and as diagnostic indicators in the detection of disease. Furthermore an understanding of the specifity, regulation, structure, and mechanism of action of enzymes provides a major contribution to the understanding of the functioning of the living cell, (Robyt, 1987).

In the construction of excellent enzyme models, cyclodextrins (CDs) seem to have attracted much attention. They are slightly V-shaped macro rings which are composed of α-(1,4)-linked D(+)-glucopyranose units. The three

practically important, industrially produced CDs are α-CD having 6, β-CD having 7 and γ-CD having 8 glucose units which are shown in as 1.1. Because they have apolar, hydrophobic character of the cavity which are similar to active sites of the majority of enzymes, they behave as enzyme-like catalysts in a mechanistic sense. The hydrophobic interactions form the main force in guest complexation with CDs among others.

All current developments amplify the importance of the basic understanding of structures and mechanisms of enzymes. Fundamental knowledge on enzyme structures and mechanisms is important for effective utilization and improvement of existing enzymes and the development of new enzymes, (Breslow, 1998).

1.6. General Hydrolytic Enzymes

Water is not just the solvent in which the chemical reactions occur; but also it is directly involved in those reactions. Hydrolysis reactions are responsible for the enzymatic addition of the elements of water, to the transferable functional group of the donor. However, a transfer reaction takes place in some systems in which a suitable acceptor, if present in adequate concentrations, may compete successfully with water to capture the donor moiety.

Most of the hydrolases studied so far are relatively simple, stable, low molecular weight enzymes, and the hydrolysis reactions they catalyze are not difficult to monitor experimentally. The general catalytic system of hydrolytic reactions is:

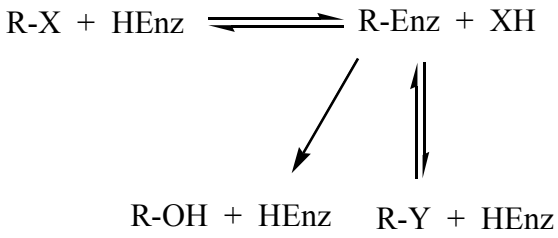

Where R-X is the substrate or the donor system, R is the transferable functional group, Y is the general acceptor system, and H_2O is the special acceptor system. Based on the nature of the reaction catalyzed, typical hydrolases are Phosphatases, Proteolytic enzymes, Glycosidases, Lipases and Esterases.

Phosphatases are defined as enzymes that catalyze the hydrolysis of phosphoric acid esters. They are divided into four subgroups according to the nature of the substrate attacked (Table 1.1).

1. Phosphomonoesterases are believed to have an essential role in important processes of intermediary metabolism. Their function is to provide inorganic phosphate (Table 1.1) for metabolic, excretory, and some secretory purposes. Glucose-6-phosphatase and alkaline phosphatase are important examples of phosphomonoesterases.

2. Phosphodiesterases are enzymes hydrolysing diesterified phosphate (Table 1.1). It is proposed to subdivide them into nucleases, those that hydrolyse nucleic acids and their derivatives; and lipophosphodiesterases, those that hydrolyse phospholipids and their derivatives. The best known example is ribonuclease.

3. Pyrophosphatases are responsible for the hydrolysis of inorganic pyrophosphate into orthophosphate (Table 1.1). Inorganic pyrophosphatases are divided into three groups based on their pH optimum values: i) Those which are active at pH 7.5 require Mg^{2+} and inhibited by F^- ii) Those whose optimum pH is 5.5 are also inhibited by F^- iii) The last group involves ATPases that are active at pH 4.

4. Metaphosphatases catalyzes the rapid reaction of unstable metaphosphate ion with water to give inorganic phosphate (Table 1.1). However it is unclear whether this mechanism occurs frequently during enzymatic catalysis.

Proteolytic Enzmes or proteases are responsible for catalyzing the hydrolysis of peptides or proteins. When the susceptible peptide bond is some internal bond, the enzyme is said to be an endopeptidase. When it is at the amino or carboxyl terminus of a protein substrate, the enzyme is termed an exopeptidase.

Glycosidases specifically hydrolyse the glycosidic bonds. Lysozyme and amylase are the well known glycosidases.

Esterases and Lipases hydrolyse esters of organic acids with alcohols. Lipases from different sources split esters of different types at different rates. In the same manner, liver esterase tends to cleave esters of short-chain fatty acids and monohydric alcohols, whereas pancreatic lipases tend to split esters of long-chain fatty acids and polyhydric alcohols. Acetylcholinesterase is of considerable importance.

Table 1.1. Classification of Phosphatases and the Reactions They Catalyze

Phosphatases	Nature of the reaction catalyzed
phosphomonoesterases	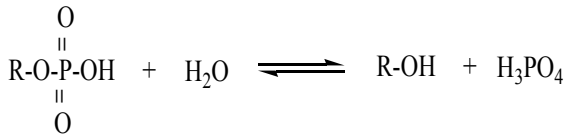
phosphodiesterases	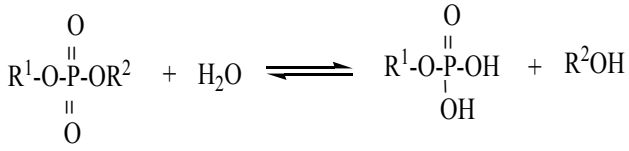
pyrophosphatases	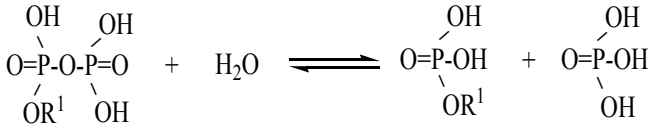
metaphosphatases	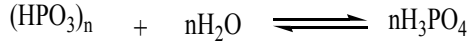

1.7. Artificial Enzymes

The field of artificial enzymes is very active, and the goals and likely achievements are exiciting. The hope is to develop catalysts for general use, as in the manifacture of medicines and other important chemicals, that combine the effectiveness and selectivity of natural enzymes. Also, artificial enzymes could represent a new class of medicinal agents, catalyzing reactions in vivo. Such catalysts need to be more stable and easily handled than natural enzymes, and also available to catalyze all reactions of interest, not just those that play a role in natural biochemical processes, (Breslow, 1998).

Enzyme catalysis depends on the preferential complexation and stabilization of transition states over their corresponding starting materials and products, (Boger et. al., 1978). An important goal in the development of artificial enzymes must, therefore, involve the construction of synthetic receptors that are complementary to the electrostatic and spatial features of transition-state structures, (Tecilla et al., 1990).

Selectivity of enzyme catalysis reactions is as important as the speed of enzyme-catalyzed reactions. Enzymes bind their substrates before catalyzing reactions, and one aspect of selectivity is their ability to bind only particular substrates in a soup of different molecules. For example; without such selectivity the genetic control of protein synthesis would not be possible. Selective binding is also seen with antibodies, which can frequently bind their target molecule with very high affinity. Many workers have built mimics of antibodies, and in appropriate cases very strong and selective binding has been observed. The goal is to use such strong selective artificial antibodies to bind to biological molecules such as hormones, so as to prevent them from binding to their natural receptors, (Breslow, 1998).

One another goal for development of the artificial enzymes is utilization of them as catalysts for reactions which can not be mediated by natural enzymes, (Murakami, 1996)**.**

Since metal ions are often very effective catalysts, and many enzymes take advantage of this, it has been attractive to synthesize enzyme mimics that combine metal ion catalysis with substrate binding. In fact, the first compound called an " artificial enzyme " in the literature was the one that combines a cyclodextrin binding group with a metal ion catalytic group. It catalyzes the hydrolysis of substrates that bind into the cyclodextrin cavity (1.16), Figure 1.11. (Breslow, 1970).

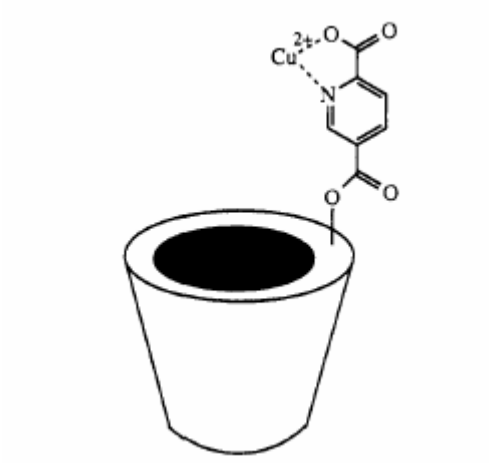

1.16

Figure 1.11. The first compound called "artificial enzyme".

Cyclodextrins have emerged as important enzyme models to use because of their ability for hydrophobic binding in the central cavitiy. A number of these miniature molecules have been introduced to mimic processes of hydrolytic enzymes.

An artificial enzyme chymotrypsin-like activity (hydrolysis of esters) has been constructed by designing a catalytic group (an imidazolyl benzoic acid) to the secondary side (C2 or C3) of β-cyclodextrin. This model hydrolyzes m-*t*-butylphenyl ester at twice the rate of chymotrypsin-catalyzed hydrolysis of p-nitrophenyl acetate shown in Figure 1.12a, (D'Souza et al., 1987).

Breslow et al. (1980) designed a synthetic transaminase by linking pyridoxamine to β-cyclodextrin via a thioether linkage and have shown that it catalyzes a transamination reaction (α-keto acid $\rightleftharpoons$ amino acid) with stereoochemical selectivity in substrates, Figure 1.12b.

Cyclodextrin dimers linked by a metal-binding group have been constructed that mimic metalloenzymes. Ester substrates with hydrophobic substituents at both ends can then bind to the dimer, with the carbonyl group positioned close to the metal catalytic group. Hydrolysis of the ester involves the attack of a metal hydroxide species as observed in typical metalloenzymes, Figure 1.12c, (Breslow and Zhang, 1992).

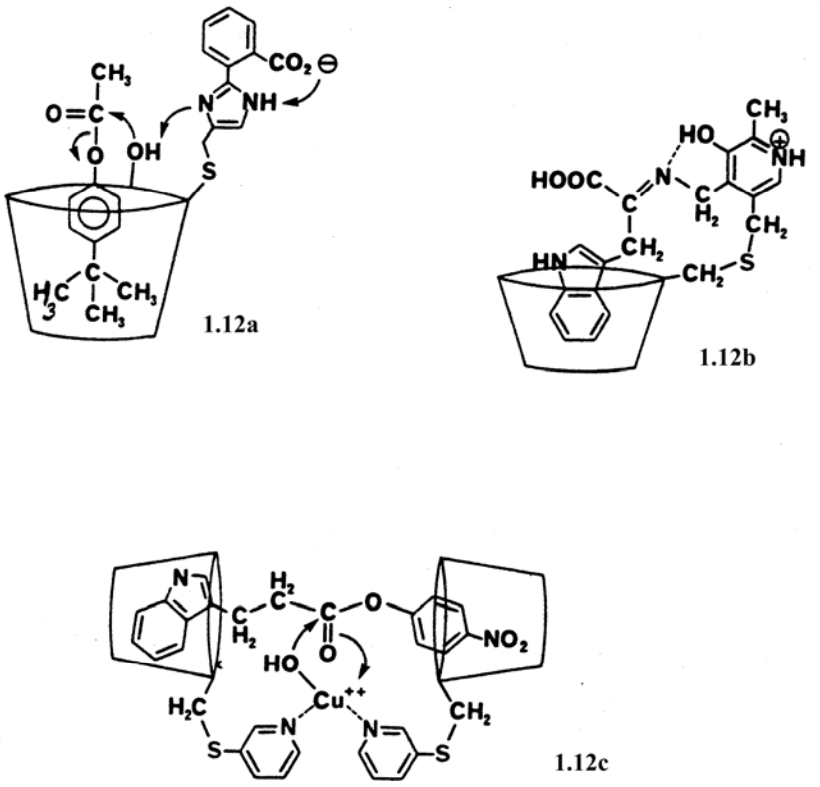

Figure 1.12. Structures of cyclodextrin based artifical enzymes.

Recently, Ikeda and co-workers (1996) have synthesized an imidazole appended 2,6-dimethyl-β-CD (1.17), given in Figure 1.13, as an artificial hydrolase. Their model caused about 1000-fold acceleration of the hydrolysis of *p*-nitrophenyl acetate, and k_{cat} for this reaction was 2.67×10^{-2} s^{-1}, which is over twice as much as that of α-chymotrypsin.

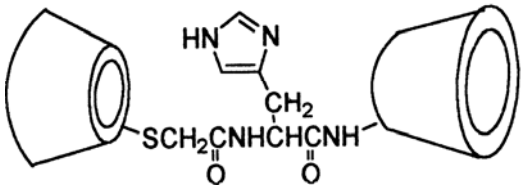

1.17

Figure 1.13. Imidazole appended β-CD dimer as an artificial hydrolase.

Artificial models for the dinuclear metalloenzymes increase the understanding of enzymatic cleavage of chemically stable phosphate esters and possible applications in biotechnology. Several artificial active site models have been reported in which two metal ions, like Zn(II), Cu(II), Co(III), and lanthanides(III), are held apart by appropriate ligands. Nonenzymatic phosphate ester cleavage is effectively facilitated by the strongly Lewis acidic Co(III) and lanthanide(III) ions. However, for application as artificial nucleases the use of Co(III) is not attractive since it forms substitutional inert complexes with the products. The disadvantage of lanthanide(III) ions is their toxicity and the laborious formation of sufficiently stable complexes, (Molenveld, 1998).

Cryptands were also used as ligands an artificial enzyme model which are structurally or functionally mimics the natural enzymes. Koike and his collaborators (1996) have shown that an octaazacryptand forms a novel dinuclear Zinc(II)cryptate(Zn_2L) (L=alokoxide form of HL) (1.18) in aqueous solution, Figure 1.14.

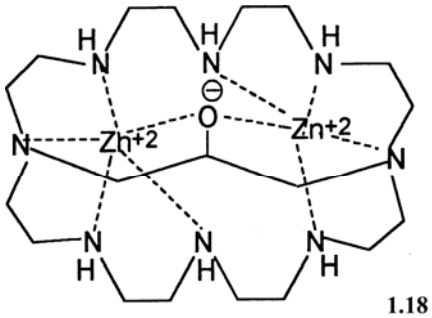

1.18

Figure 1.14. Di-nuclear Zn(II)cryptate(Zn_2L).

1.8. Acid-base Catalysis

A crucial factor in whether or not an acid-base catalyst is effective is whether or not it is in the correct ionization state under the reaction conditions: an acid has to be in acidic form to be an acid catalyst, and a base in its basic form. The most effective acid-base catalysts at pH 7.0 are those whose pK_a's are about 7. This accounts for the widespread involvement of histidine, with an imidazole pK_a of 6 to 7, in enzyme catalysis (Fersht, 1985).

In all enzymatic reactions, involving proton transfer, acid-base catalysis take place. Therefore; there are not many enzymes which do not have acidic or basic groups in their active sites. Non-enzymatic reactions may be carried out in in a wide range of pH conditions while enzymatic reactions have a strict limitation for pH. They are active at physiological pH, in the range 5-9.

When the substrate is protonated by a catalytic residue in the active site of the enzyme, it causes a general acid catalysis to occur. As a result of this event this residue loses a proton**,** (Figure 1.15A). So, the acidic groups involving the enzymatic reactions must have a pK_a above the physiological pH (range of 7.0-10), and they can be protonated at physiological pH.

When the substrate is deprotonated or when water is deprotonated and attacks the substrate, it causes a general base catalysis to occur. (Figure 1.15B) So, the bases in the active site of the enzyme must have pKa value below the physiological pH, and can be deprotonated at physiological pH.

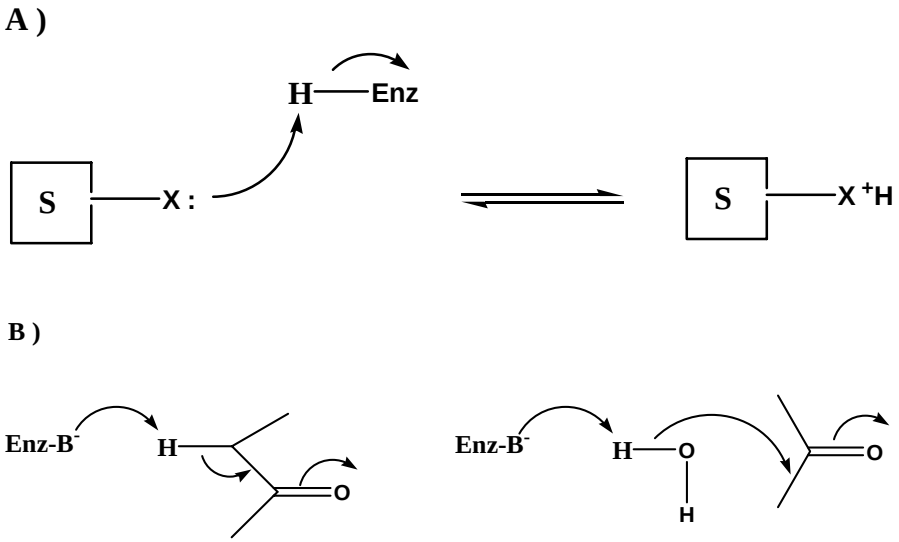

Figure 1.15. A) General acid catalysis B) General base catalysis

The pKa values of the acidic and basic groups can be influenced by their microenviroment. For example; the enzyme acetoacetate decarboxylase have a lysine residue in the active site which forms an imine linkage with its substrate and shows a pK_a value about 5.9, much less than the expected value.

Enzymes have the ability to cary out bifunctional catalysis: protonation and deprotonation of the substrate at the same time but in different parts of the substrate. An example of such an enzyme is ketosteroid isomerase, in which

aspartate is the acidic group and tyrosine is the basic group in the active site of the enzyme, (Figure 1.16) (Bugg, 1997).

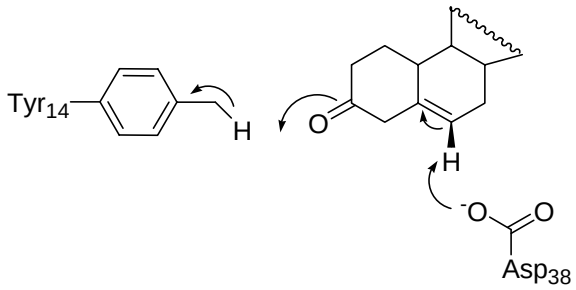

Figure 1.16. Bifunctional catalysis in the ketosteroid isomerase.

1.9. Metal ions in Biochemistry and Metalloenzymes

One third of all known enzymes are metalloenzymes, the unique class of enzymes in which discrete active centers are formed when metal ions or metal containing cofactors are incorporated into proteins, (Noodleman, 2003).

Nature has developed many hydrolytic metalloenzymes. Transition metal ions are essential components of many biological systems. They catalyze many difficult and critical reactions in biological systems, evolving to hydrolyze some of the most important molecules of life including proteins, phospholipids, and DNA, (Chin, 1991).

The importance of metal ions to the vital functions of living organisms has become increasingly apparent. Metal ions with certain nucleotides serve as cofactors for various enzymatic reactions. They can also mediate oxidation-reduction reactions by reversible changes in the metal ion's oxidation state. Also, ionic interactions between an enzyme-bound metal and the substrate can

help to orient the substrate for a reaction or stabilize charged reaction transition state. For catalytic activity, enzymes require one or more metal ions, (Barrett, et. al., 1995).

One rol for metals in metalloenzymes is to act as electrophilic catalysts, stabilizing the increased electron density or negative charge that can develop during reactions. Among the enzymes that function in this manner is liver alcohol dehydrogenase.

Another potential function of metal ions is to provide a powerful nucleophile at neutral pH. Coordination to a metal ion can increase the acidity of a nucleophile with an ionizable proton:

$$M^{2+} + NucH \rightleftharpoons M^{2+}(NucH) \rightleftharpoons M^{2+}(Nuc^{-}) + H^{+}$$

The reactivity of the coordinated, deprotonated nucleophile is typically intermediate between that of the un-ionized and ionized forms of the nucleophile. For example, carboxypeptidase contains an active site Zn^{2+}, which facilitates deprotonation of a water molecule in this manner, (Garrett & Grisham**,** 1995).

Over the years there has been a great deal of interest in developing artificial hydrolytic metalloenzymes that hydrolyze the phosphate diester bonds in nucleic acids and the amide bonds in protein molecules, (Komiyama, et. al., 1992). Lanthanide metal ions and their complexes have recently been shown to be highly reactive for hydrolyzing phosphate diesters including RNA, (Takasaki & Chin, 1993).

A metal ion can accelerate the rate of the phosphate ester hydrolysis in several ways. The three direct modes of activation are;

1. Lewis acid activation
2. Nucleophile activation
3. Leaving group activation

In addition, metal ions may indirectly activate these reactions. A metal coordinated hydroxide can act as an intramolecular general base catalyst, or metal coordinated water molecules can act as an intramolecular general acid catalyst, (Chin, 1997).

In nature, multinuclear metalloenzymes serve as catalysts for several acyl and phosphoryl transfer reactions. Chin et al. (1993) chose a binuclear copper complex to accelerate the reaction of a phosphoric acid diester anion (1.19) shown in Figure 1.17. This reaction can be considered a model for the first step of the hydrolysis of RNA. When the binuclear copper complex was compared with the analogous mononuclear complex, the approximately 50 times larger rate constant of binuclear complexs shows that, here, the two metal ions probably cooperate.

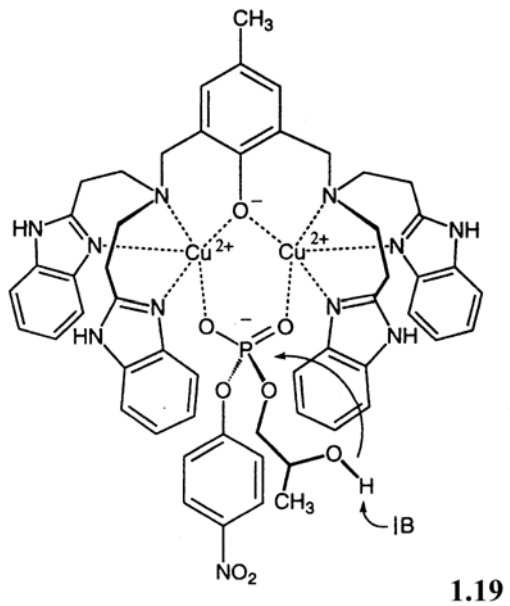

1.19

Figure 1.17. Model reaction for the first step of the hydrolysis of RNA. B=base.

In recent studies with carefully designed binuclear complexes have demonstrated that how the catalytic efficiency depends critically on the distance between the metal centers and the conformation of the spacer. In the Co^{3+} binuclear complex (1.20), the two metal ions are held so far apart by the spacer that no direct dimerization of the two subunits through oxygen is possible, Figure 1.18. This complex accelerates the hydrolysis of phosphoric acid diester anions by seven orders of magnitude, but still does not exceed the activity of mononuclear complexes. The postulated mechanism for the hydrolysis of phosphoric acid diester (1.21) is given in Figure 1.19. On the other hand, this complex increases the rate of hydrolysis of phosphoric acid monoesters about ten times more than the corresponding mononuclear complexes (1.22), which hydrolysis mechanism is also shown in Figure 1.19, (Czarnik, 1993).

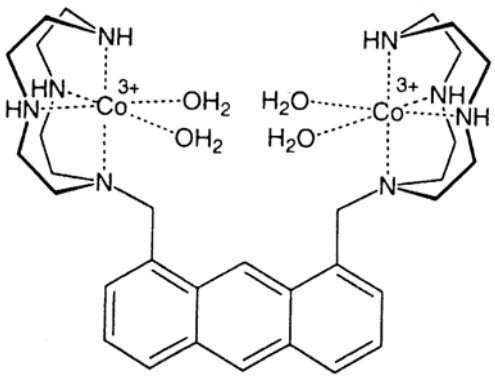

1.20

Figure 1.18. The dinuclear Co^{3+} complex.

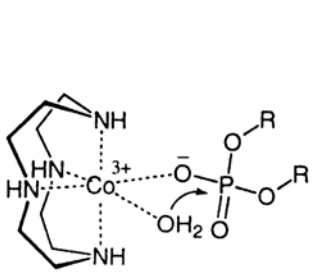

1.21

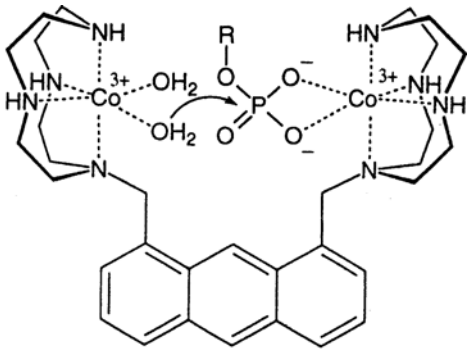

1.22

Figure 1.19. Postulated mechanisms for the hydrolysis of phosphoric acid esters (1.21 and 1.22).

1.10. Zinc Enzymes

Zinc is an essential component in biochemistry, and forms part of the active site of more than 100 enzymes, (Steed & Atwood, 2000).

Substantial quantities of firmly bound zinc in RNA and DNA have revealed additional important avenues of its role in biology. Zinc appears to stabilize the secondary and tertiary structure of RNA and to play an important role in protein synthesis.

Zinc is also an essential cofactor, and critical for numerous cellular functions. The combination of its unique chemical properties and its central role in processes including gene expression, apoptosis, enzyme regulation, and neurotransmission suggest that Zn^{2+} may be a major regulatory ion in the metabolism of cells, (Walkup et al., 2000).

In recent years the variety and importance of zinc functions in biology and medicine has expanded dramatically. Whereas a decade ago, zinc was viewed mainly as a component of metalloenzymes and transcription factors, there is now growing consensus that zinc also functions as a signal ion, somewhat analogous to calcium, among a variety of cell types**,** (Thompson, 2002).

The roles of zinc in metalloenzymes can be divided into four categories: catalytic, structural, regulatory-or modulatory, and noncatalytic.

Zinc is said to have a catalytic role when it is essential for and directly involved in catalysis by the enzyme; carbonic anhydrase, carboxypeptidase, thermolysin, and aldolases are examples of this type.

Zinc plays a structural role when it is required solely for the structural stability of the protein, being necessary for activity only to the extent that the overall conformation of the enzyme affects its action. The examples for this type can be in B.subtilis α-amylase, and aspartate transcarbamylase.

A regulatory role is indicated when zinc regulates, but is not essential for, enzymatic activity (which is present in the absence of metal) or for the stability of the protein. Regulatory zinc may act either as an activator or inhibitor as in bovine lens leucine aminopeptidase and fructose 1,6-biphosphatase respectively.

Some metalloenzymes which have zinc in are neither involved directly in catalysis nor essential for the maintenance of the tertiary structure of the enzyme, so that its function is yet clear. In the absence of specific knowledge on how the metal acts, it is referred to as noncatalytic. Examples for this type may be alcohol dehydrogenase and E. coli alkaline phosphatase

Metal exchange studies have shown that the replacement of catalytic and regulatory zinc with other metal ions can affect activity, while that of structural and noncatalytic zinc atoms seems to have only minor consequences, (Spiro, 1991).

Much of the importance of zinc enzymes derives from their peptidase and amidase activity involving the cleavage of RC(O)-NH(R^1) amide bonds. In addition to the cleavage of amide bonds, zinc enzymes play an important role in the cleavage of the P-OR bond in phosphates as exemplified by their nuclease activity pertaining to the hydrolysis of DNA and RNA. The importance of zinc enzymes is not, however, restricted to their role in cleaving amide and phosphate bonds. It is therefore, evident that zinc plays multifaceted roles in biological systems, (Parkin, 2004).

The first enzyme shown to require Zn(II) for its biological activity is Carbonic anhydrase (CA). Its major function is the catalysis of the hydration of CO_2 and dehydration of H_2CO_3 or HCO_3^-.

Among the physiologically relevant metal ions, Zn(II) is probably the best suited metal ion for the development of artificial metallonucleases. In fact, being a strong Lewis acid and exchanging ligands very rapidly, it is an ideal candidate to play the role of hydrolytic catalysts. However, its reactivity is somewhat lower than that of the other commonly employed transition-metal ions, and this probably explains that why the examples of Zn(II)-based artificial nucleases reported to date are very few**,** (Boseggia, 2004).

The study of Molenveld et al. (1997) presents calix[4]arene (1.23), functionalized with two Zn(II) centers at the distal positions of the upper rim, as the first example of a dinuclear complex. The molecule shows both strong binding to a phosphate diester substrate, 2-(hydroxypropyl)-p-nitrophenyl phosphate (HPNP), and high catalytic activity. The catalytic activity of the mono-nuclear calix[4]arene Zn(II) complex (1.24) is 50 times lower than that of (1.23), emphasizing the importance of synergism of the two Zn(II) centers in (1.23) (Figure 1.20).

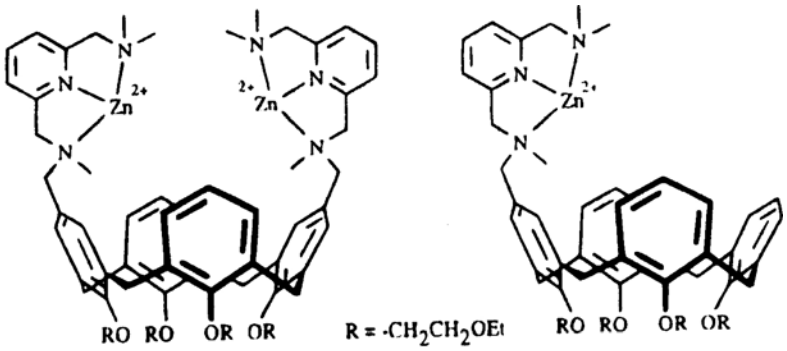

1.23 1.24

Figure 1.20. Structures of di- (1.23) and mono-nuclear (1.24) calix[4]arene Zn(II) complexes.

Breslow and co-workers (1988) described a catalyst (1.25) in Figure 1.21 in which two bound Zn(II) ions cooperate in the cleavage of a phosphate triester or carboxylic ester. The catalyst showed a 5-fold increase in the rate with p-nitrophenyl diphenyl phosphate and a 7-fold increase with p-nitrophenyl acetate, compared to the rate with a single ligand group.

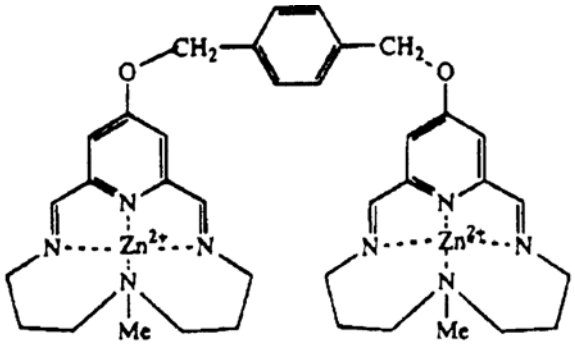

1.25

Figure 1.21. An example of zinc containing enzyme.

Yashiro and his colleagues (1997) also showed the cooperation effect of three zinc(II) ions in phosphoester hydrolysis, since three Zn^{2+} ions have been suggested to participate in enzymatic reactions, (Volbeda, 1991). They reported that the trinuclear complex Zn_3L^3 hydrolyses diribonucleotides much more efficiently than dinuclear Zn_2L^2 complex, (Figure 1.22).

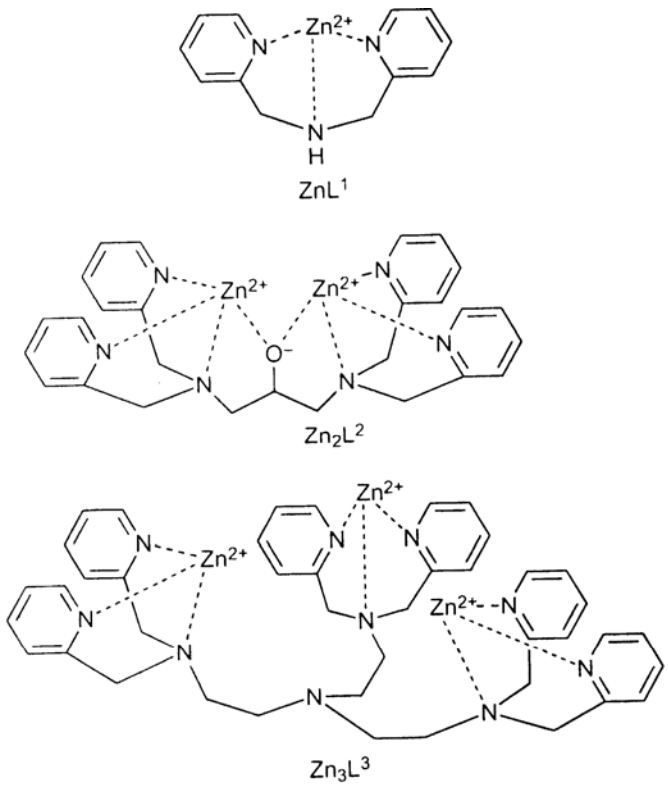

Figure 1.22. Structures of ligands.

1.11. Aim of the Study

Recognition at the molecular level is a fundamental characteristic of biochemical systems. Recent models developed in bioorganic chemistry have rvealed the importance of complementarity in size, shape and functional groups in molecular recognition. Structures that feature a cleft are particularly effective in regard to complementarity since functional groups attached to the interior of the cleft converge on substrates held inside. Thus, the molecular clefts offer the advantage of efficient construction. The catalytic effects of enzymes and the specifity of biogenic receptors also illustrate the remarkable properties of properly ordered functional group arrays.

To have a better of understanding of the mechanism of enzyme catalysis, it would be useful to have a relatively simple model systems which exhibit some of the important characteristics of enzyme-catalyzed reactions. Artificial enzyme design is an active field of supramolecular chemistry. Metalloenzymes are attractive targets in such studies, because in these enzymes active sites feature metal ions, and the hydrolytic activity of these complexed ions can be relatively easily approximated in model systems. Many hydrolytic enzymes carry one or more metal centers, and in most cases there is a cooperativity between the metal centers. However, in enzymes, there are always additional interactions; in fact, enzymatic catalysis is essentially a 'multifuctional' catalysis. Nucleophilic, general acid and general base catalysis are very common catalytic effects observed in hydrolytic enzymes. Combination of such hydrolytic functions, typically result in 'larger than additive' effects.

Xanthene derivatives proved to be very useful rigid scaffolds in supramolecular chemistry. In this study, in order to demonstrate the utility of multifunctional catalysis over simple metal catalysis, we aimed to design and synthesize novel xanthene derivatives carrying two cyclen **(2.16)**, one cyclen and

one imidazole **(2.17)** and one cyclen and one hydroxymethyl **(2.18)** units which are functionalized with one and two Zn(II) centers, and studied hydrolytic activities of these enzyme models for the hydrolyses of the model substrate, *p*-nitrophenylacetate (PNPA) **(2.15)**.

These biomimetic enzyme models are such examples for binuclear, bifunctional and mononuclear metalloenzymes, respectively. Thus, this set of xanthene derivatives would allow us to assess relative contributions of different catalytic modes.

CHAPTER II

MATERIALS AND METHODS

2.1. Materials

^{1}H and ^{13}C NMR spectra were recorded on a Bruker Instruments Avance Series-Spectrospin DPX-400 Ultra shield (400 MHz) High Performance digital FT-NMR spectrometer (METU NMR Laboratory). All chemical shifts are referenced to residual solvent signals previously referenced to TMS (tetramethylsilane) and splitting patterns are designated as s (singlet), d (dublet), t (triplet), q (quartet), m (multiplet), and br (broad).

Absorption spectrometry was performed using Shimadzu UV-1600PC spectrophotometer. Kinetics of the reactions were studied in aqueous buffer solutions, following the increase in the absorption at 400 nm due to the release of the *p*-nitrophenolate ion Mass analysis of the compounds were obtained from the TUBITAK (The Scientific and Technical Research Council of Turkey) Instrumental Analysis Laboratory.

Chemical and solvents were purchased from Aldrich and used without further purification. Column chromatography of all the products were performed using Merck Silica Gel 60 (particle size: 0.040-0.063 mm, 230-400 mesh ASTM)

pretreated with the eluent. Reactions were monitored by thin layer chromatography using fluorescent coated aluminum sheets (20x20 cm).

2.2. Synthesis of 2,7-Di-*tert*-butyl-4,5-bis-chloromethyl-9,9-dimethyl-9*H*-xanthene (2.2)

The synthesis was carried out as mentioned by Grummit and Buck (1999). 2,7-di-*tert*-butyl-9,9-dimethyl-9*H*-xanthene (1.55 mmol, 500 mg), paraformaldehyde (200 mg) , acetic acid (0.6 ml) , phosphoric acid (0.13 ml) , and concentrated hydrochloric acid (0.6 ml) were placed in a sealed tube and stirred at 90 ^{o}C for overnight. Then, water (10 ml) was added into the reaction mixture and the mixture was extracted with CH_2Cl_2 (3x10 ml). The organic phase was collected, dried with Na_2SO_4 and the solvent was removed under reduced pressure Yield:for **(2.2)** 585 mg (90 %).

^{1}H NMR (400 MHz, $CDCl_3$,) δ(ppm) 1.27 (18 H, s, $C(CH_3)_3$), 1.57 (6H, s, CH_3), 4.75 (4H, s, CH_2), 7.17 (2H, s, Ar-H), 7.28 (2H, s, Ar-H).
^{13} C NMR (100 MHz, $CDCl_3$) δ(ppm) 31.9, 32.0, 32.8, 34.9, 42.5, 123.9, 124.4, 125.9, 130.0, 146.1, 146.4.

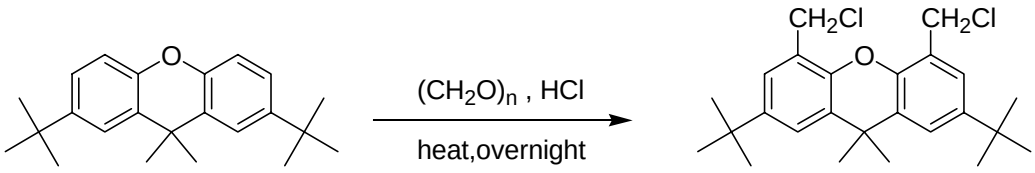

2.1 **2.2**

Figure 2.1. Synthesis of 2,7-Di-*tert*-butyl-4,5-bis-chloromethyl-9,9-dimethyl-9*H*-xanthene (2.2).

2.3. Synthesis of 1,4,7 Tris (tert-butyloxycarbonyl)-1,4,7,10-tetraazacyclo-dodecane (Tris-Boc-cyclen) (2.4)

Di-*tert*-butyl dicarbonate (2.0 g, 9.16 mmol) in $CHCl_3$ (50 ml, passed through Al_2O_3) was slowly added (in 3 hrs) into a solution of 1,4,7,10-tetraazacyclododecane (0.56 g, 3.24 mmol) and triethylamine (1.01 g, 9.98 mmol) in $CHCl_3$ (60 ml) at room temperature. Then, the reaction mixture was stirred for 24 h at room temperature (Kimura et. al., 1997). The organic solvent was evaporated under reduced pressure. The product (2.4) was purified by silica gel column chromatography (ethyl acetate/hexane/methanol). Yield:for **(2.4)** 1.03 g (67 %).

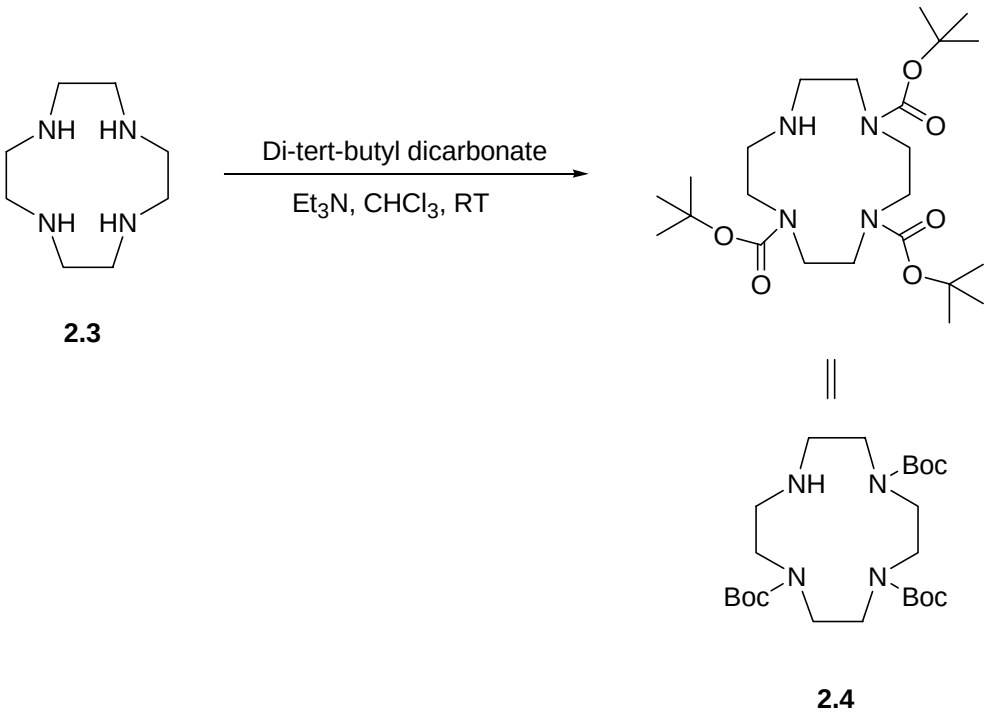

2.3

2.4

Figure 2.2. Synthesis of 1,4,7 tris(tert-butyloxycarbonyl)-1,4,7,10-tetraazacyclo-dodecane (2.4).

2.4. Synthesis of and isolation of the dicyclen derivative (2.5) and the mono-substitution product (2.6)

2,7-Di-*tert*-butyl-4,5-bis-chloromethyl-9,9-dimethyl-9H-xanthene **(2.2)** (1.2 mmol, 500 mg) and tris(boc)-cyclen (4.8 mmol, 2.26 g) in toluene (6 ml) were refluxed for 2 days. The reaction mixture was then concentrated under reduced pressure. The products were separated and purified by column chromatography (silica gel, $CHCl_3$ / MeOH 100:7, eluent).
Yield for **(2.5)** 725 mg (47 %) and for **(2.6)** 450 mg (42 %).

2.5: ^{1}H NMR (400 MHz, $CDCl_3$) δ(ppm) 1.35 (18 H, s, $C(CH_3)_3$), 1.51 (54 H, s, $C(CH_3)_3$), 1.62 (6H, s, CH_3), 2.66-2.85 (8H, m, N-CH_2), 3.20-3.65 (24H, m, N-CH_2), 4.0 (4H, s, Ar-CH_2-), 7.24 (2H, s, Ar-H), 7.37 (2H, s, Ar-H).
^{13} C NMR (100 MHz, $CDCl_3$) δ(ppm) 28.8, 31.9, 34.8, 35.4, 48.9, 50.0, 52.7, 55.9, 57.5, 79.8, 121.7, 123.7, 130.9, 145.4, 147.9, 156.0, 156.5.

2.6: ^{1}H NMR (400 MHz, $CDCl_3$) δ(ppm) 1.19 (9H, s, $C(CH_3)_3$), 1.24 (9H, s, $C(CH_3)_3$), 1.33 (27H, s, $C(CH_3)_3$), 1.51 (6H, s, CH_3), 2.60-2.80 (4H, m, N-CH_2), 3.12-3.49 (12H, m, N-CH_2), 3.95 (2H, s, N-CH_2), 4.65 (2H, s, Ar-CH_2-), 7.06 (1H, s, Ar-H), 7.11 (1H, s, Ar-H), 7.20 (2H, s, Ar-H), 7.26 (1H, s, Ar-H).
^{13} C NMR (100 MHz, $CDCl_3$) δ(ppm) 28.9, 31.9, 34.7, 34.9, 35.3, 42.6, 48.8, 50.2, 54.9, 56.9, 79.8, 121.8, 123.5, 124.0, 126.0, 127.6, 130.6, 131.0, 145.6, 146.0, 147.3, 147.7, 155.9, 156.6.

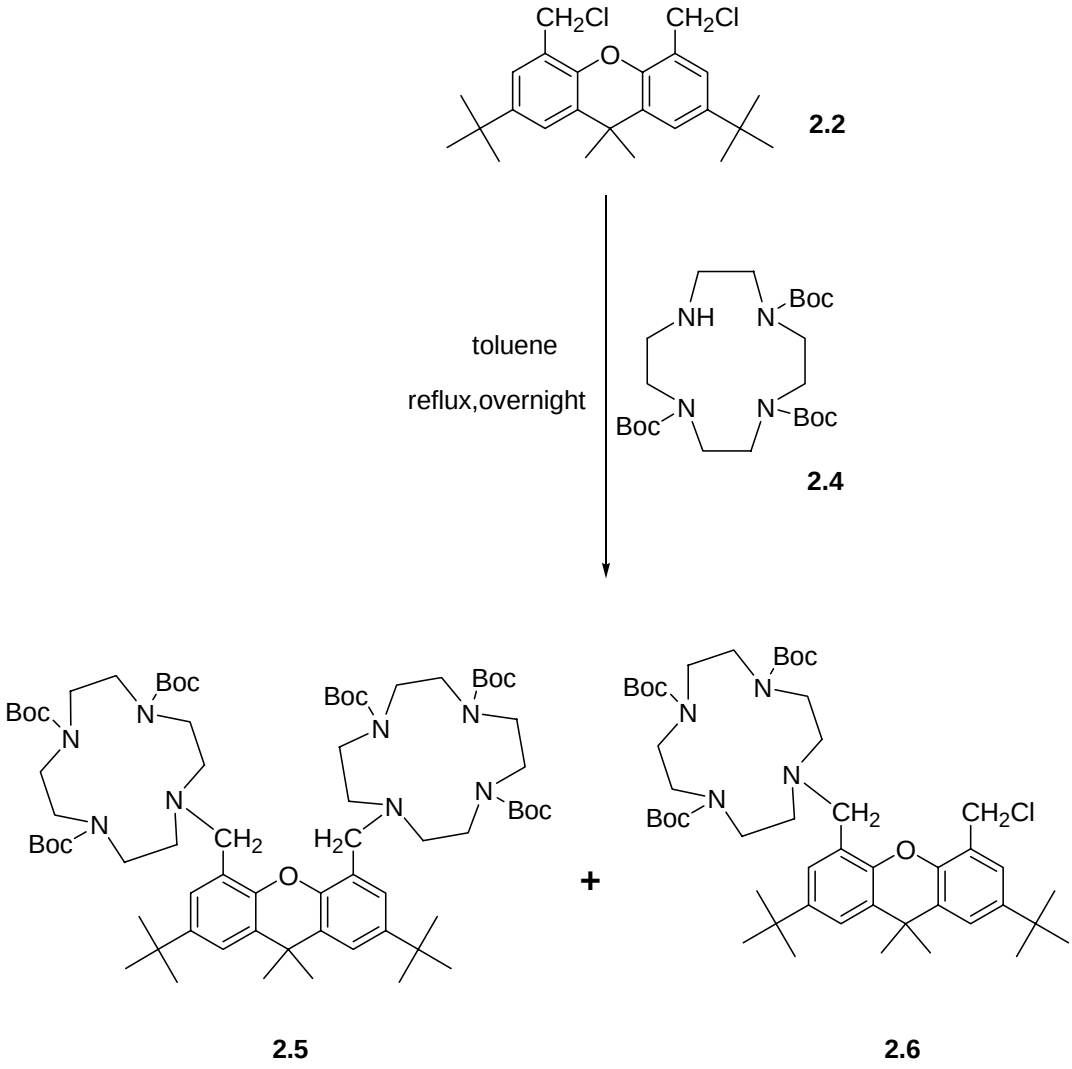

Figure 2.3. Synthesis of and isolation of the dicyclen derivative (2. 5) and the mono-substitution product (2. 6).

2.5. Deprotection of 2.5

Disubstitution product **(2.5)** (0.19 mmol, 250 mg) was dissolved in TFA-CH_2Cl_2 mixture (4 ml 50:50) and stirred at room temperature for overnight. Then

the reaction mixture neutralized and washed with 10 % NaOH (3x10 ml) and organic phase was dried with $NaSO_4$ and removed under reduced pressure.
Yield: for **(2.7)** 90 mg (68 %).

^{1}H NMR (400 MHz, $CDCl_3$) δ(ppm) 1.08 (18 H, s, $C(CH_3)_3$), 1.34 (6H, s, CH_3), 2.25-2.35 (8H, m, CH_2), 2.36-2.62 (24H, m, CH_2), 3.57 (4H, s, CH_2), 7.02 (2H, s, Ar-H), 7.18 (2H, s, Ar-H).
^{13} C NMR (100 MHz, $CDCl_3$) δ(ppm) 32.0, 34.9, 35.2, 46.0, 47.1, 47.8, 52.1, 52.8, 125.6, 125.8, 130.1, 145.2, 147.4.

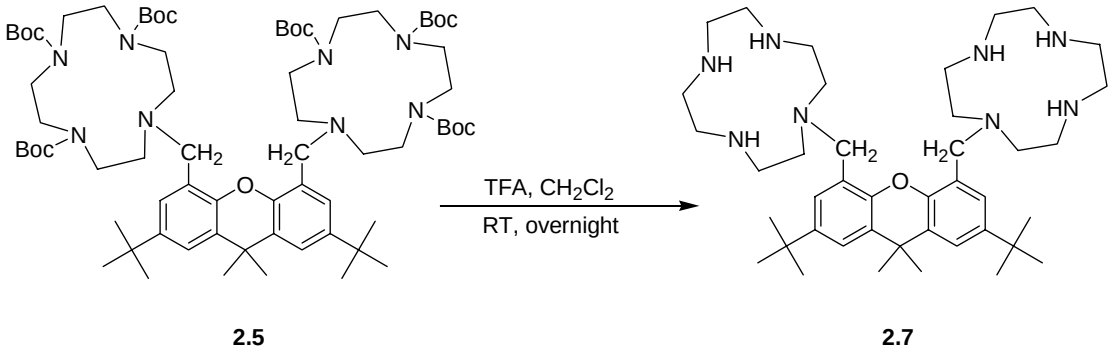

2.5 **2.7**

Figure 2.4. Deprotection of (2.5).

2.6. The reaction of compound (2.6) with imidazole to yield compound (2.8)

Mono-cyclen substituted xanthene derivative **(2. 6)** (0.23 mmol, 200 mg) and imidazole (0.23 mmol, 16 mg) were refluxed in 2 ml toluene for 2 days. The reaction mixture was then concentrated under reduced pressure. The product **(2. 8)** was purified by column chromatography (silica gel, $CHCl_3$ / MeOH 100:7, eluent). Yield: for **(2.8)** 143 mg (69.5 %).

^{1}H NMR (400 MHz, $CDCl_3$) δ(ppm) 1.29 (9H, s, $C(CH_3)_3$), 1.32 (9H, s, $C(CH_3)_3$), 1.48 (27H, s, $C(CH_3)_3$), 1.68 (6H, s, CH_3), 2.06 (2H, s, CH_2), 2.60-3.65 (16H, m, CH_2), 3.80 (2H, s, CH_2), 5.34 (2H, s, CH_2), 6.80 (1H, s, Ar-H), 6.95 (1H, s, Ar-H), 7.10 (1H, s, Ar-H), 7.15 (1H, s, Ar-H), 7.33 (1H, s, Ar-H), 7.40 (1H, s, Ar-H), 7.55 (1H, s, Ar-H).

^{13} C NMR (100 MHz, $CDCl_3$) δ(ppm) 14.5, 21.4, 23.1, 28.9, 29.7, 31.8, 31.9, 34.9, 35.2, 46.9, 60.8, 79.9, 119.8, 122.0, 123.2, 129.7, 130.7, 137.6, 146.4.

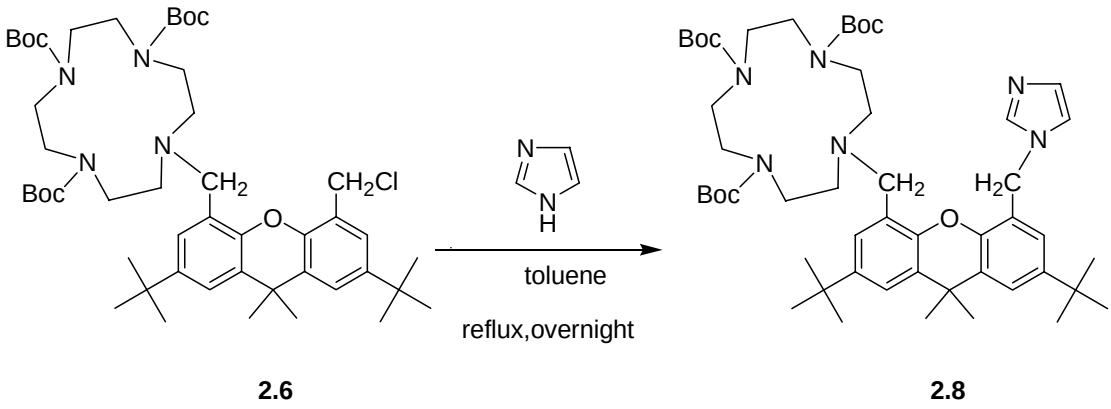

2.6 **2.8**

Figure 2.5. Synthesis of 10-(2,7-Di-*tert*-butyl-5-imidazol-1-ylmethyl-9,9-dimethyl-9*H*-xanthen-4-ylmethyl)-1,4,7,10tetraaza-cyclododecane-1,4,7-tricarboxylic acid tri-*tert*-butyl ester (2.8).

2.7. Deprotection of 2.8

Compound **(2. 8)** was deprotected (0.24 mmol, 215 mg) in TFA-CH_2Cl_2 mixture (6 ml, 50:50). The solution was stirred at room temperature for overnight. Then the reaction mixture neutralized and washed with 10 % NaOH (3x10 ml)

and the organic phase was dried with $NaSO_4$. The solvent was removed under reduced pressure. Yield: for **(2.9)** 49 mg (35 %).

^{1}H NMR (400 MHz, $CDCl_3$) δ(ppm) 1.40 (9H, s, $C(CH_3)_3$), 1.46 (9H, s, $C(CH_3)_3$), 1.75 (6H, s, CH_3), 2.63-2.97 (16H, m, CH_2), 3.81 (2H, s, CH_2), 5.44 (2H, s, CH_2), 6.93 (1H, s, Ar-H), 7.04 (1H, s, Ar-H), 7.17 (1H, s, Ar-H), 7.40 (1H, s, Ar-H), 7.49 (1H, s, Ar-H), 7.54 (1H, s, Ar-H), 7.68 (1H, s, Ar-H).
^{13} C NMR (100 MHz, $CDCl_3$) δ(ppm) 30.1, 31.8, 32.5, 45.7, 46.8, 47.6, 52.2, 52.5, 119.7, 121.8, 122.7, 123.3, 124.3, 126.0, 129.4, 129.9, 130.6, 137.8, 146.0, 146.4, 146.5.

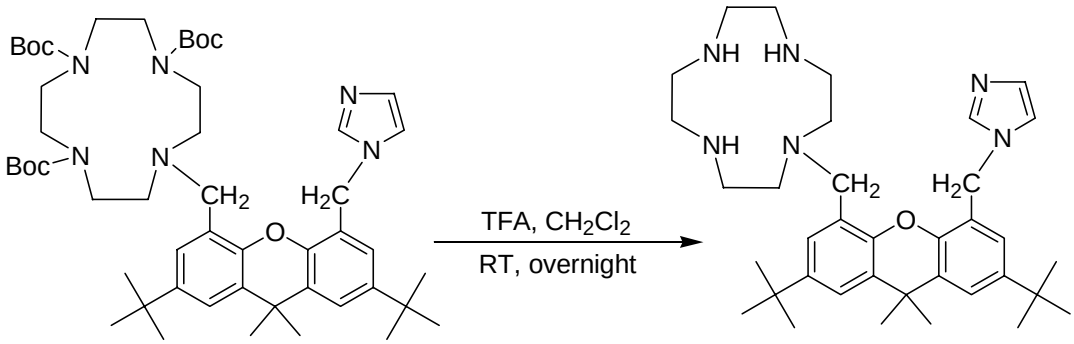

2.8 **2.9**

Figure 2.6. Synthesis of 1-(2,7-Di-*tert*-butyl-5-imidazol-1-ylmethyl-9,9-dimethyl-9*H*-xanthen-4-ylmethyl)-1,4,7,10tetraaza-cyclododecane (2.9).

2.8. The reduction of 2,7-di-*tert*-butyl-9,9-dimethyl-4,5-xanthenedicarboxylic acid (2.10)

$LiAlH_4$ (1.22 mmol, 500 mg) in 15 ml dry THF was cooled to 0 ^oC in an ice bath (Brown et. al., 1966) and then 2,7-di-*tert*-butyl-9,9-dimethyl-4,5-xanthenedicarboxylic acid (**2. 10**, 1.5 mmol, 600 mg) in 10 ml of THF solution was added in portions. The solution was stirred at RT for four days. The carboxylic acid proved to be highly resistant to complete reduction and even an aldehyde product was isolated from the reaction mixture. After 4 days the reaction mixture was first treated with H_2O until no bubbling observed and then extracted with ether. The solvent was removed under reduced pressure, and then purified by column chromatography (silica gel, $CHCl_3$ / MeOH 100:3, eluent).
The yield of the desired product **(2. 11)** was 165 mg (35.2 %).

^1H NMR (400 MHz, $CDCl_3$) δ(ppm) 1.26 (18H, s, $C(CH_3)_3$), 1.57 (6H, s, CH_3), 3.38 (2H, brs, OH), 4.64 (4H, s, CH_2), 7.07 (2H, s, Ar-H), 7.28 (2H, s, Ar-H).
^{13}C NMR ($CDCl_3$) δ(ppm) 30.1, 32.0, 32.5, 34.9, 62.5, 122.6, 125.3, 127.5, 129.9, 145.5, 147.3.

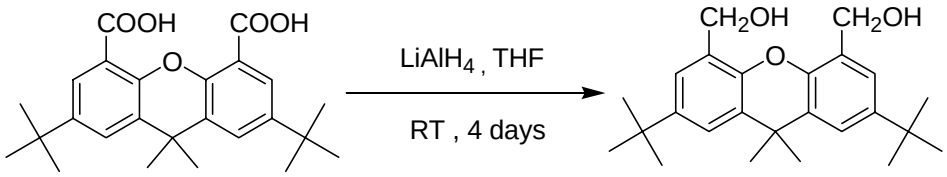

2.10 **2.11**

Figure 2.7. Synthesis of 2,7-Di-*tert*-butyl-5-hydroxymethyl-9,9-dimethyl-9*H*-xanthen-4-yl)-methanol (2. 11).

2.9. Synthesis of the monochlorinated compound (2.12)

(2,7-Di-*tert*-butyl-5-hydroxymethyl-9,9-dimethyl-9*H*-xanthen-4-yl) methanol (**2.11**, 0.13mmol, 50 mg) and $SOCl_2$ (8 ml) put into a flask and refluxed for 1 hour. Then the solvent was removed under reduced pressure, and the compound **(2.12)** was isolated in good yield from the reaction mixture. Yield for **(2.12)** 34 mg (65 %).

^{1}H NMR (400 MHz, $CDCl_3$) δ(ppm) 1.18 (9H, s, $C(CH_3)_3$), 1.27 (9H, s, $C(CH_3)_3$), 1.57 (6H, s, CH_3), 3.40 (1H, br s, OH), 4.77 (4H, d, CH_2), 7.18 (2H, s, Ar-H), 7.30 (2H, s, Ar-H).

^{13} C NMR ($CDCl_3$) δ(ppm) 23.1, 29.8, 32.3, 32.8, 34.9, 42.5, 124.6, 125.9, 127.0, 128.2, 128.6, 130.0, 132.6, 146.1, 146.4, 146.7.

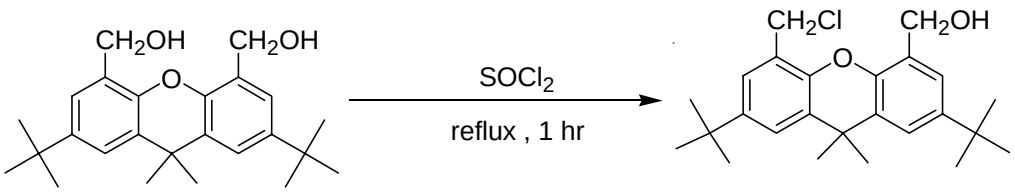

2.11 **2.12**

Figure 2.8. Synthesis of (2,7-Di-*tert*-butyl-5-chloromethyl-9,9-dimethyl-9*H*-xanthen-4-yl)-methanol; compound with methane (2.12).

2.10. Synthesis of compound (2.13)

The product was synthesized by the procedure published by Koçak et. al. (1994). Tris(boc)-cyclen (0.46 mmol, 220 mg) was dissolved in DMF (4 ml) and

then K_2CO_3 (200 mg) was added. The mixture was stirred at room temperature for 1 hour. Then the monochloromethyl derivative (**2.12**, 0.3 mmol, 120 mg) in DMF (5 ml) was added dropwise to the tris(boc)cyclen solution. The reaction mixture was heated at 80 ^{0} C for 2 days. Then H_2O (15 ml) was added to the solution and the resulting white solid was collected by filtration. The product was purified by column chromatography {silica gel, EtOAc: Hexane (1:5), eluent). Yield for **(2.13)** 115 mg (45.7 %).

^{1}H NMR (400 MHz, $CDCl_3$) δ(ppm) 1.24 (9H, s, $C(CH_3)_3$), 1.27 (9H, s, $C(CH_3)_3$), 1.40 (27H, s, $C(CH_3)_3$), 1.54 (6H, s, CH_3), 2.65-2.80 (4H, m, CH_2), 3.18-3.60 (12H, m, CH_2), 3.99 (2H, s, CH_2), 4.69 (2H, s, CH_2), 7.07 (1H, s, Ar-H), 7.15 (1H, s, Ar-H), 7.24 (1H, s, Ar-H), 7.30 (1H, s, Ar-H).

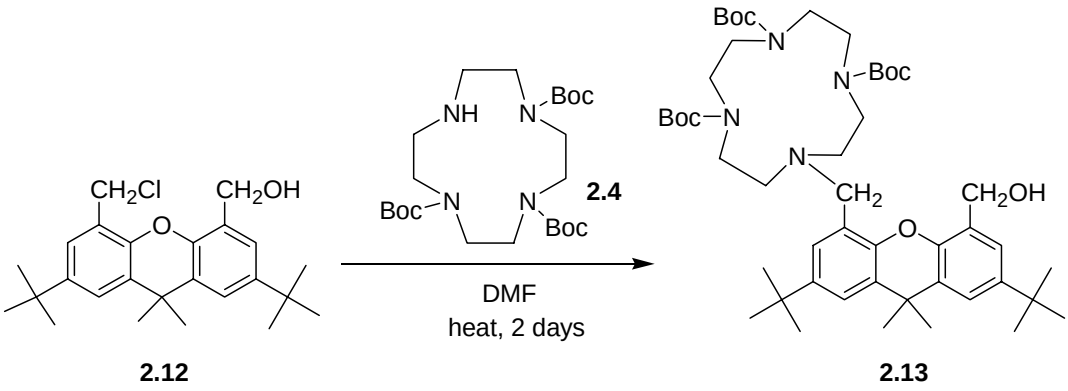

Figure 2.9. Synthesis of 10-(2,7-Di-*tert*-butyl-5-hydroxymethyl-9,9-dimethyl-9*H*-xanthen-4-ylm ethyl)-1,4,7,10-tetraaza-cyclododecane-1,4,7-tricarboxylic acid tri-*tert*-butyl ester (2.13).

2.11. Deprotection of compound (2.13)

The protected compound (**2.13**) (0.14 mmol, 120 mg) was dissolved in TFA**:**CH_2Cl_2 (2 ml**:**2 ml). The reaction mixture was stirred at room temperature for overnight. The reaction mixture was then washed with 10 % NaOH (3x10 ml) and the organic phase was dried with $NaSO_4$. The solvent was removed under reduced pressure. Yield for **(2.14)** 25 mg (33.2 %).

^{1}H NMR (400 MHz, $CDCl_3$) δ (ppm) 1.26 (18 H, s, $C(CH_3)_3$), 1.51 (6H, s, CH_3), 2.35-2.67 (16H, m, CH_2), 3.73 (2H, s, CH_2), 4.64 (2H, s, CH_2), 7.03 (2H, s, Ar-H), 7.23 (1H, s, Ar-H), 7.27 (1H, s, Ar-H).

^{13} C NMR ($CDCl_3$) δ(ppm) 30.0, 32.0, 34.8, 34.8, 35.7, 45.5, 46.2, 47.3, 52.3, 56.0, 57.0, 121.1, 121.3, 126.0, 126.6, 127.2, 129.3, 131.8, 132.2, 145.2, 146.0.

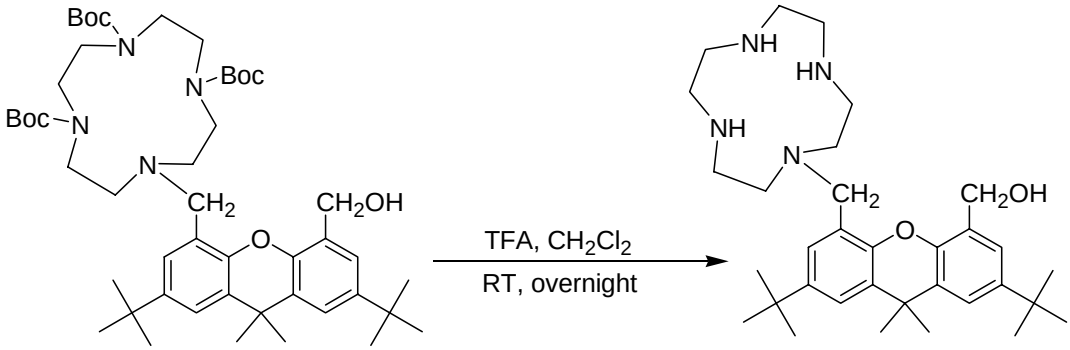

2.13 **2.14**

Figure 2.10. Synthesis of [2,7-Di-*tert*-butyl-9,9-dimethyl-5-(1,4,7,10-tetraaza-cyclododec-1-ylm ethyl)-9*H*-xanthen-4-yl] methanol (2.14).

2.12. Kinetics

Kinetic reactions were carried out by following the appearance of p-nitrophenolate from the enzyme-catalyzed hydrolysis of the model substrate; p-nitrophenylacetate (PNPA) **(2.15).**

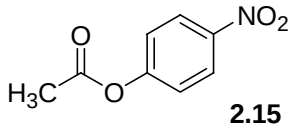

2.15

Figure 2.11. Structure of p-nitrophenylacetate.

Hydrolysis of PNPA in the presence of enzyme models shown in Figure 2.12. were studied in four different pH. For pH 7.0 and 7.5 MOPS and for pH 8.0 and 8.5 TRIS was used as buffering material. The blank solution contained appropriate buffer solutions that were used in the sample compartment. The reactions were followed for more than 8 half-lives.

The ligand **2.7** (200 µl, 40 mM in CH_3CN) and $Zn(ClO_4)_2$ (400 µl, 40 mM in H_2O) were added to a cuvet containing 0.336 ml 0.15 M buffer at room temperature. After a couple of minutes of equilibration, PNPA **(2.15)** (40 µl 5 mM in CH_3CN) was added, and the increase in UV absorption at 400 nm was recorded. Final concentrations were 2 mM in di-cyclenyl-ligand, 4 mM Zn^{2+}, 50 µM in PNPA and 0.126 M in buffer.

For the ligands **2.9** and **2.14** (200 µl, 40 mM in CH_3CN) and $Zn(ClO_4)_2$ (200 µl, 40 mM in H_2O) were added to a cuvet containing 0.356 ml 0.15 M buffer at room temperature. After a couple of minutes of equilibration, PNPA **(2.15)** (40

μl 5 mM in CH3CN) was added, and the increase in UV absorption at 400 nm was recorded. Final concentrations were 2 mM in monocyclenyl and monocyclenyl+imidazole ligands, 2 mM Zn^{2+}, 50 μM in PNPA and 0.133 M in buffer.

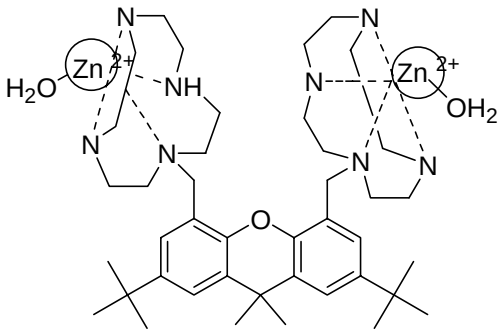

2.16

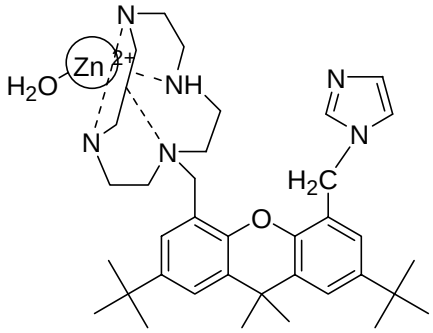

2.17

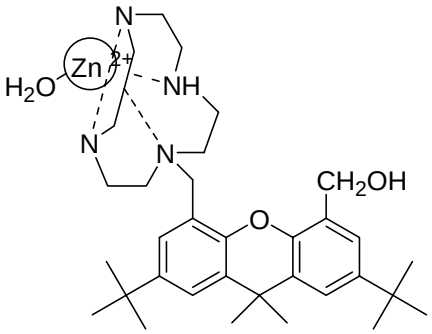

2.18

Figure 2.12. Illustrations of dinucleating **(2.16)** and mononucleating (**2.17** and **2.18**) complexes.

Calculations were carried out using s plot of $\ln(A_\infty\text{-}A/A_\infty)$ versus time from the absorbance versus time data transferred to Excel. The slope and intercept

were obtained by linear regression and pseudo-first order rate constants were obtained.

In a first order reaction, the rate is given by the following equation:

$$-R = - d[A] / dt = k[A]$$

Rearranging the equation, we get;

$$d[A] / [A] = -kdt$$

On integration, and further manipulation,

$$[A_t] = [A_0] e^{-kt}$$

In our experimental system, the product concentration is followed, therefore;

$$[P_t] = [A_0] – [A_t]$$

$[A_0] = [P_\infty]$ so making the appropriate substitutions;

since, $[P_t] = [A_0] – [A_t]$

$[P_t] = [P_\infty] – [A_t]$ $\longrightarrow$ $[A_t] = [P_\infty] – [P_t]$

$$[P_\infty] – [P_t] = [P_\infty] e^{-kt}$$

since $At = [P_t] \ell \varepsilon$

$$A_\infty - A_t / A_\infty = e^{-kt}$$

Taking the natural logarithm of both sides,

$\ln A_\infty - A_t / A_\infty = -kt$

pseudo-first order rate constant is obtained from the plot of ($\ln A_\infty - A_t / A_\infty$) versus time graphs.

CHAPTER III

RESULTS AND DISCUSSION

We present the synthesis, and characterization of di-cyclen derivative (DC) **(2.7)**, mono-cyclen-imidazole derivative (MC-Im) **(2.9)**, mono-cyclen derivative (MC) **(2.14)** ligands; and the formation of corresponding Zn(II) complexes ($DC[Zn^{2+}]_2$) **(2.16)**, ($MC\text{-}Im[Zn^{2+}]$) **(2.17)**, and ($MC[Zn^{2+}]$) **(2.18),** respectively, (Figure 2.12) and finally the kinetic studies of the catalytic activities in the hydrolysis of model substrate *p*-nitrophenylacetate (PNPA) **(2.15)** (Figure 2.11).

The characterization of supramolecular systems depend upon a complete analysis of the structural attributes. In this regard, NMR data are very important to serve a direct information of the chemical structure of our models. ^{1}H and ^{13}C NMR were performed at 400 MHz and the obtained results confirmed the structures we synthesized throughout the project. ^{1}H and ^{13}C NMR spectra of compounds **2.2 – 2.14** are in the appendix A1-A19.

The rate of PNPA hydrolysis in the presence and absence of enzyme models were studied at four different pH solutions: 7.0, 7.5, 8.0, 8.5. The absorbance versus time plots and $\ln[(A_\infty\text{-}A)/A_\infty]$ versus time plots reletad to these experiments have been shown in Figures 3.1. to 3.24.

The initial rate constants for both the catalyzed (k_{cat}) and uncatalyzed (k_{uncat}) reactions were calculated from the increase in absorbance at λ=400 nm due to the release of p-nitrophenolate.

3.1. Hydrolysis of PNPA by di-cyclen derivative-$[Zn^{2+}]_2$ (DC$[Zn^{2+}]_2$) (2.16)

We present kinetic studies of the catalytic hydrolysis of *p*-nitro phenylacetate as a substrate model by di-cyclen derivative-$[Zn^{2+}]_2$ (DC$[Zn^{2+}]_2$) (2.16).

The enzyme model 2.16 at $2x10^{-3}$ M concentration accelerates the hydrolysis of the substrate PNPA, generating 2 equivalents of p-nitrophenolate ion which has an intense absorbance at 400 nm.

At pH 7.0 rate acceleration of 428.5, at pH 7.5 rate acceleration of 7.0, at pH 8.0 rate acceleration of 7.4, and at pH 8.5 rate acceleration of 7.5 were obtained over the uncatalyzed reaction, (Table 3.1).

The hydrolysis reaction gets faster by the enzyme model 2.16 with increased pH, which indicates that the hydroxide promoted hydrolysis becomes more dominant over the reaction.

The absorbance versus time plots and $\ln[(A_\infty-A)/A_\infty]$ versus time plots releted to these experiments have been presented in Figures from 3.1. through 3.8. According to these data, the enzyme model (2.16) shows the highest rate acceleration in comparison with the uncatalyzed reaction at pH 7.0. However; k_{cat} ($9x10^{-4}$ s^{-1}) value for this pH gives the lowest one.

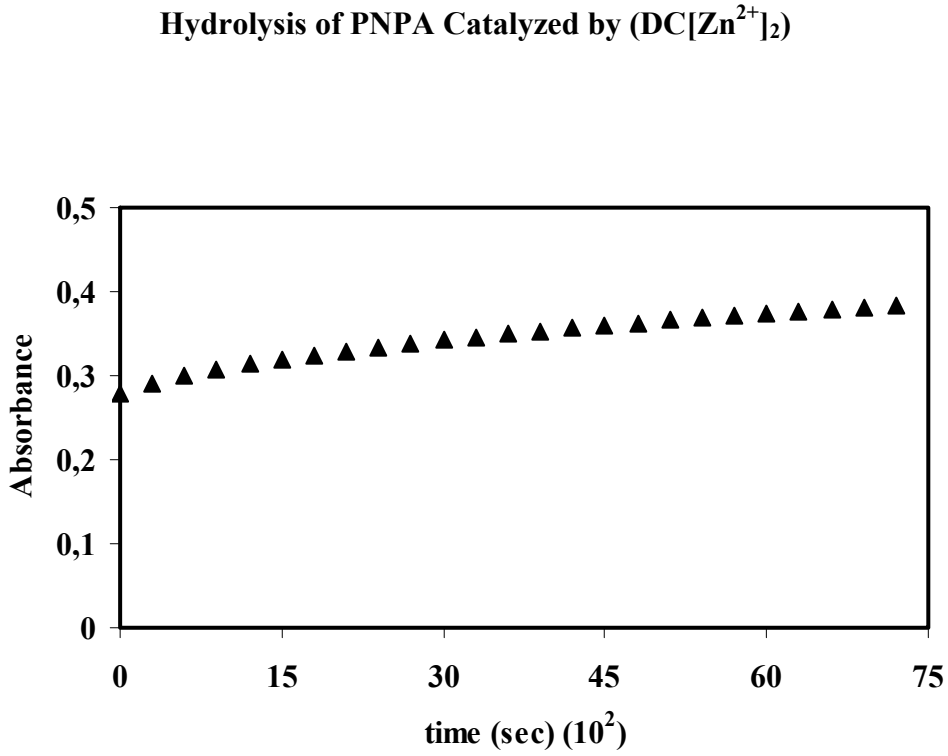

Figure 3.1. Absorbance of p-nitrophenolate ion at 400 nm as a function of time, in the hydrolysis of PNPA catalyzed by $2x10^{-3}$ M of the compound 2.7 and $4x10^{-3}$ M Zn^{2+} ions in $12.6x10^{-2}$ M MOPS buffer at pH 7.0 and 25°C.

Figure 3.1 shows the increase in the absorbance of p-nitrophenolate at 400 nm as a function of time for the hydrolysis of PNPA catalyzed by our enzyme model. When we compare the rate accelerations between the presence and absence of our enzyme model, it is seen that presence of enzyme increased the rate by 428.5-fold.

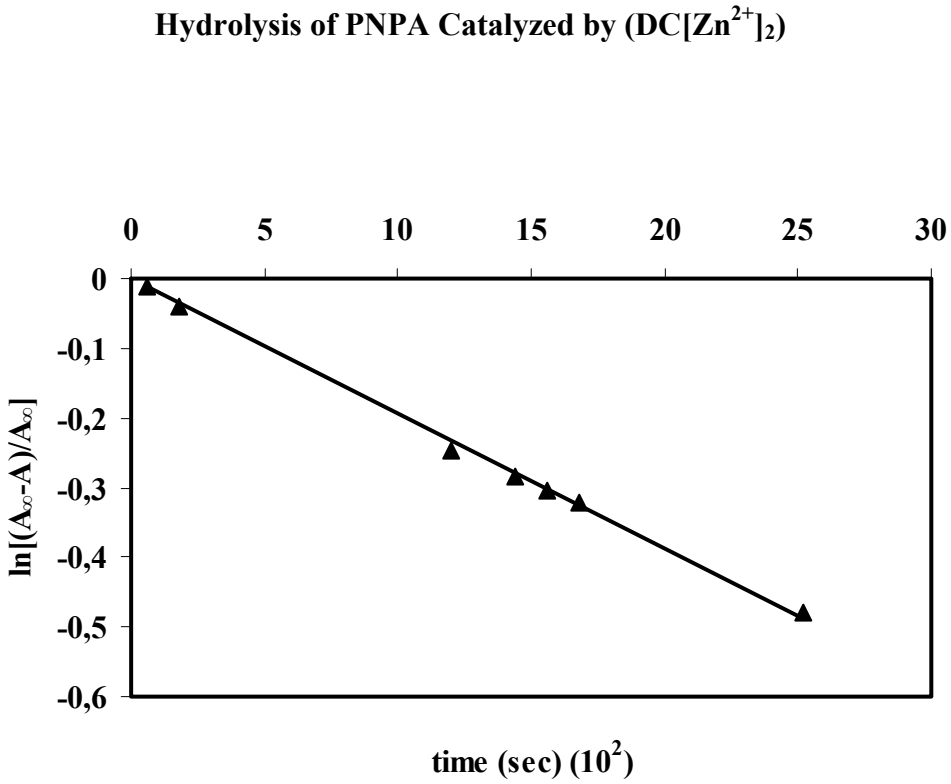

Figure 3.2. The plot of $\ln[(A_\infty-A)/A_\infty]$ as a function of time for 2×10^{-3} M compound 2.7 and 4×10^{-3} M Zn^{2+} ions in 12.6×10^{-2} M MOPS buffer at pH 7.0 at 25°C, yielding a pseudo-first order rate constant ($k_{cat}=0.9\times10^{-3}$ s^{-1}) and $R^2=0.995$.

$\ln[(A_\infty-A)/A_\infty]$ was plotted as a function of time and pseudo-first order rate constant of $k_{cat}=0.9\times10^{-3}$ s^{-1} was obtained.

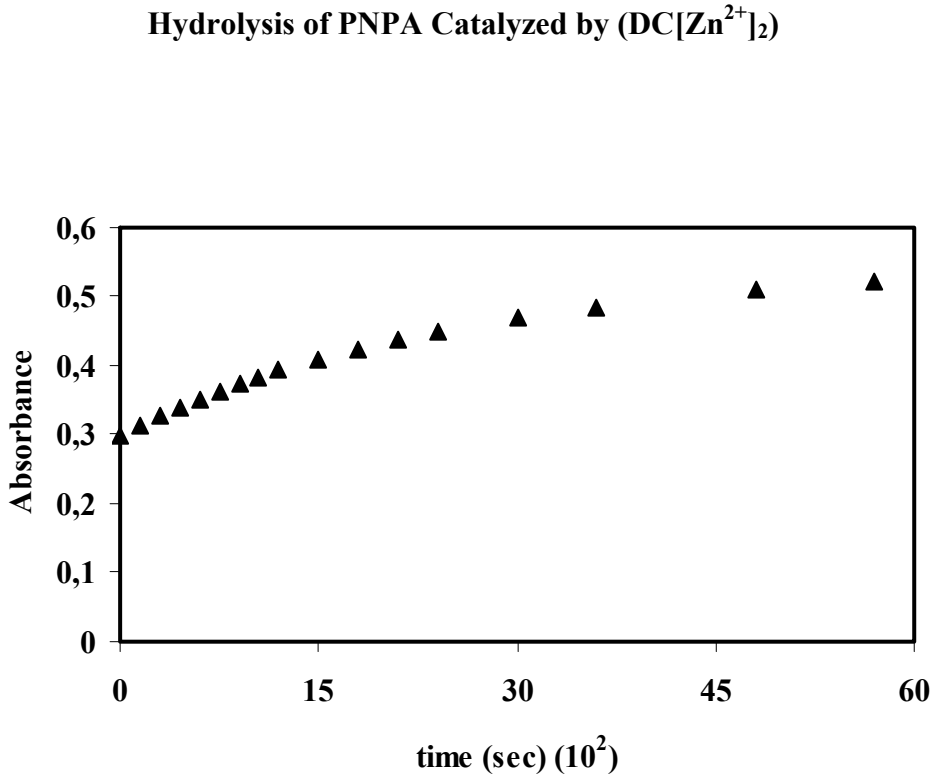

Figure 3.3. Absorbance of p-nitrophenolate ion at 400 nm as a function of time, in the hydrolysis of PNPA catalyzed by $2x10^{-3}$ M of the compound 2.7 and $4x10^{-3}$ M Zn^{2+} ions in $12.6x10^{-2}$ M MOPS buffer at pH 7.5 and 25°C.

Figure 3.3. shows the increased yield of PNPA hydrolysis at pH 7.5. Hydrolysis reaction was completed in about 1.5 h.

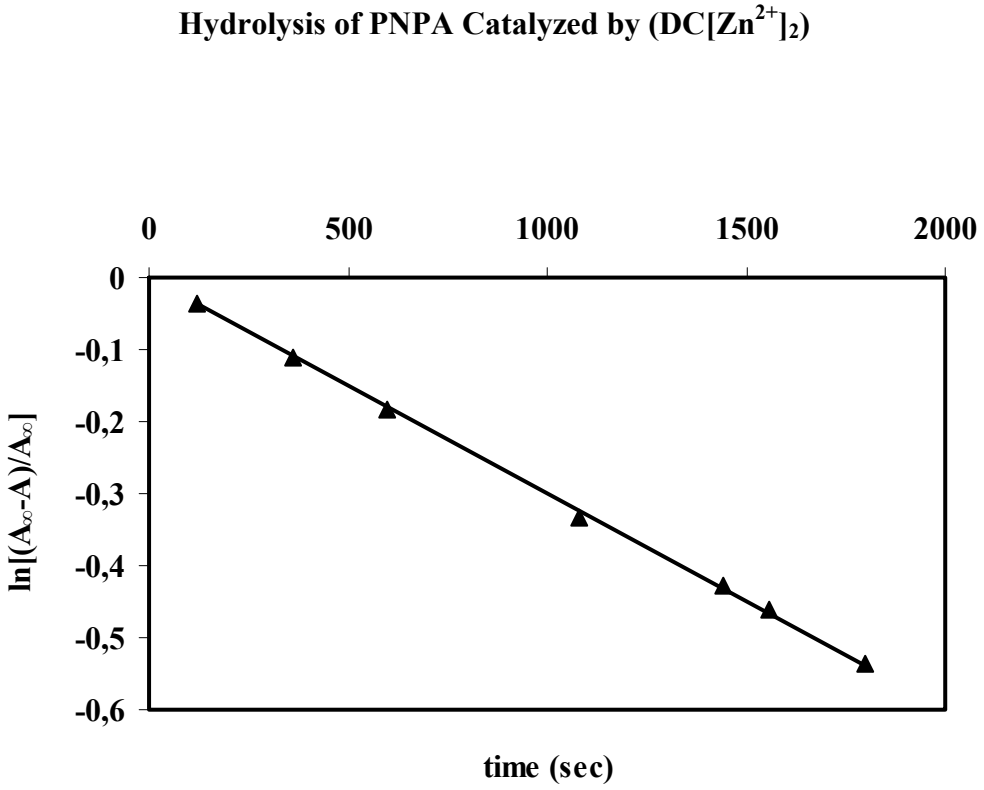

Figure 3.4. The plot of $\ln[(A_\infty-A)/A_\infty]$ as a function of time for $2x10^{-3}$ M compound 2.7 and $4x10^{-3}$ M Zn^{2+} ions in $12.6x10^{-2}$ M MOPS buffer at pH 7.5 and 25°C, yielding a pseudo-first order rate constant ($k_{cat}=1.6x10^{-3}$ s^{-1}) and $R^2=0.9964$.

By plotting $\ln[(A_\infty-A)/A_\infty]$ as a function of time in the presence of pH 7.5 MOPS buffer, a pseudo-first order rate constant of 1.6x10-3 s^{-1} is obtained. Rate enhancement in the hydrolysis of PNPA is 7.

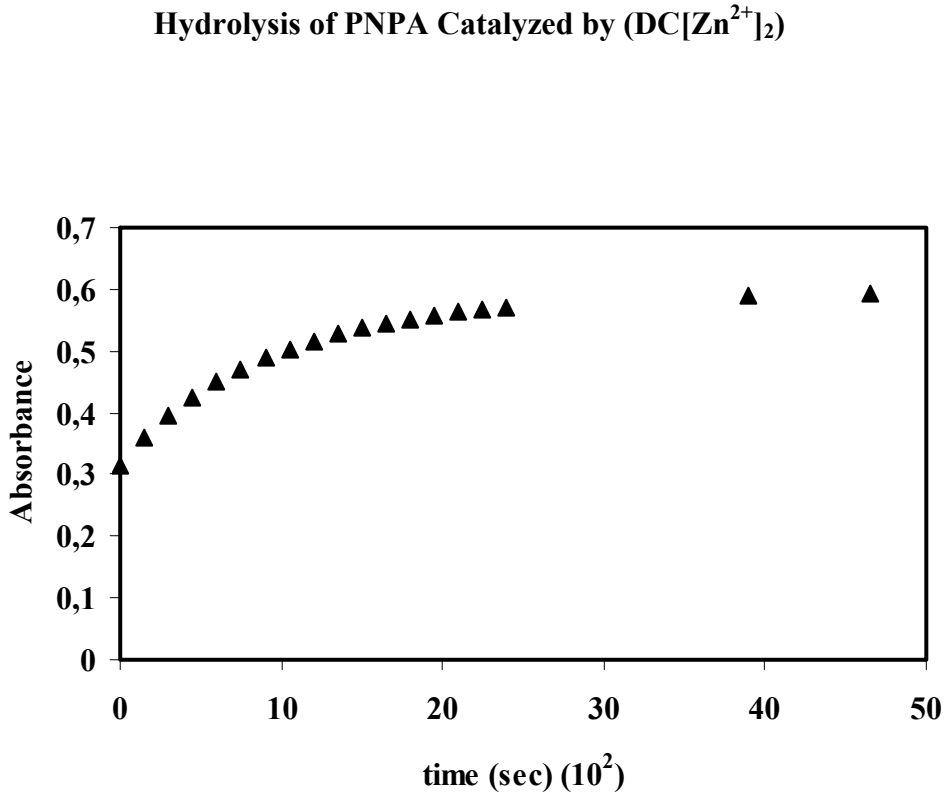

Figure 3.5. Absorbance of p-nitrophenolate ion at 400 nm as a function of time, in the hydrolysis of PNPA catalyzed by $2x10^{-3}$ M of the compound 2.7 and $4x10^{-3}$ M Zn^{2+} ions in $12.6x10^{-2}$ M TRIS buffer at pH 8.0 and 25°C.

Figure 3.5. shows the increase in the absorbance of p-nitrophenolate as a function of time at 400 nm for the cleavage of PNPA at pH 8.0. The hydrolysis is faster than that of at PH 7.0, completed to about 20 minutes.

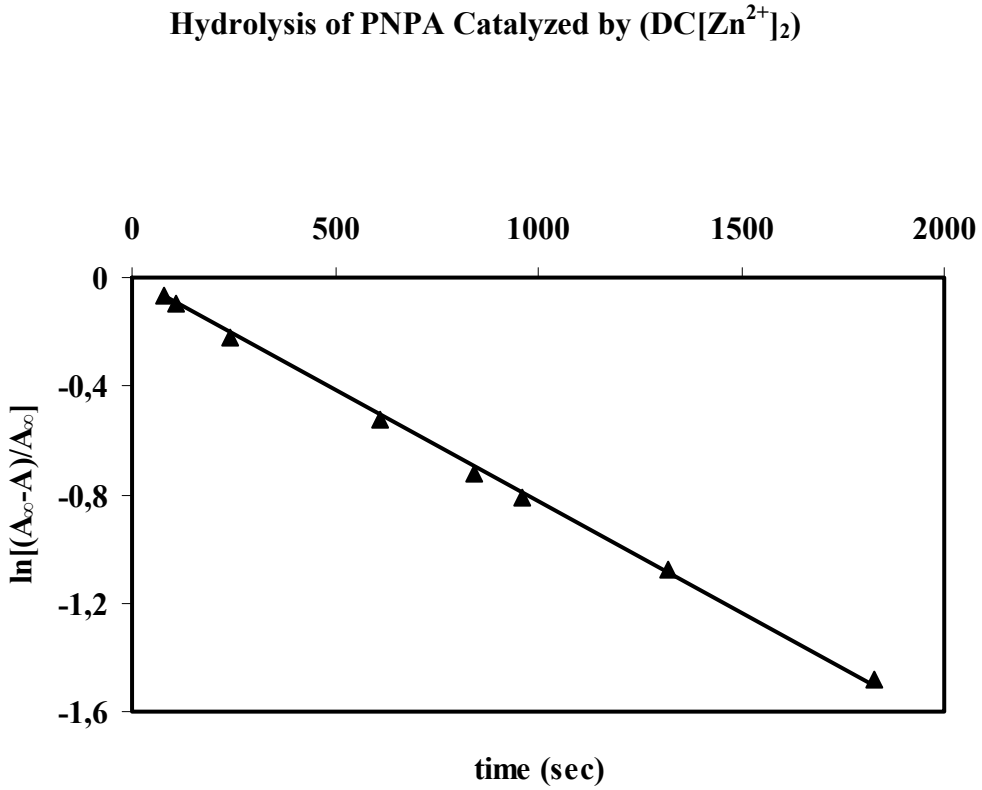

Figure 3.6. The plot of $\ln[(A_\infty-A)/A_\infty]$ as a function of time for $2x10^{-3}$ M compound 2.7 and $4x10^{-3}$ M Zn^{2+} ions in $12.6x10^{-2}$ M TRIS buffer at pH 8.0 and 25°C, yielding a pseudo-first order rate constant ($k_{cat}=4.5x10^{-3}$ s^{-1}) and $R^2=0.9978$.

The $\ln[(A_\infty-A)/A_\infty]$ was plotted as a function of time and pseudo-first order rate constant of $4.5x10^{-3}$ s^{-1} was obtained.

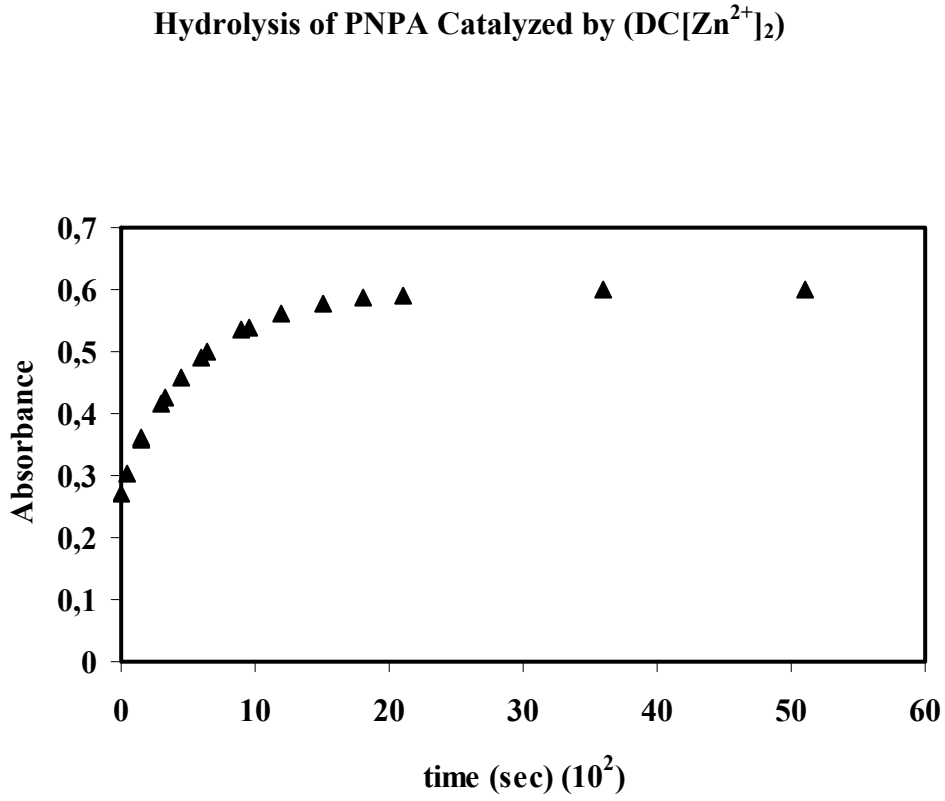

Figure 3.7. Absorbance at 400 nm as a function of time, in the hydrolysis of PNPA catalyzed by $2x10^{-3}$ M of the compound 2.7 and $4x10^{-3}$ M Zn^{2+} ions in $12.6x10^{-2}$ M TRIS buffer at pH 8.5 and 25°C.

The hydrolysis of the model substrate at pH 8.5 was carried out by following the increase in the absorbance at 400 nm., (Figure 3.7). The hydrolysis of PNPA occurs 7.5 times more rapidly compared to that of uncatalyzed reaction at pH 8.5.

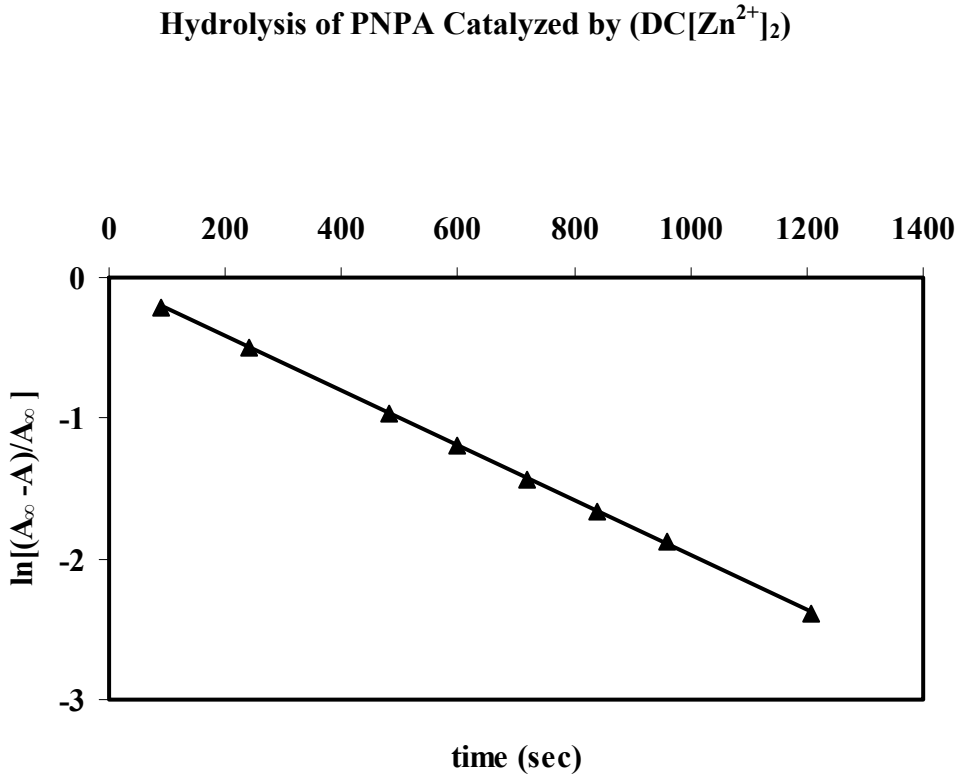

Figure 3.8. The plot of $\ln[(A_\infty-A)/A_\infty]$ as a function of time for $2x10^{-3}$ M compound 2.7 and $4x10^{-3}$ M Zn^{2+} ions in $12.6x10^{-2}$ M TRIS buffer at pH 8.5 and 25°C, yielding a pseudo-first order rate constant ($k_{cat}=12x10^{-3}$ s^{-1}) and $R^2=0.9998$.

The best line yields a pseudo-first order rate constant of $12x10^{-3}$ s^{-1}, which has increased compared to the rate constant at pH 7.0.

3.2. Hydrolysis of PNPA by mono-cyclen-imidazole derivative-[Zn^{2+}] (MC-Im[Zn^{2+}]) (2.17)

The activity of the mono-cyclen-imidazole derivative-[Zn^{2+}] complex was studied. The pseudo-first rate constants for both catalyzed (k_{cat}) and (k_{uncat}) reactions were calculated from the increase in absorbance at 400 nm due to the release of *p*-nitrophenolate.

The kinetic hydrolysis of the *p*-nitrophenolate (PNPA) was studied in the absence and presence of our model 2.17 at pH 7.0, 7.5, 8.0, and 8.5. The absorbance versus time and pseudo-first order kinetics are shown in Figures 3.17-3.24.

Comparison of (MC-Im[Zn^{2+}]) enzyme model with the di- and mono-derivative enzyme models at the same pH's demonstrated that the faster hydrolysis of PNPA by the mono-cyclen-imidazole derivative-[Zn^{2+}] was observed.

Mono-cyclen-imidazole derivative-[Zn^{2+}] complex showed a high catalytic activity at pH 7.0 with a rate acceleration of a factor 5714 over the uncatlyzed reaction. Whereas at pH 7.5 rate acceleration of 11, at pH 8.0 rate acceleration of 7.9, and at pH 8.5 rate acceleration of 4.7 were observed, (Table 3.1).

The great rate enhancement in the hydrolysis of PNPA with 2.17 showed the catalytic role of imidazole unit on the mono-cyclen-imidazole derivative-[Zn^{2+}] enzyme model. This is a very important point for the applications of general acid-general base catalysis.

Depending on the obtained results, enzyme model 2.17 shows the highest rate acceleration with the fast k_{cat} value of $12x10^{-3}$ s^{-1} at pH 7.0.

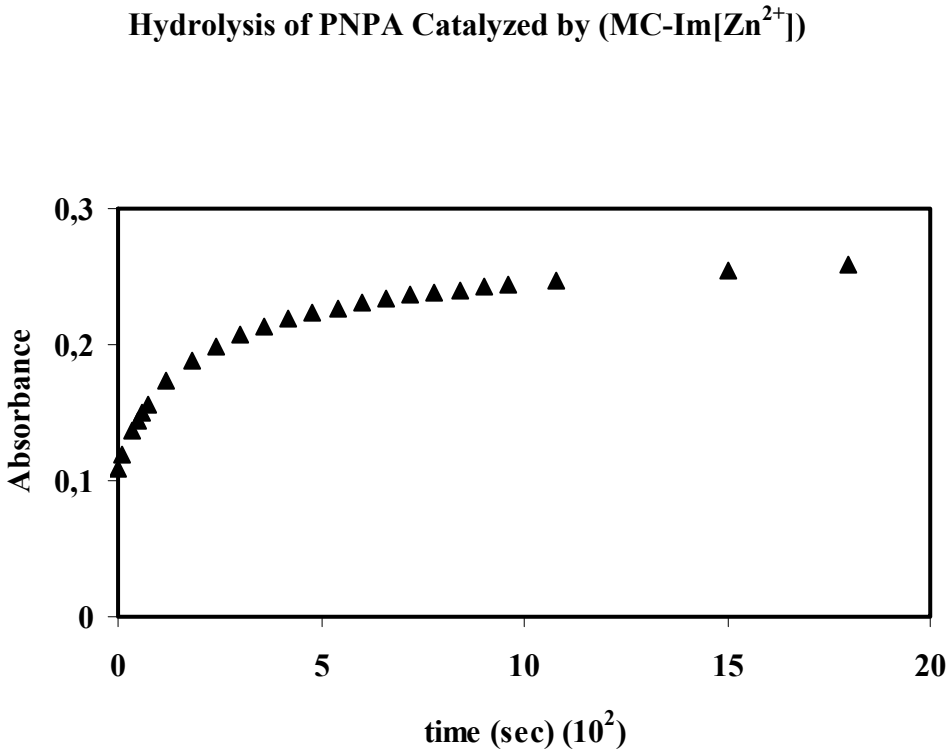

Figure 3.9. Absorbance at 400 nm as a function of time, in the hydrolysis of PNPA catalyzed by $2x10^{-3}$ M of the compound 2.9 and $2x10^{-3}$ M Zn^{2+} ions in $13.3x10^{-2}$ M MOPS buffer at pH 7.0 and 25°C.

Figure 3.9. shows the increased yield of PNPA hydrolysis at pH 7.0. The saturation obseved in less than 5 minutes.

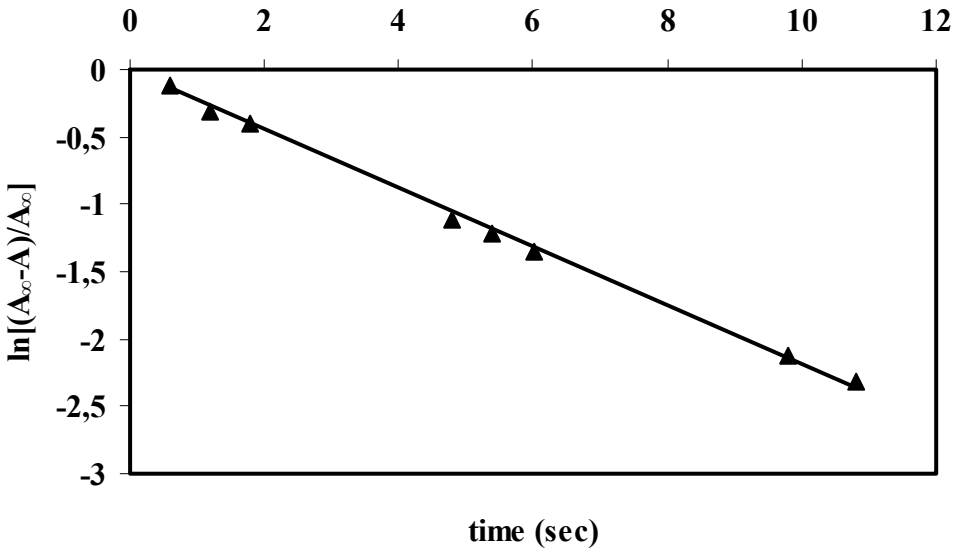

Figure 3.10. The plot of $\ln[(A_\infty-A)/A_\infty]$ as a function of time for $2x10^{-3}$ M compound 2.9 and $2x10^{-3}$ M Zn^{2+} in $13.3x10^{-2}$ M MOPS buffer at pH 7.0 and 25°C, yielding a pseudo-first order rate constant ($k_{cat}=12x10^{-3}$ s^{-1}) and $R^2=0.999$.

The $\ln[(A_\infty-A)/A_\infty]$ was plotted as a function of time and pseudo-first order rate constant of $k_{cat}=12x10^{-3}$ s^{-1} was obtained.

At pH 7.0 the enzyme model (2.17) shows the maximum rate acceleration with 5714-fold compared to the uncatalyzed reaction.

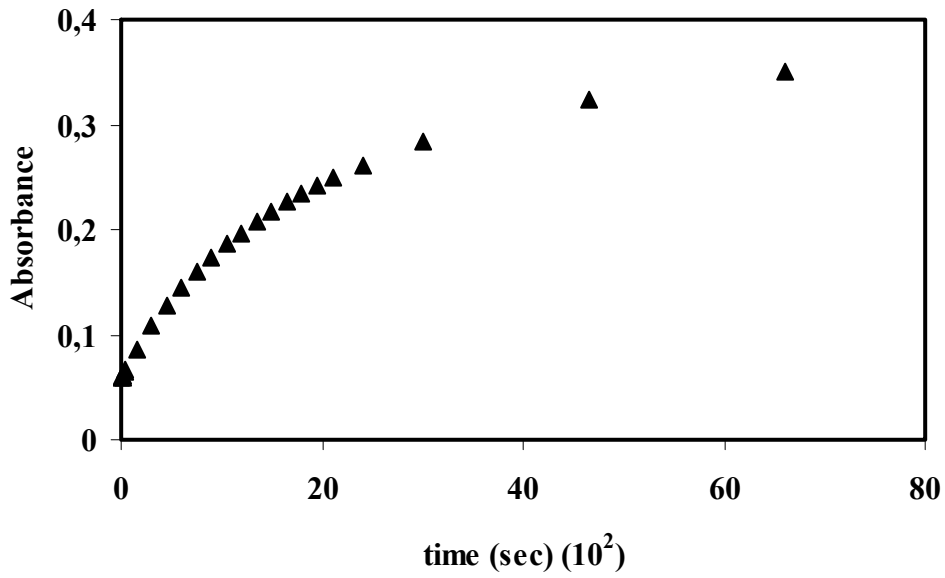

Figure 3.11. Absorbance at 400 nm as a function of time, in the hydrolysis of PNPA catalyzed by $2x10^{-3}$ M of the compound 2.9 and $2x10^{-3}$ M Zn^{2+} ions in $13.3x10^{-2}$ M MOPS buffer at pH 7.5 and 25°C.

Absorbance at 400 nm as a function of time for the hydrolysis of PNPA by the action of enzyme model 2.17 at pH 7.5 is shown. Hydrolysis was completed in about 30 minutes.

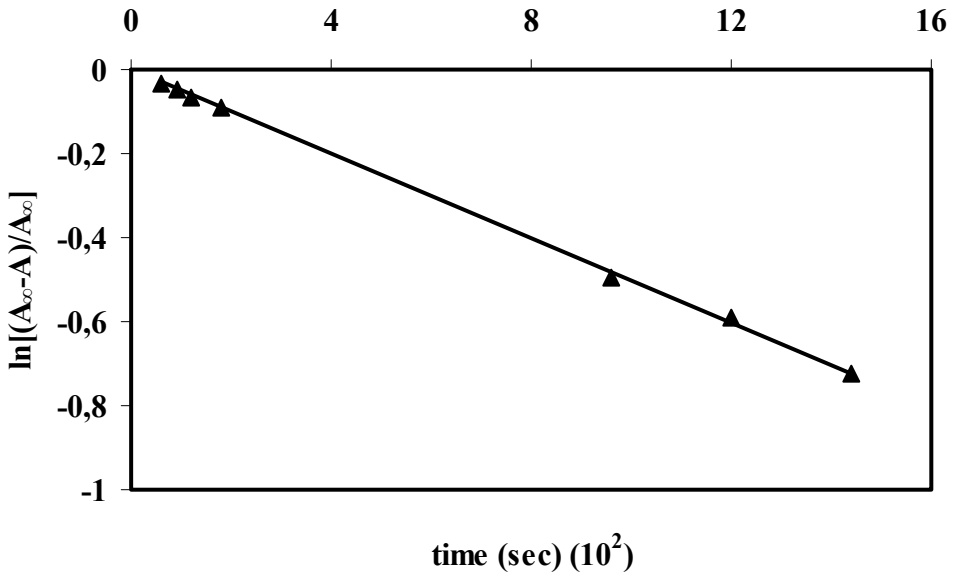

Figure 3.12. The plot of $\ln[(A_\infty-A)/A_\infty]$ as a function of time for $2x10^{-3}$ M compound 2.9 and $2x10^{-3}$ M Zn^{2+} in $13.3x10^{-2}$ M MOPS buffer at pH 7.5 and 25°C, yielding a pseudo-first order rate constant ($k_{cat}=2.5x10^{-3}$ s^{-1}) and $R^2=0.9967$.

By plotting $\ln[(A_\infty-A)/A_\infty]$ as a function of time in the presence of MOPS buffer at 7.5, a pseudo-first order rate constant of $2.5x10^{-3}$ s^{-1} was obtained. The rate acceleration is 11 times more efficient in hydrolysis of PNPA compared to uncatalyzed hydrolysis reaction.

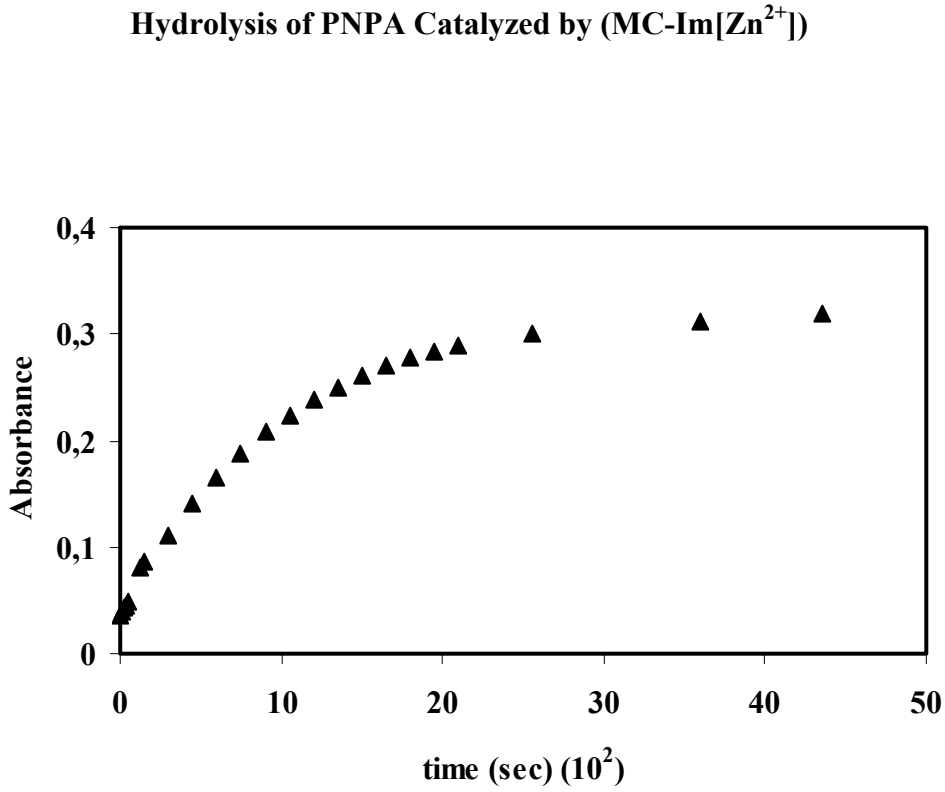

Figure 3.13. Absorbance of p-nitrophenolate ion at 400 nm as a function of time, in the hydrolysis of PNPA catalyzed by $2x10^{-3}$ M of the compound 2.9 and $2x10^{-3}$ M Zn^{2+} ions in $13.3x10^{-2}$ M TRIS buffer at pH 8.0 and 25°C.

Figure 3. 13. shows the increase of absorbance as a function of time at 400 nm for the cleavage of PNPA at pH 8.0. The hydrolytic cleavage is slower compared to the reaction catalyzed by the enzyme model at pH 7.0.

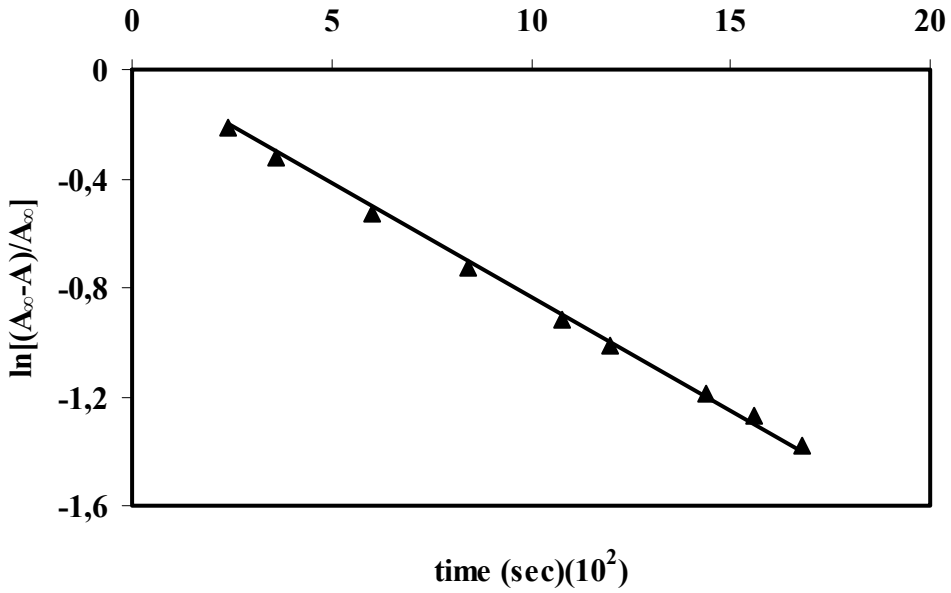

Figure 3.14. The plot of $\ln[(A_\infty-A)/A_\infty]$ as a function of time for $2x10^{-3}$ M compound 2.9 and $2x10^{-3}$ M Zn^{2+} in $13.3x10^{-2}$ M TRIS buffer at pH 8.0 and 25°C, yielding a pseudo-first order rate constant ($k_{cat}=4.8x10^{-3}$ s^{-1}) and $R^2=0.9975$.

The $\ln[(A_\infty-A)/A_\infty]$ was plotted as a function of time and pseudo-first order rate constant of $k_{cat}=4.8x10^{-3}$ s^{-1} was obtained.

The rate acceleration is about 8-fold over the uncatalyzed hydrolysis at pH 8.0.

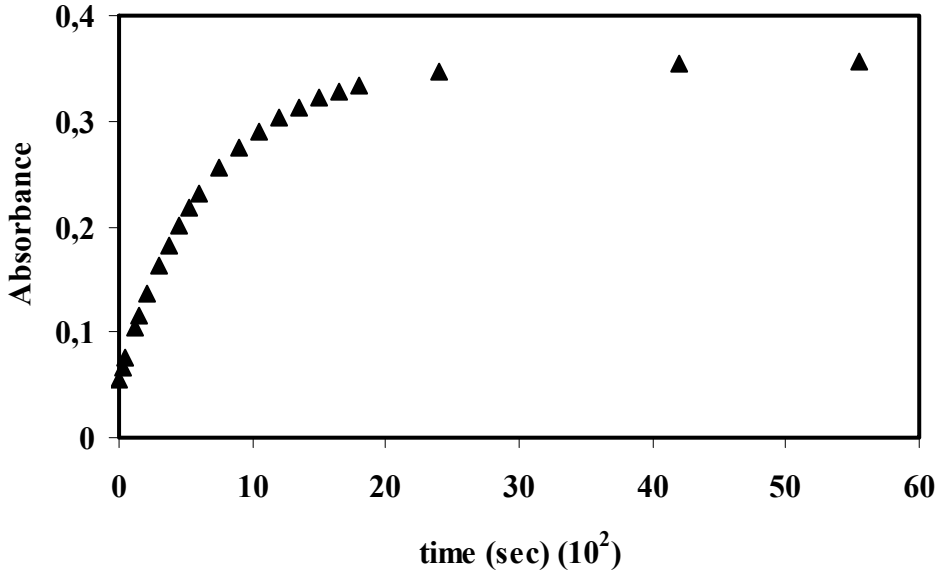

Figure 3.15. Absorbance of p-nitrophenolate ion at 400 nm as a function of time, in the hydrolysis of PNPA catalyzed by $2x10^{-3}$ M of the compound 2.9 and $2x10^{-3}$ M Zn^{2+} ions in $13.3x10^{-2}$ M TRIS buffer at pH 8.5 at 25°C.

The increase in absorbance due to the release of p-nitrophenolate was observed at 400 nm.

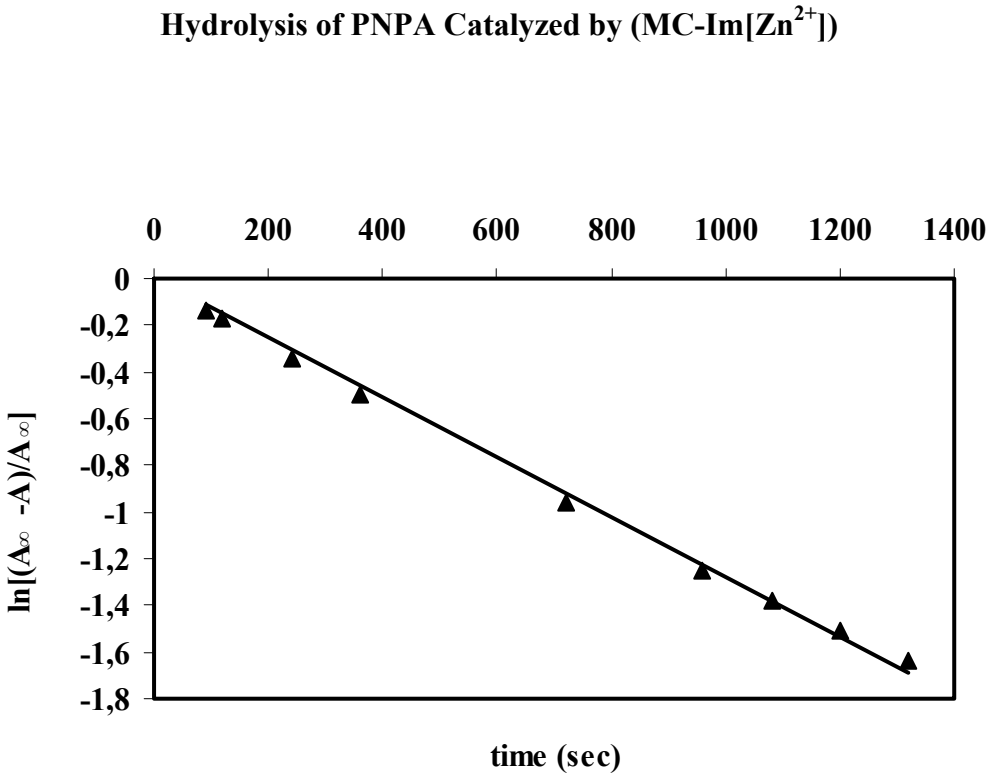

Figure 3.16. The plot of $\ln[(A_\infty-A)/A_\infty]$ as a function of time for $2x10^{-3}$ M compound 2.9 and $2x10^{-3}$ M Zn^{2+} in $13.3x10^{-2}$ M TRIS buffer at pH 8.5 and 25°C, yielding a pseudo-first order rate constant ($k_{cat}=7.5x10^{-3}$ s^{-1}) and $R^2=0.9987$.

Pseudo-first order rate constant was $7.5x10^{-3}$ s^{-1} with the rate acceleration of 5 which gives the lowest rate enhancement over the uncatalyzed reaction.

3.3. Hydrolysis of PNPA by monocyclen derivative-[Zn^{2+}] (MC[Zn^{2+}]) (2.18)

The monocyclen derivative-[Zn^{2+}] complex (MC[Zn^{2+}]) (2.18) was formed by mixing compound 2.14 with one equivalent of $Zn(ClO_4)_2$ and tested for its catalytic activity in the hydrolysis of the substrate of *p*-nitrophenylacetate (PNPA).

The catalytic activity of the PNPA was studied in the absence and presence of compound 2.16 at 7.0, 7.5, 8.0, and 8.5. The increase in the absorbance at 400 nm is due to the release of p-nitrophenolate. The absorbance as a function of time and pseudo-first order kinetics are shown in Figures 3. 17-3.24.

At pH 7.0 the rate acceleration of 714 ($k_{cat}=1.5x10^{-3}$), at pH 7.5 rate acceleration of 6.9 ($k_{cat}=1.6x10^{-3}$), at pH 8.0 rate acceleration of 5.9 ($k_{cat}=3.6x10^{-3}$ and at pH 8.5 rate acceleration of 8.4 ($k_{cat}=5.1x10^{-3}$) were observed, (Table 3.1).

The hydrolysis of the model substrate is followed by the increase in p-nitrophenolate at 400 nm as a function of time. Pseudo-first order rate constants were obtained by plotting the $\ln[(A_\infty-A)/A_\infty]$ as a function time. The results obtained are given in Figure 3.17-3.24. Depending on these results, the enzyme model presents the highest rate acceleration of 714-fold at pH 7.0.

On the other hand; pseudo-first order rate constants of the hydrolysis reactions increase due to the high pH.

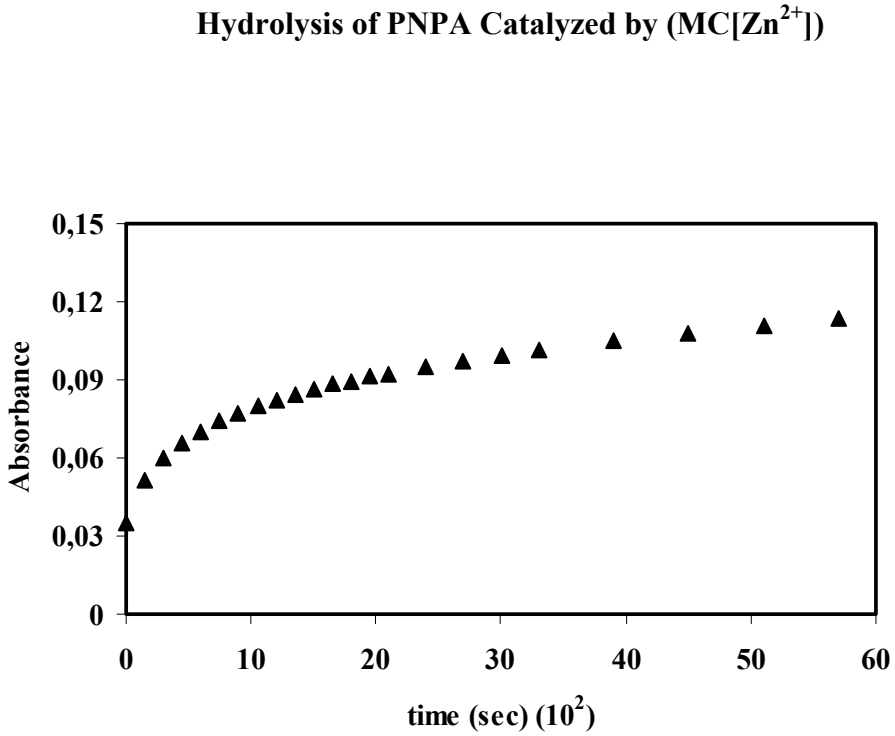

Figure 3.17. Absorbance at 400 nm as a function of time, in the hydrolysis of PNPA catalyzed by $2x10^{-3}$ M of the compound 2.14 and $2x10^{-3}$ M Zn^{2+} ions in $13.3x10^{-2}$ M MOPS buffer at pH 7.0 and 25°C.

Figure 3.17. shows the increaseof absorbance of p-nitrophenolate as a function of time at 400 nm for hydrolysis of PNPA in the presence of enzyme model (2.18) at pH 7.0. The highest rate acceleration is observed at this pH.

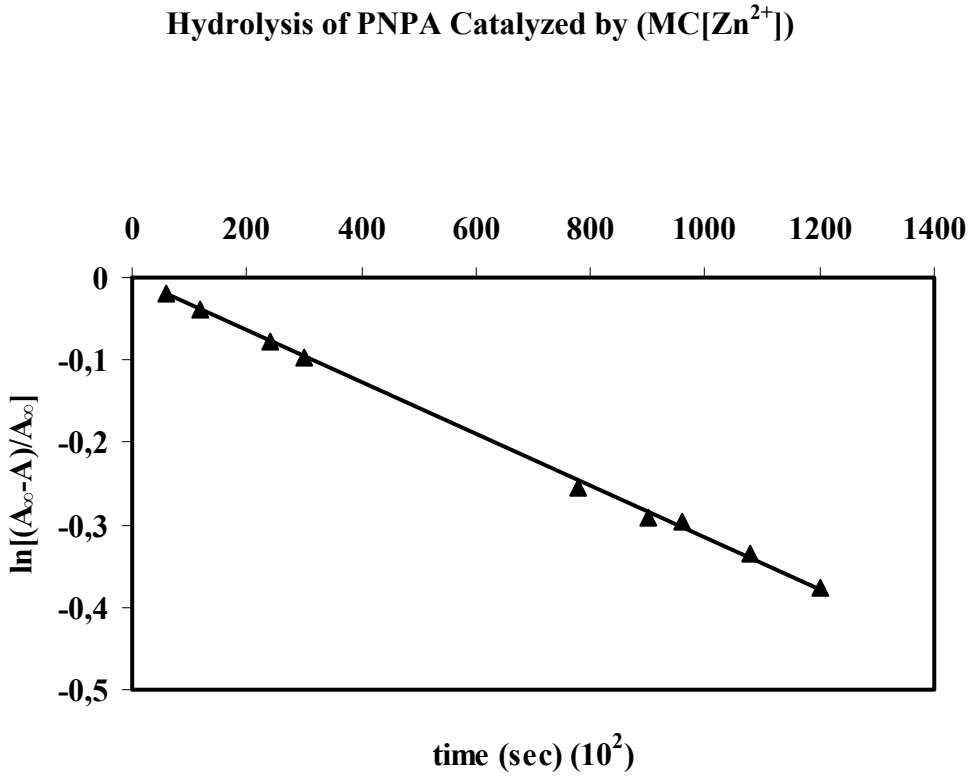

Figure 3.18. The plot of $\ln[(A_\infty-A)/A_\infty]$ as a function of time for $2x10^{-3}$ M compound 2.14 and $2x10^{-3}$ M Zn^{2+} in $13.3x10^{-2}$ M MOPS buffer at pH 7.0 and 25°C, yielding a pseudo-first order rate constant ($k_{cat}=1.5x10^{-3}$ s^{-1}) and $R^2=0.996$.

Pseudo-first order rate constant for the hydrolysis at pH 7.0 was obtained by plotting the $\ln[(A_\infty-A)/A_\infty]$ as a function time, (Figure3.18). The slope and intercept were obtained by linear regression, yielding a k_{cat} of $1.5x10^{-3}$ s^{-1} with the rate acceleration of 714.

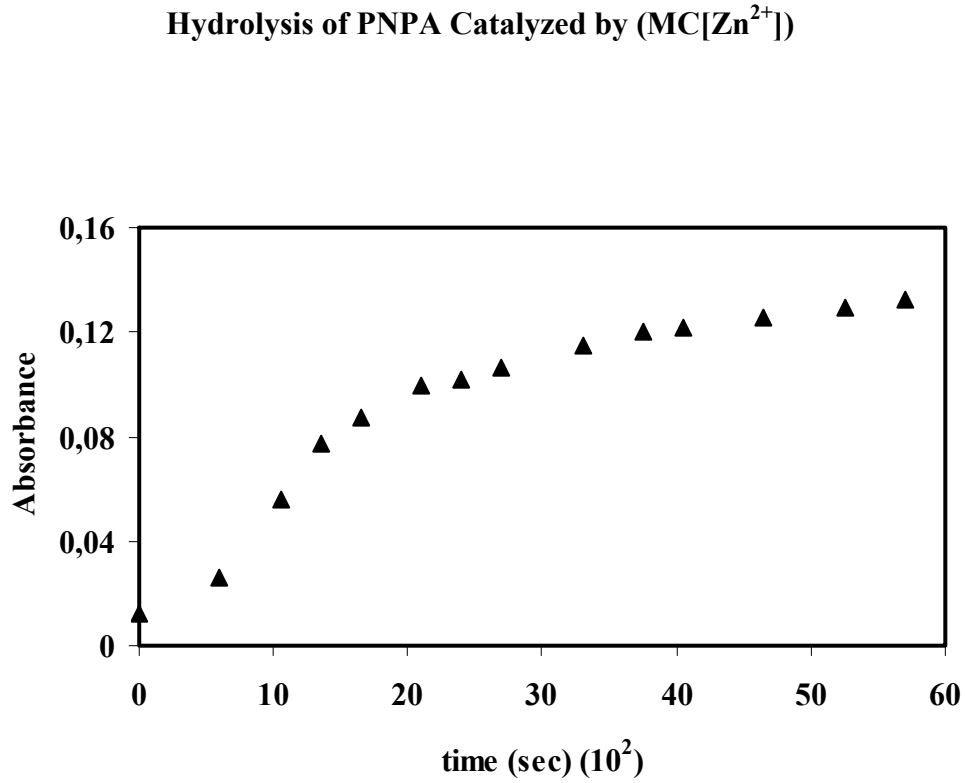

Figure 3.19. Absorbance of p-nitrophenolate ion at 400 nm as a function of time, in the hydrolysis of PNPA catalyzed by $2x10^{-3}$ M of the compound 2.14 and $2x10^{-3}$ M Zn^{2+} ions in $13.3x10^{-2}$ M MOPS buffer at pH 7.5 and 25°C.

In Figure 3.19. the increase of the absorbance due to the release of the p-nitrophenolate at 400 nm by hydrolysis of PNPA at pH 7.5 is shown. The hydrolysis reaction was completed in about one hour in the presence of enzyme model 2.18.

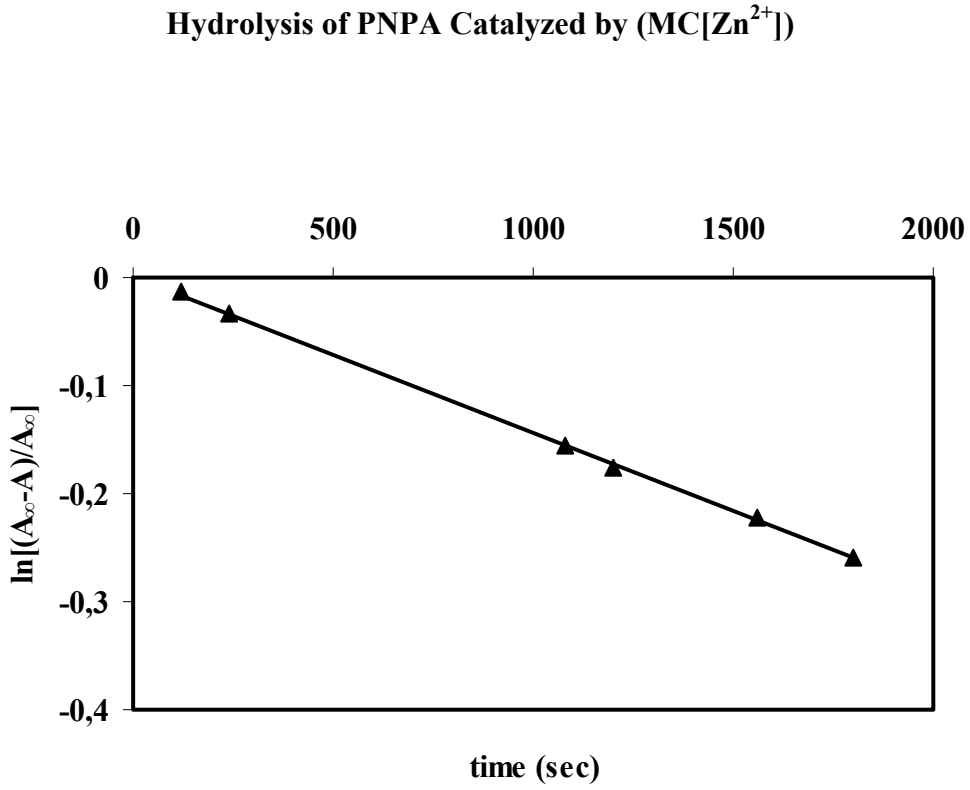

Figure 3.20. The plot of $\ln[(A_\infty-A)/A_\infty]$ as a function of time for $2x10^{-3}$ M compound 2.14 and $2x10^{-3}$ M Zn^{2+} in $13.3x10^{-2}$ M MOPS buffer at pH 7.5 and 25°C, yielding a pseudo-first order rate constant ($k_{cat}=1.6x10^{-3}$ s^{-1}) and $R^2=0.994$.

By plotting $\ln[(A_\infty-A)/A_\infty]$ as a function of time in the presence of MOPS buffer at pH 7.5, a pseudo-first order rate constant of $1.6x10^{-3}$ s^{-1} was obtained. The rate acceleration is 6.9 times more efficient in hydrolysis of PNPA compared to uncatalyzed hydrolysis reaction.

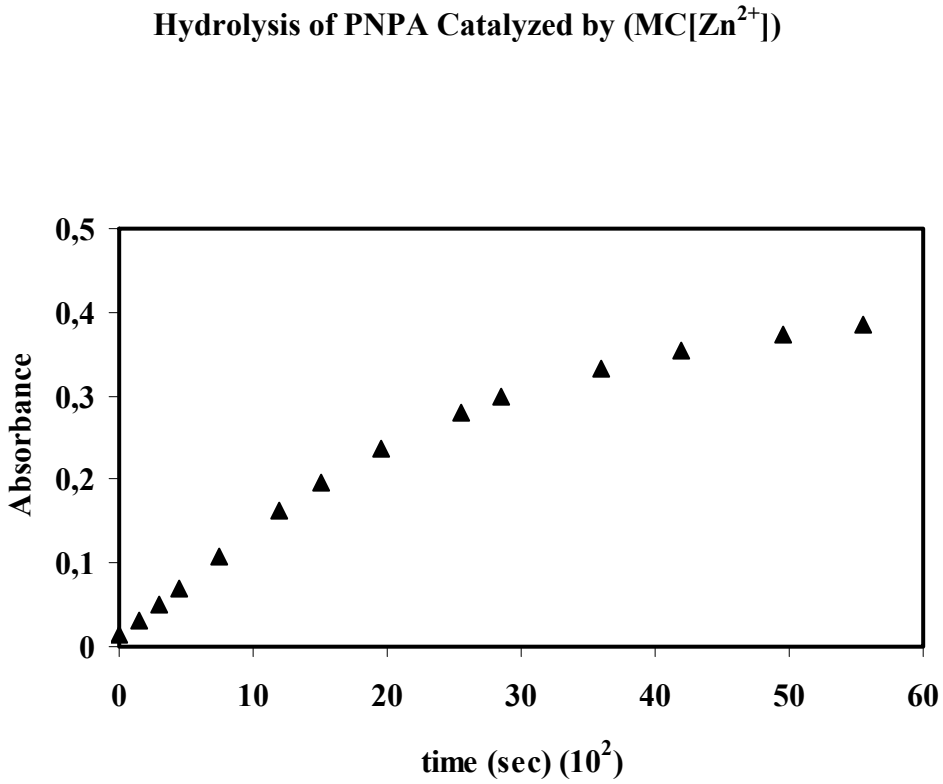

Figure 3.21. Absorbance of p-nitrophenolate ion at 400 nm as a function of time, in the hydrolysis of PNPA catalyzed by $2x10^{-3}$ M of the compound 2.14 and $2x10^{-3}$ M Zn^{2+} ions in $13.3x10^{-2}$ M TRIS buffer at pH 8.0 and 25°C.

Figure 3.21. shows the hydrolysis of the substrate as followed by the increase in absorbance at 400 nm, this time at pH 8.0. Hydrolysis reaction of PNPA was decreased to 40 minutes.

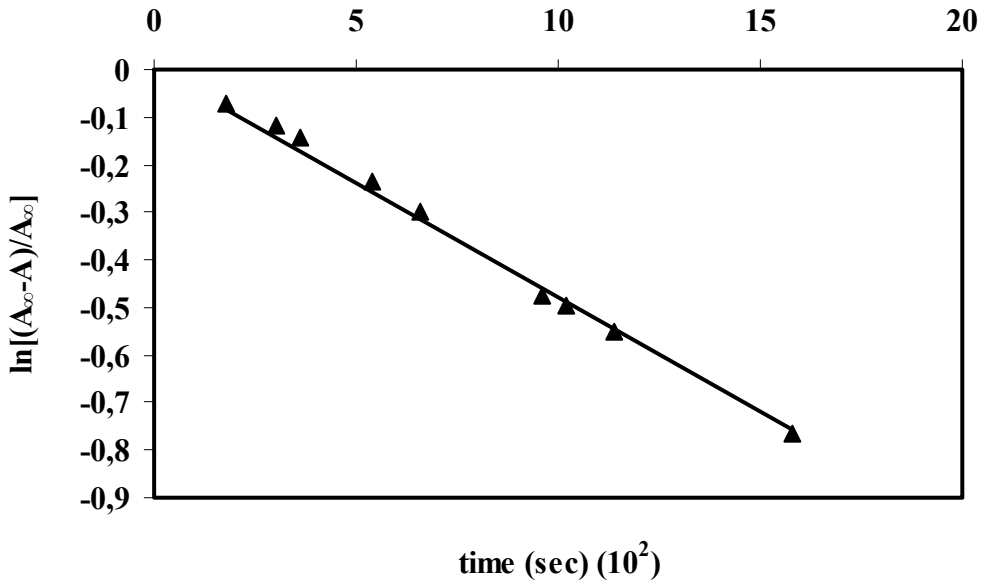

Figure 3.22. The plot of $\ln[(A_\infty-A)/A_\infty]$ as a function of time for $2x10^{-3}$ M compound 2.14 and $2x10^{-3}$ M Zn^{2+} in $13.3x10^{-2}$ M TRIS buffer at pH 8.0 and 25°C, yielding a pseudo-first order rate constant ($k_{cat}=3.6x10^{-3}$ s^{-1}) and $R^2=0.9922$.

As it is shown in Figure 3.22. a pseudo-first order rate constant of $3.6x10^{-3}$ s^{-1} was obtained for this reaction.

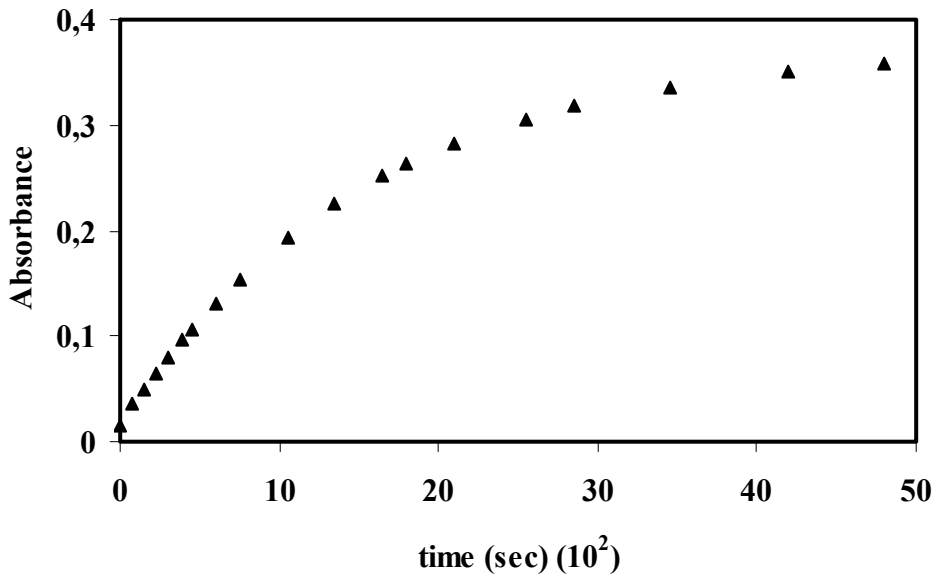

Figure 3.23. Absorbance at 400 nm as a function of time, in the hydrolysis of PNPA catalyzed by $2x10^{-3}$ M of the compound 2.14 and $2x10^{-3}$ M Zn^{2+} ions in $13.3x10^{-2}$ M TRIS buffer at pH 8.5 and 25°C.

The increase in absorbance due to the release of the p-nitrophenolate was observed at 400 nm.

The hydrolysis reaction was slower compared to the reaction catalyzed by ($DC[Zn^{2+}]_2$) enzyme model 2.16 at the same pH.

Hydrolysis of PNPA Catalyzed by (MC[Zn^{2+}])

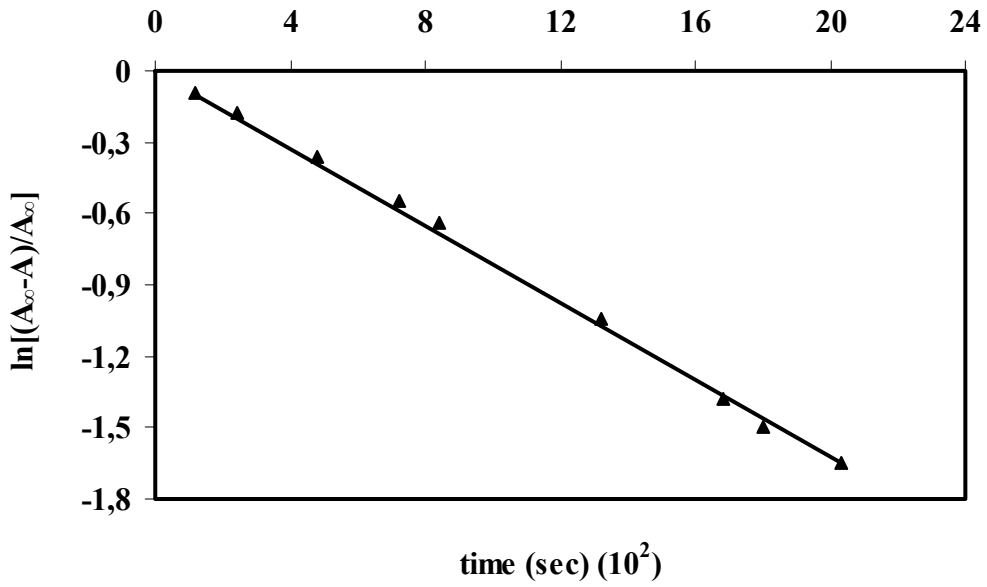

Figure 3.24. The plot of $\ln[(A_\infty-A)/A_\infty]$ as a function of time for $2x10^{-3}$ M compound 2.14 and $2x10^{-3}$ M Zn^{2+} in $13.3x10^{-2}$ M TRIS buffer at pH 8.5 and 25°C, yielding a pseudo-first order rate constant ($k_{cat}=5.1x10^{-3}$ s^{-1}) and $R^2=0.9972$.

The plot of $\ln[(A_\infty-A)/A_\infty]$ as a function of time gave the pseudo-first order rate constant of $5.1x10^{-3}$ s^{-1} and rate acceleration of 8.4 (k_{cat}/k_{uncat}).

Table 3.1. Kinetic data for hydrolysis of PNPA[(a,b,c)] by complexes 2.16, 2.17 and 2.18

Enzyme Model	pH	$k_{cat}(s^{-1})$	k_{cat}/k_{uncat}
$DC[Zn^{2+}]_2$	7.0	$0.9x10^{-3}$	428.5
	7.5	$1.6x10^{-3}$	7.0
	8.0	$4.5x10^{-3}$	7.4
	8.5	$12.0x10^{-3}$	7.5
MC-Im[Zn^{2+}]	7.0	$12.0x10^{-3}$	5714.0
	7.5	$2.5x10^{-3}$	11.0
	8.0	$4.8x10^{-3}$	7.9
	8.5	$7.5x10^{-3}$	4.7
MC[Zn^{2+}]	7.0	$1.5x10^{-3}$	714.0
	7.5	$1.6x10^{-3}$	6.9
	8.0	$3.6x10^{-3}$	5.9
	8.5	$5.1x10^{-3}$	8.4

[a] The reactions were carried out in 0.15M buffer solutions at the indicated pH, in the presence of 2mM catalyst and $Zn(ClO_4)_2$ (4mM for compound **2.16** and 2mM for compounds **2.17** and **2.18)**. For pH 7.0 and 7.5 MOPS and for pH 8.0 and 8.5 tris was used as buffering material.
[b] The substrate (p-nitrophenolate) concentration was 50 μM.
[c] The reactions were carried out at 298 K.

Cyclen-complexed Zn^{2+} carries a water molecule as an additional ligand in aqueous solutions. Thus, the substrate does not bind directly to the metal and that zinc mediates its function through the metal-bound-water molecule, which is not displaced on the binding substrate. Zinc lowers the pK_a of the bound-water molecule from ~14 to ~7. The resultant metal-bound hydroxide ion can then attack the substrate. The function of zinc is to activate the water molecule that acts as a nucleophile. Coordination to a metal ion increases the acidity of nucleophile and provides a powerful nucleophile at neutral pH. In addition, the metal through its flexible coordination geometry, would act as a template to bring together the substrate and nucleophile; this suggestion is consistent with the entatic nature of the metal.

On the other hand; full cooperative action between the metal centers has been shown in binuclear complexes. In these type of models, two functional groups are expected to functionally complement to each other resulting to satisfactory catalysts. Our designed complex DC[Zn^{2+}]$_2$ 2.16 is also significant catalysis in this manner, but the bifunctional model 2.17 provides much more better catalysis.

The mechanism of the hydrolysis promoted by our enzyme model, mono-cyclen+imidazole derivative-[Zn^{2+}] (2.17) depends on general acid-general base catalysis. Figure 3.25 shows the schematic representation of the hydrolysis by the enzyme MC-Im[Zn^{2+}]. Nearly all enzyme reactions involve some degree of acid or base catalysis. In general acid-base catalysis, the buffer can donate or accept a proton in the transition state and apparently stabilizes it. The acceleration of the reaction, therefore, is achieved by the catalytic transfer of a proton.

At pH 7.0, our model compound MC-Im[Zn^{2+}] gives the maximum rate acceleration with 5714-fold compared to the uncatalyzed hydrolysis of *p*-nitrophenolate and demonstrates the efficiency of bifunctional catalysis. An

increase on pH results the reaction rate of hydrolysis of PNPA to decrease. This interesting finding is a proof for the catalytic role of the imidazole unit as a general acid. In solutions with the pH is higher than 7.0, imidazole is deprotonated and no longer facilitates as a general acid catalyst. In accordance with our expectations, in the pH range 7.0-8.5 uncatalyzed reaction rate increases as the pH increases.

The reaction rate by bifunctional compound (2.17) differs from binuclear (2.16) and mononuclear (2.18) models only by an order of magnitude. However; the difference is significant and the given values are the avareges of five different runs.

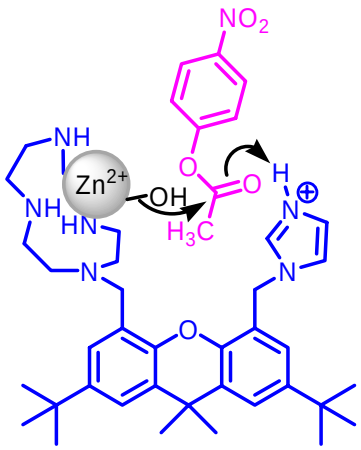

Figure 3.25. The mechanism of *p*-nitrophenylacetate hydrolysis with the enzyme model 2.17.

CHAPTER IV

CONCLUSION

Enzymes set chemists a high standard for synthetic catalysts with their high selectivity and enormous acceleration of reactions. This goal is very difficult to achieve. The elucidation of enzyme mechanisms is therefore counted among the important tasks of science, to which a wide variety of research disciplines can contribute. It is suggested that the active sites of enzymes involved structures that are complementary to transition state. Recently, the importance of having the correct orientation of functional groups in the substrate-catalyst complexes has been highlighted. This directionality is very well pronounced with the xanthene-based molecules.

In our work, we have derivatized xanthene framework which carries adjacent hydrolytically active units. Obtained compounds have two cyclen (2.16), one cyclen and one imidazole (2.17) and one cyclen and one hydroxymethyl (2.18) in which ^{1}H and ^{13}C NMR data confirmed. Then the formation of corresponding Zn(II) complexes resulted binuclear ($DC[Zn^{2+}]_2$) **(2.16)**, bifunctional ($MC\text{-}Im[Zn^{2+}]$) **(2.17)**, and mononuclear ($MC[Zn^{2+}]$) **(2.18)** metalloenzymes**,** respectively.

Studing the hydrolytic activities of these enzyme models for the hydrolyses of the model substrate *p*-nitrophenyl acetate (PNPA) (2.15) at four different pH demonstrated that mono-cyclen-imidazole derivative-[Zn^{2+}] (MC-Im[Zn^{2+}]) (2.17) seems to be the most active catalyst**.** The compound hydrolyzes PNPA (2.15) far more efficiently than the other two metalloenzme models (2.16 and 2.18) with the large rate acceleration of 5714-fold at pH 7.0. Decreasing the reaction rate on going to more alkaline pH's proves the catalytic role of the imidazole unit as a general base.

In summary, this study has underlined the potential of such multifunctional enzyme models. Well-designed models of enzyme active sites with critically located multiple functionalities are promising candidates for biomimetic catalysts.

CHAPTER V

INTRODUCTION

5.1. Chemosensors

A sensor is a device that interacts with matter or energy and yields a measurable signal in response. Many microscopic devices are used in everyday life like thermometers, or in laboratories like a pH electrode, as sensors. In nano-world, the supramolecules, molecular assemblies or even small molecules can act as sensors for detecting presence or absence of "matter" and "energy" as their macroscopic relatives do. They are 'devices' in the eyes of the scientists; to be constructed from the very beginning and to be operated in use.

One approach to have such a sensor is to use what nature uses: biosensors. Selective binding to analyte, which is one of the vital points to be accomplished by a sensor, is demonstrated in many biological compounds such as enzymes, transport proteins and antibodies. To date, the sensors directly used or derived from biological sensors have had a great utility. However, the kinds of of ions and molecules that can be sensed by the biosensors of today are limited in number. Also, bioreceptors often have low stabilities, making them hard to keep on shelf for a long-time. Additionally, the large-scale productions of these biosensors are usually expensive.

The transduction of information from the molecular world to ours can be achieved naturally by means of light signals arising from molecular species. There are various strategies for introducing a signal transduction pathway into a particular device. Most options include electrochemical (potentiometric, amperomrtric) and optical (UV-VIS-NIR, fluorescence).

Chemosensors may be considered as two-component molecules in which a receptor moiety is covalently connected to a light sensitive group, and exhibit selective complexation affinity toward a given species and undergo photophysical changes upon guest binding. There are mainly two types of chemosensors; intrinsic and conjugate ones shown in Figure 5.1. Intrinsic chemosensors are the ones in which the mechanism for signal transduction involves interaction of the analyte with a ligand that is a part of the fluorophore π-system. In conjugate chemosensors, the mechanism for signal transduction involves interaction of the analyte with a ligand electronically-insulated from the fluorophore π-system, (Czarnik, 1993).

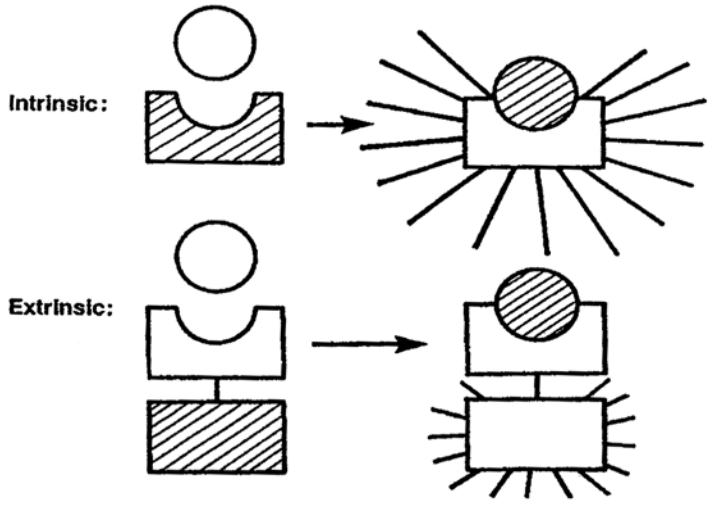

Figure 5.1. Demonstration of intrinsic and extinsic chemosensors.

Conjugaton of chromophores and fluorophores to antibodies and enzymes generally proceed with poor site selectivity, resulting in uncertain communication with the binding site to which the optical sensing component is extrinsic. Another approach is to combine the binding and sensing functions in a single subunit in the system. When both the chromophores and fluorophores are combined into a designed binding site, it produces an intrinsic optical sensing moiety. This approach usually improves the optical effects with the optical effects with the help of appropriate local electronic polarization, desolvation and conformational changes, (Minta et al., 1989).

Recognition of ions requires special attention in the design of fluorescent probes for selectivity in binding and the photophysical effects upon binding. Scientists try to answer three basic questions essential for a good design of chemosensors.

- How can bind a molecular entity with high selectivity to the analyte?
- How can one generate signals that are easily measurable from such binding processes?
- What mechanisms for binding and signal transduction intersect?

The medium in which the recognition takes place is also very important since the nature of the solvent, pH, ionic strength affect the efficiency of the photophysical characteristics of the chemosensor. Also, water soluble chemosensors are of great achievement as most of the biological applications need aqueous enviroments.

The photophysical changes of a chemosensor on ion binding can involve various photoinduced processes: energy transfer, electron transfer, charge transfer, excimer or exciplex formation or disappearance. These changes on recognition

should be markable. Chemosensors undergoing shifts of emission and/or excitation spectra are preferred to the probes whose fluorescence intensities only change. By this way, the ion or molecule concentration which is independent of the probe concentration, can be measured from the ratio of the fluoroscence intensities at two appropriate emission or excitation wavelengths and the measurement will be insensitive to intensity of incident light, inner-filter effects, scattering, and photobleaching, (Valeur, 1994).

In order to make use of advantages of chemosensors, a chemosensor must satisfy a number of requirements.

- The binding site should be able to select the desired analyte to bind among the other species present in the medium.
- The analyte should be able to dissociate from the binding site in real-time.
- The excitation wavelength should correspond to that of an inexpensive, portable laser source.
- The emission wavelength should be consistent with inexpensive detectors and removed from that of fluorescent impurities in the media.
- Long-wavelength fluorophores (i.e. near-IR) should be designed in order to avoid autofluororescence which is a background signal in most biological samples up to 650 nm, (Lakowicz et al., 1992).

5.2. The Anion Coordination Chemistry

Over the past years, chemosensors which detect cations have been successfully developed. Conversely, the development of anion sensors has been less successful and it has only been in the last twenty years that sustained effort has been applied to the problems inherent in binding anions. There are a number

of reasons for this sudden growth in this new area of coordination chemistry. Anions are essential throughout biological systems. They carry genetic information (DNA is a polyanion) and the majority of enzyme substrates and co-factors are anionic (e.g.; carboxypeptidase). Anions also play roles in the area of medicine, e.g. the metabolities of nitrate are proven to cause carcinogenesis and cystic fibrosis is one of the medical conditions in which misregulation of anion transport is responsible.. Also, the production of pertechnetate during the processing of nuclear fuel and the use of phosphate–containing fertilizers are a threat for the water resources, (Moss, 1996).

Recognition and sensing of anions has been a subject of intensive current interest and hydrogen bonding is one of the important recognition elements in anion sensing. Like the cation chemsosensor, an anion chemosensor consists of a recognition moiety and a signal reporter that are either directly linked to allow for a highly efficient communication between the recognition moiety and the reporter or connected by a flexible spacer to ensure an optimal approaching of them, (Wu et al., 2002).

The design of anion receptors is particularly challenging. There are numerious reasons for this. These are;

- Anions are relatively large and therefore require receptors of considerably greater size than cations.
- Even simple inorganic anions occur in a range of shapes and geometries, e.g. spherical, linear, planar, tetrahedral, octahedral, as well as more complicated examples as in the case of biologically important oligo-phosphate anions.
- In comparison to cations of similar size, anions have high free energies of solvation and hence anions hosts must compete more effectively with the surrounding medium.

- Many anions exist only in a relatively narrow pH window, which can cause problems especially in the case of receptors based on poly-ammonium salts where the host may not be fully protonated in the pH region in which the anion is present in the desired form.
- Anions are usually saturated coordinatively and therefore bind only via weak forces such as hydrogen bonding and van der waals interactions.

Anion recognition chemsitry has its roots in work conducted in the late 1960s around the same time that Pedersen reported the synthesis and coordination chemistry of crown ethers and Lehn published the cation coordination chemistry by cryptands.

Auseful way of categorizing anion receptors is to consider the types of non-covalent interaction used to complex the anionic guests. These are hydrogen bonding, electrostatic interactions, hydrophobicity, coordination to a metal ion, and combinations of these interactions working together, (Beer and Gale, 2001).

5.2.1. Hydrogen bonds

Hydrogen bonds allow to design specific shaped receptors that are capable of differentiating between anionic guests with different geometries. In 1986, Pascal prepared the first purely amide-based anion receptor and showed evidence of binding fluoride ions, (Figure 5.2).

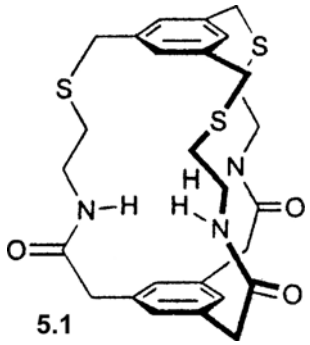

5.1

Figure 5.2. The first purely amide-based anion receptor.

In another example, Choi and Hamilton have described the synthesis and anion binding properties of a new family of cyclic tri-amides such as the one given in Figure 5.3.

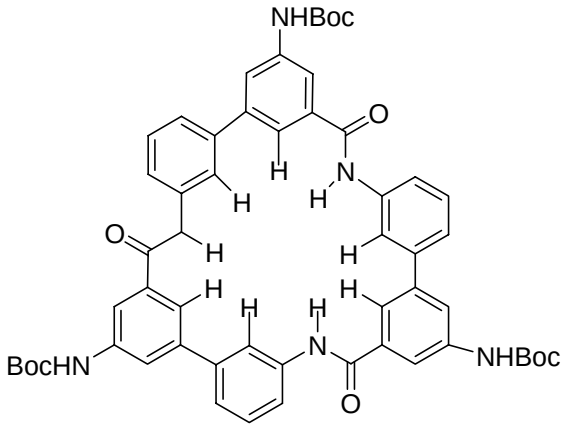

5.2

Figure 5.3. Another example for amide based anion receptor.

Urea and thiourea are particularly good hydrogen-bond donors and are excellent receptors for Y-shaped anions such as carboxylate through the formation of two hydrogen bonds. Kelley and Kim (1994) showed that the very simple urea-

based receptor given in Figure 5.4**.** demonstrates increasingly stable complexes with more highly charged and more basic bidentate anions.

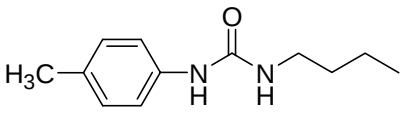

5.3

Figure 5.4. A urea-based anion receptor.

In a recent study , Lee et al. (2001) developed an azaphenol-thiourea based anion sensor which acts as colorimetric sensor for selected anions by means of hydrogen-bonding interactions. The system allows for the selective colorimetric detection of dihydrogen phosphate, fluoride and acetate anions (Figure 5.5).

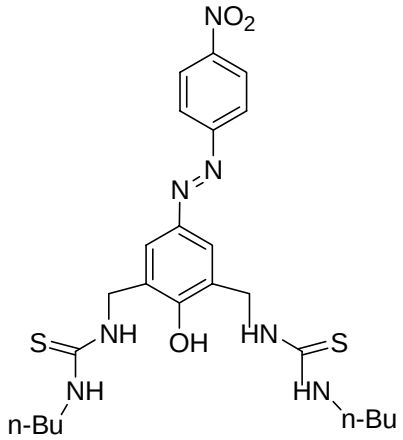

5.4

Figure 5.5. The azaphenol-thiourea based chromophore anion sensor.

In 1999 Sato et al. and Alcalde et al. have reported that receptors with 1,3-disubstituted imidazolium groups bind anions by forming C-H---X^- hydrogen bonds between the imidazolium rings and the guest anion. Three years later, Yun and his co-workers synthesized a positively charged tripodal receptor containing three imidazolium groups and demonstrated the enhancement in the anion binding strength by the nitro groups based on the theoretical understanding of the $(C\text{-}H)^+$---X^- hydrogen bonding interaction and charge-dipole interaction in molecular recognition (Figure 5.6). They have also proved that the receptor recognizes effectively and selectively the chloride anion over other halide ions. In addition, the molecule showed reasonably high affinity toward the biologically important diphosphate anion.

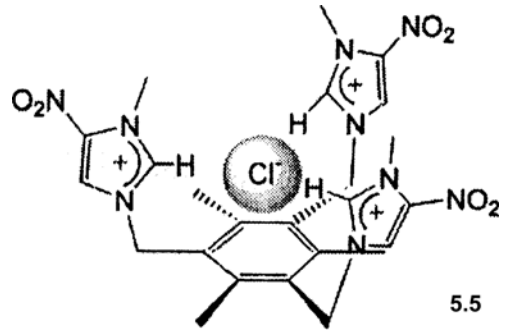

Figure 5.6. Schematic representation of a positively charged tripodal receptor.

5.2.2. Electrostatic Interactions

In the late 1970s, Schmidtchen produced a couple of macrotricyclic quaternary ammonium hosts and found that these receptors formed complexes with a variety of anionic guests in water. The cavity in the first receptor formed a strong complex with iodide ion whereas the second recoptor which is larger was able to form complexes with anions such as p-nitrophenolate that are too large for

the first receptor, (Figure 5.7). Schmidtchen et al. (1994) also designed some zwitterionic receptors that are neutral and are formed stronger complexes with chloride, bromide, and iodide ions than the first receptor. Two of these receptors are also given in Figure 5.7.

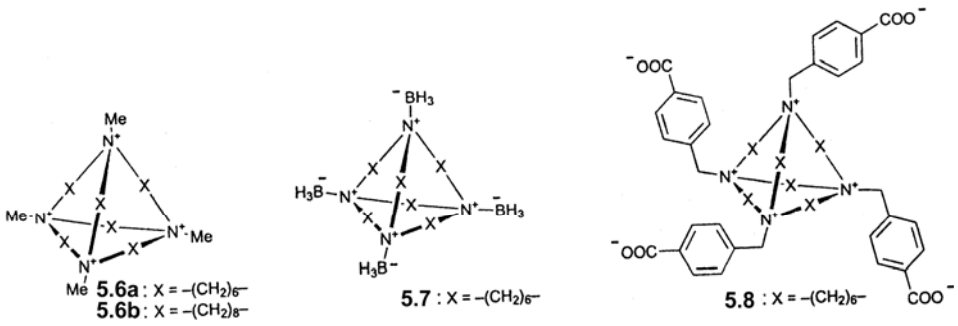

Figure 5.7. Molecules designed by Schmidtchen et al.

5.2.3. The Hydrophobic effect

Inclusion complaxation of a series naphthalenesulfonates with β-cyclodextrin (Figure 1.1) in water showed that the binding interaction in these complexes is primarily a result of the hydrophobic effect, (Inoue et al., 1993). The naphthalene residue displaces water molecules from the internal cavitiy of the cyclodextrin while the anionic sulfonate group remains outside the cavity in contact with the solvent, thereby controlling the orientation of the naphthalene group within the cavity.

5.2.4. Metal Ion Coordination

Electron-deficient Lewis-acidic centers are able to bind to anions by an orbital overlap that causes a bonding interaction. This has led to the production of many chelating and macrocyclic hosts for anions containing atoms such as boron, mercury, germanium, tin, and silicon.

Azuma et al. (1984) have done studies on the synthesis of a series of tin-based macrocycles and showed that this family of macrocycles would form 1:1 and 1:2 host:anion complexes with chloride anions, respectively (Figure 5.8).

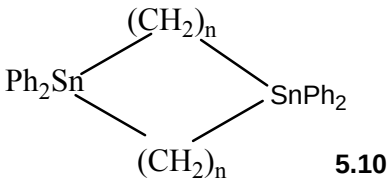

5.10

n= 4, 5, 6, 8, 10, 12

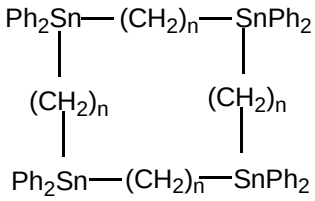

5.11

Figure 5.8. A series of examples for tin-based macrocycles.

Later on**,** a variety of germanium- and silicon-based receptors have been synthesized by several authors, (Aoyaki et al., 1994; Tamao et al., 1996). Some examples of these receptors are shown in Figure 5.9.

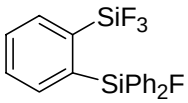

5.12

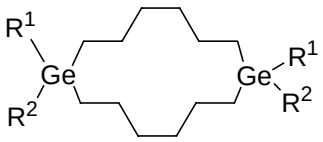

$R^1 = R^2 = Me$

$R^1 = Cl, R^2 = Me$

5.13

Figure 5.9. The silicon- and germanium-based receptors.

5.2.5. Electrostatic Interactions and Hydrogen Bonds

Hydrogen bonds and electrostatic interactions can be used together to produce very effective receptors for anions. Park and Simmons (1968) reported the first example of a macrocyclic synthetic anion receptor bound anions by a combination of these interactions. They produced several macrobicyclic ammonium cages given in Figure 5.10 which coordinate to halide ions through electrostatic interactions and hydrogen bonds. NMR and crystallographic analysis showed that the halide ions are bound within the cage between the two protonated nitrogen atoms.

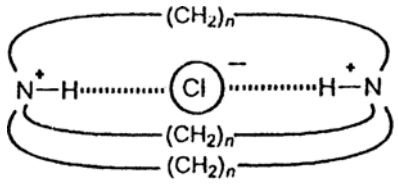

5.14 : $n = 9$
5.15 : $n = 10$

Figure 5.10. Macrocyclic anion receptors represented by Park and Simmons.

The protonated version of hexaazametacyclophane has been shown to bind AMP, ADP, and ATP in aqueous solution, (Aguliar et al., 1995). The anionic phosphate groups of the nucleotides coordinate to the macrocycle through a combination of electrostatic and hydrogen-bonding interactions (Figure 5.11).

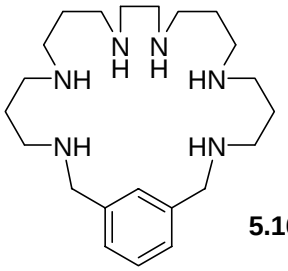

5.16

Figure 5.11. An example of electrostatic and hydrogen-bonding interactions.

5.3. Fluorisis

Fluoride is a natural mineral that is found in various concentrations in all drinking water and soil. Being a beneficial nutrient it is the only one that reduces the occurrence and prevalence of dental caries (cavities) in both children and adults. Scientists believed that dental decay could be prevented by increasing fluoride amounts in the water supply. Hence, it is essential to maintain the F^- concentration between 0.8 to 1.0 mg/L in drinking water. Among the many methods suggested for the determination of fluoride ion in water, the colorimetric method (SPADNS) & the ion selective electrode method are the most satisfactory and applicable to variety of samples.

Tap water is not the only source of fluoride. Nowadays we get fluoride in toothpaste, soft drinks, air pollution, fruit juice, children's vitamin supplements. Studies over time seem to show that rising exposure to fluoride from other sources makes water fluoridation less protective of teeth and more likely to cause fluorisis which results to the tooth and bone decalcification. While much has been written about the effects of too much fluoride on teeth and bones, little is known about that of on the rest of the body. From a lot of research it seems that fluoride causes joint problems, skeletal deformations, osteoporosis, and that it can even cause bone cancer. Also the brain cannot escape from it. Fluoride has a negative

influence on the nervous system and the immune system, and in children it can lead to (chronic) fatigue, a lower IQ, learning disabilities, and depression. Enzyme systems react to fluoride in different ways; some are activated and others are inhibited. Lipase (essential for the digestion of fat) and phosphatases (needed for the breakdown of phosphates) are very sensitive to fluoride. In patients with skeletal fluorisis, succinate dehydrogenase activity is inhibited. Fluoride has even been shown to affect the pituitary gland, which controls growth rate by regulating the production of thyroid hormones, (Menda, 2000).

5.4. Chloride Channels and Cystic Fibrosis

Ion channels are a crucial part to all cells. They are responsible for allowing ions in and out of the cell, which permit such things as muscle contraction to occur. Cystic fibrosis (CF) is a genetically inherited disease in which chloride transport is the root cause of its symptoms. CF is caused by mutations in the CFTR (cystic fibrosis transmembrane conductive regulator) gene that encodes a cAMP-regulated chloride channel. The CFTR protein is embedded in the cell membrane, forming a channel. It is 1480 amino acids long and it has carbohydrate side-chains attached. The R-domain can bind phosphate groups and, together with two adjacent sites which bind and cleave ATP, regulates the opening and closing of the channel which is shown in Figure 5.12.

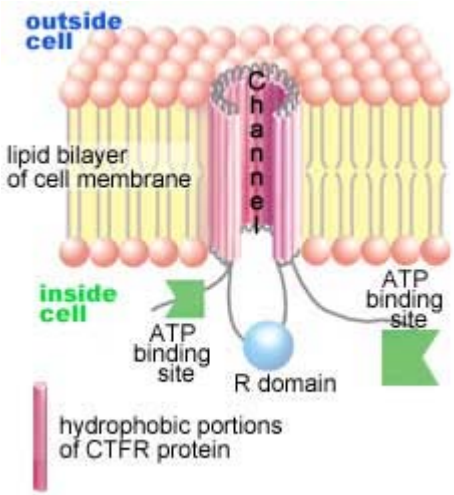

Scheme 5.1. Section through the cell membrane of an epithelial cell. The CFTR channel is shown open.

The major mutation occurring in CF patients is a 3-base pair deletion resulting in the loss of phenylalanine. As a result, the CFTR protein is not correctly trafficked to the surface membrane and does not become inserted. In cystic fibrosis, because the gene produces a faulty protein, there is a build up of sodium and chloride that causes the body to make sticky, thick mucus which is the most characteristic symptom of CF. This mucus prevents pancreatic enzymes from breaking down food, prevents the intestines from absorbing important nutrients and causes lung disease. Most individuals with the disease die by the time they reach their mid-thirties because of lung infections. Salt absorption in the sweat ducts is also impaired, and CF patients produce extremely salty sweat. Based on this observation, a sweat test has been developed to diagnose CF. This test is still the standard for diagnosis, (Nagel et al., 2001).

5.5. Calixpyrroles

The calix[4]pyrroles are octamethyl substituted form of porphyrinogens that were first synthesized by Baeyer in the nineteenth century by condensing pyrrole and acetone in the presence of an acid, (Baeyer, 1886) (Figure 5.12). Porphyrinogens are naturally occurring colourless macrocycles consisting of four pyrrole rings linked through the α or *meso*-like positions by sp^3 hybridized carbon atoms, (Gale et al., 1998). Subsequent to the work of Baeyer, Dennstedt and Zimmermann (1886) also studied this reaction, using 'chlorzink' as the acid catalyst. Thirty years later, Chelintzev and Tronov (1955) repeated these reactions and correctly proposed a cyclic tetrameric structure for calix[4]pyrrole.

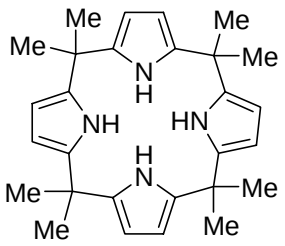

5.17

Figure 5.12. The structure of *meso*-octamethylcalix[4]pyrrole.

In the early 1970s, Brown et al.condensed cyclohexanone with pyrrole in a 1:1 ratio in the presence of acid to obtain tetraspirocyclohexyl[calix]pyrrole (Figure 5.13).

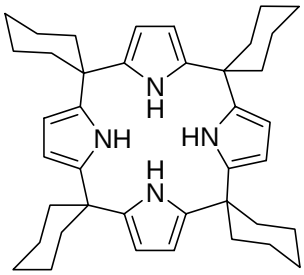

5.18

Figure 5.13. Tetraspirocyclohexyl[calix]pyrrole structure.

In the mid-1990s Sessler and co-workers discovered that the NH array present in these species can act as a binding site for anionic and neutral guest species. They prepared the compounds 5.17 and 5.18 using known literature procedures. Single crystals suitable for X-ray crystallographic analysis showed that the molecules adopt a 1,3 alternate conformation in the solid state wherein adjacent rings are oriented in opposite directions. However, X-ray crystal analysis of the tetramethylammonium chloride and tetramethylammonium fluoride complexes of compounds 5.17 and 5.18, respectively, revealed that the formation of an anion-calixpyrrole complex is accompanied by a dramatic change in the conformation of the macrocycle . In both cases the calix[4]pyrrole ligand adopts a conelike conformation such that the four NH protons can hydrogen bond to the halide anion (Figure 5.14). Up until that point these macrocycles had been known as porphyrinogens. This interesting conformational behavior drew the attention to the clear analogy between them and the calix[4]arenes. This analogy, coupled with the fact that as these species carry eight alkyl or aryl groups in the meso-positions and hence are not susceptible to oxidation to produce (e.g., porphyrin) led them proposed as calix[4]pyrroles. Analyses of the solution phase anion-binding properties of the compounds revealed that both of them are not only effective 1:1 anion-binding agents in solution, they are also selective ones; they show a marked preference for F^- relative to other anionic guests (e.g. Cl^-, Br^-, I^-, $H_2PO_4^-$and HSO_4^-).

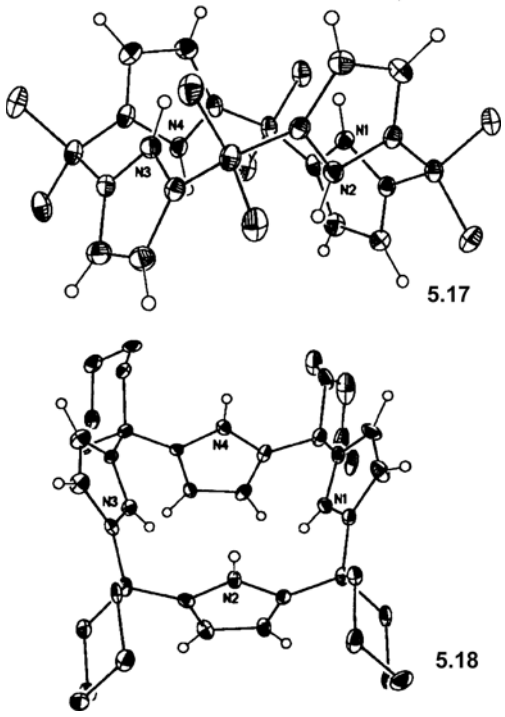

Figure 5.14. Viev of the molecular structures of 5.17 and 5.18.

Interestingly, unlike the calix[4]arenes, in calix[4]pyrroles there is no possibility for the formation of a hydrogen bonded array between the various pyrrolic NH groups. Thus, in the absence of an added substrate there is no possibility for the free macrocycles to adopt the cone conformation, a motif so common in calix[4]arene chemistry (Scheme 5.2).

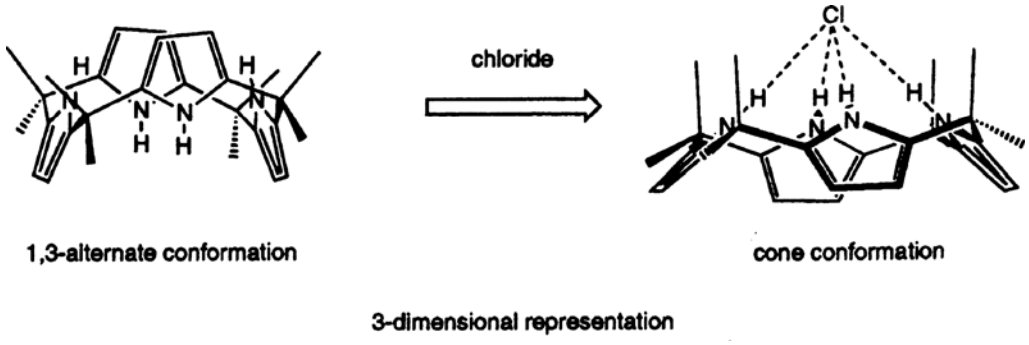

Scheme 5.2. An illustration for calix[4]pyrrole conformation.

Allen and his groups (1996) showed that the molecular recognition chemistry of the calix[4]pyrroles is not limited to anionic substrates. The coordination of neutral species was clearly achieved using *meso*-octamethylcalix[4]pyrrole 5.17. They revealed that this calix[4]pyrrole forms complexes with neutral species, including short chain alcohols, amides and other oxygen-containing neutral species. The structure of this molecule coordinated to two molecules of MeOH was determined by X-ray diffraction analysis. This group also characterized the *meso*-octamethylcalix[4]pyrrole 5.17-DMF complex. As in the bis(methanol) adduct, each of the two DMF molecules was found to be coordinated to a single calix[4]pyrrole macrocycle via two hydrogen bonds. However, in the case of the DMF complex, the calix[4]pyrrole adopts a 1,2-alternate conformation, wherein each DMF molecule is coordinated to adjacent pyrrole moieties. This complex is the first calixpyrrole in this conformation. (Figure 5.15).

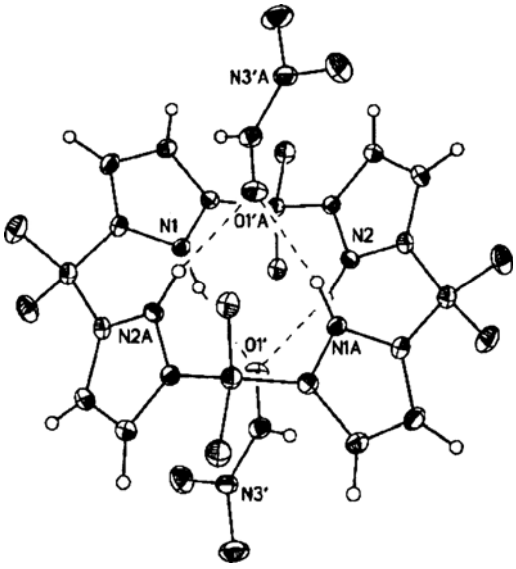

Figure 5.15. X-ray crystal structure of 5.17-DMF complex.

The effects of structural changes, specifically the presence and absence of substituents on the *meso*-like and β-pyrrolic carbons (C-rim), on anion affinities have been detailed by several authors. For this purpose, Gale et al.(1997) reported several novel calixpyrrole molecules They replaced the β-pyrrolic hydrogens of *meso*-octamethylcalix[4]pyrrole 5.17 and tetraspirocyclohexyl[calix]pyrrole 5.18. by bromine atoms (5.19) or methoxy substitutents (5.20), respectively. The results showed that receptor 5.19 exhibits higher stability constants for the binding of fluoride and chloride anions than 5.17 and 5.18 due to the electron-withdrawing nature of the eight C-rim bromine atoms increasing the acidity of the pyrrole NH protons and hence enhancing anion binding ability. Compound 5.20**,** on the other hand, has lower stability constants with these anions because the electron-donating effects of the methoxy groups decrease the acidity of the pyrrole NH protons and therefore lowers the calixpyrrole-anion complex formed (Figure 5.16).

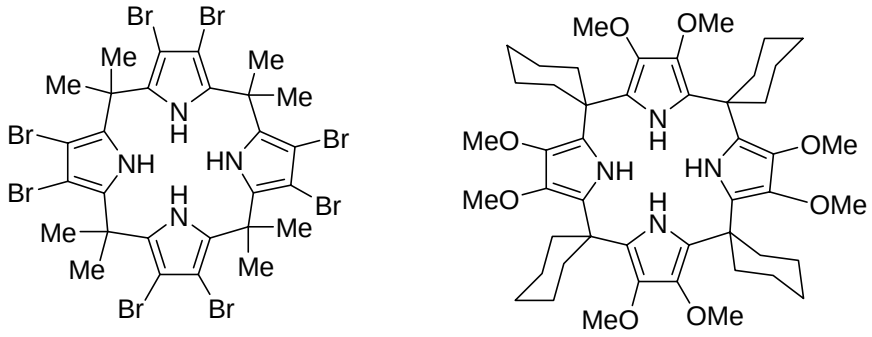

5.19 **5.20**

Figure 5.16. A couple of novel calix(4)pyrrole molecules.

Ferrocene-appended aza-macrocycles and amides have been synthesized and studied by a number of research groups, (Beer at al, 2000 and Tuntulani, 2001). Gale et al (2001) synthesized a new calix[4]pyrrole containing a ferrocene moiety attached to one of the *meso*-positions. As in the case of other calix[4]pyrrole macrocycles, the uncomplexed receptor adopts the 1,3-alternate conformation in the solid state. The crystal structure of molecule revealed that it functions as an electrochemical sensor and binds fluoride, dihydrogen phosphate and chloride anions. The structure of ferrocene-appended calix[4]pyrrole and schematic repreasentation of the ferrocene CH with calixpyrrole NH hydrogen-bonding interaction that are thought to stabilize the bound anion in complex are shown in Figure 5.17.

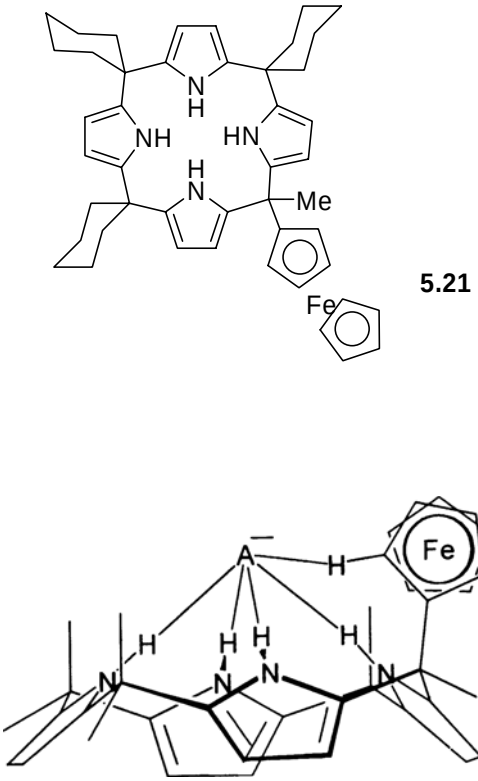

Figure 5.17. Ferrocene-appended calixpyrrole and proposed CH-anion interaction in complex.

In 2000 Sessler and his group developed a strategy to the synthesis of dimeric systems. They synthesized the acetylene-linked calix[4]pyrrole given in Figure 5.18. and a detailed study showed that there is a cooperative binding of appropriately sized dianionic substrate, e.g. isophthalate anion, to the calix[4]pyrrole dimer when compared to the control monomer, octamethyl[4]pyrrole 5.17.

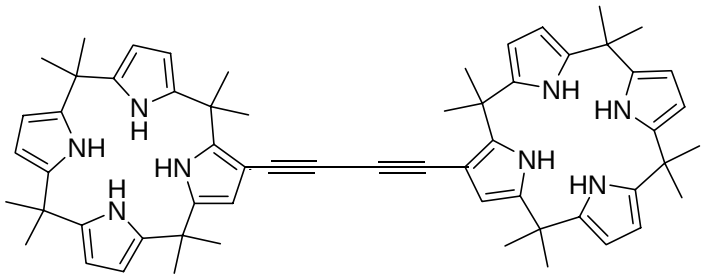

5.22

Figure 5.18. The acetylene-linked calix[4]pyrrole dimer**.**

5.6. Higher ordered calix[4]pyrroles

It is anticipated that higher order calix[4]pyrroles with larger cavities will enable selective and effective complexation of other anionic as well as uncharged species.

The first synthesis of a well characterized larger *meso*-calix[n]pyrrole, specifically calix[6]pyrrole, was achieved by Eichen and co-workers in 1998. X-ray crystallographic analysis of the calix[6]pyrrole revealed that the macrocycle adopts an asymmetric cone-like conformation in which all three diphenylmethylene bridges point above the macrocyclic plane (Figure 5.19).

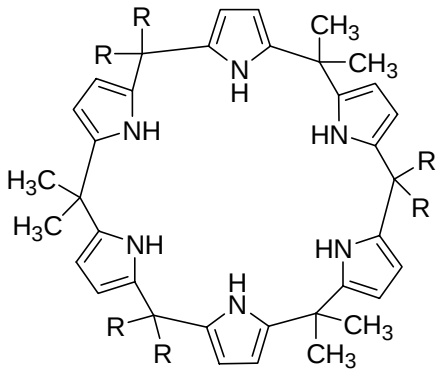

5.23

R = phenyl

Figure 5.19. The structure of well characterized calix[6]pyrrole.

Recently, Sessler et al. (2000) discovered a direct synthesis of higher order calixpyrroles. They proposed that the use of 3,4-difluoropyrrole, rather than simple pyrrole, allows for the preparation of calix[5]- 5.25 and calix[8]pyrroles 5.26 derivatives besides calix[4]pyrroles 5.24, depending on the exact ratio and concentration of fluorinated pyrrole and acetone employed.. The successful preparation of polyfluorinated calixpyrroles is particularly important because the calix[4]pyrrole with electron withdrawing substituent on the β-pyrrolic position was found to show not only enhanced affinities for various anionic substrates but also improved selectivities for phosphate and chloride anions relative to meso-octamethylcalix[4]pyrrole 5.17. It has been found that the calix[5]pyrrole analogoue 5.25 also exhibits an affinity for chloride anion that is increased by a factor of roughly four relative to the corresponding calixpyrrole analogoue 5.24.

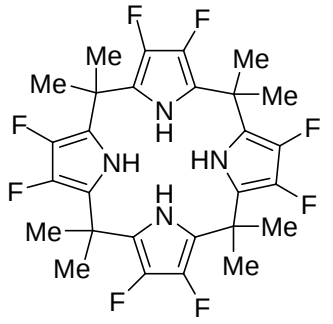

5.24

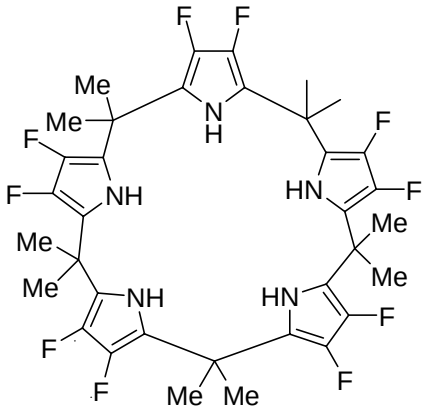

5.25

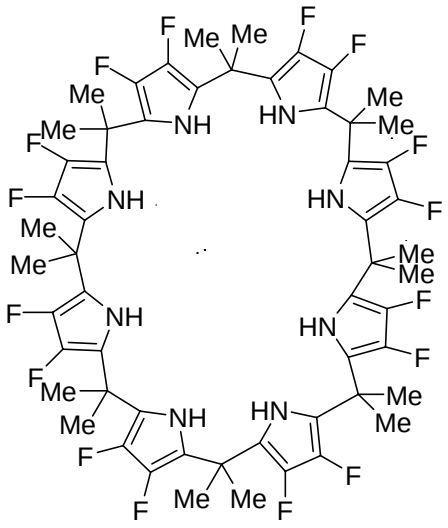

5.26

Figure 5.20. Higher ordered calixpyrrole derivatives synthesized by Sessler et al.

5.7. Calixpyrrole Based Optical Sensors

Chromogenic sensors have attracted much attention due to their capability to detect analytes by the naked eye without resorting to any expensive instruments. The development of optical sensors for biologically active molecules gives one the ability to monitor analytes during cellular processes. For example,

very effective sensors for the whole cell imaging of Ca^{2+} during cellular signaling events have been developed.

Two main approaches have been used in the production of calix[4]pyrrole based optical anion sensors (Scheme 5.3). The first of these is based on the covalent attachment of a colorimetric or fluorescent reporter group to the calix[4]pyrrole skeleton. The second strategy centers around the use of a displacement assay where a more stronger coordinating anionic analyte replaces to the initially maked calix[4]pyrrole complex involving a colored anion.

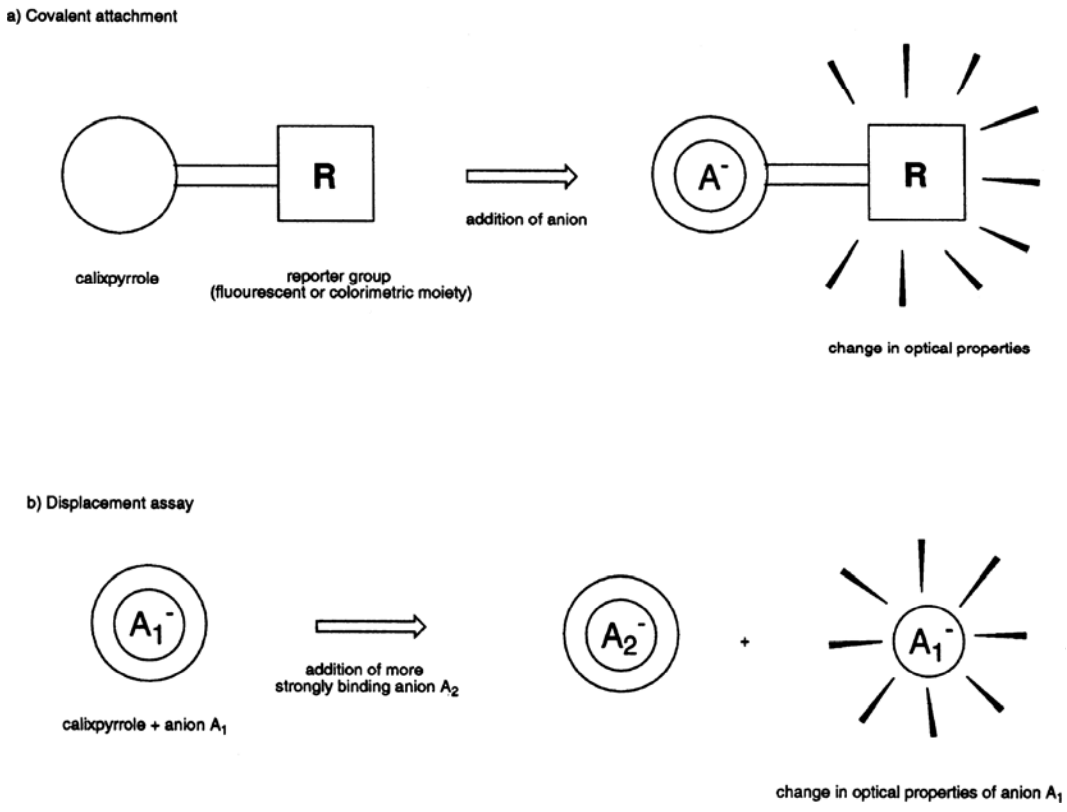

Scheme 5.3. Two approaches used to get calix[4]pyrrole based optical sensors.

Sessler et al. (1999) reported a new library of covalently linked calixpyrrole derivatives and showed that they could find application as anion sensors. The systems consisted of anthracene groups attached to the calix[4]pyrrole skeleton via amide bonds, and represented a "matched set" containing linkers of increasing length (Figure 5.21).

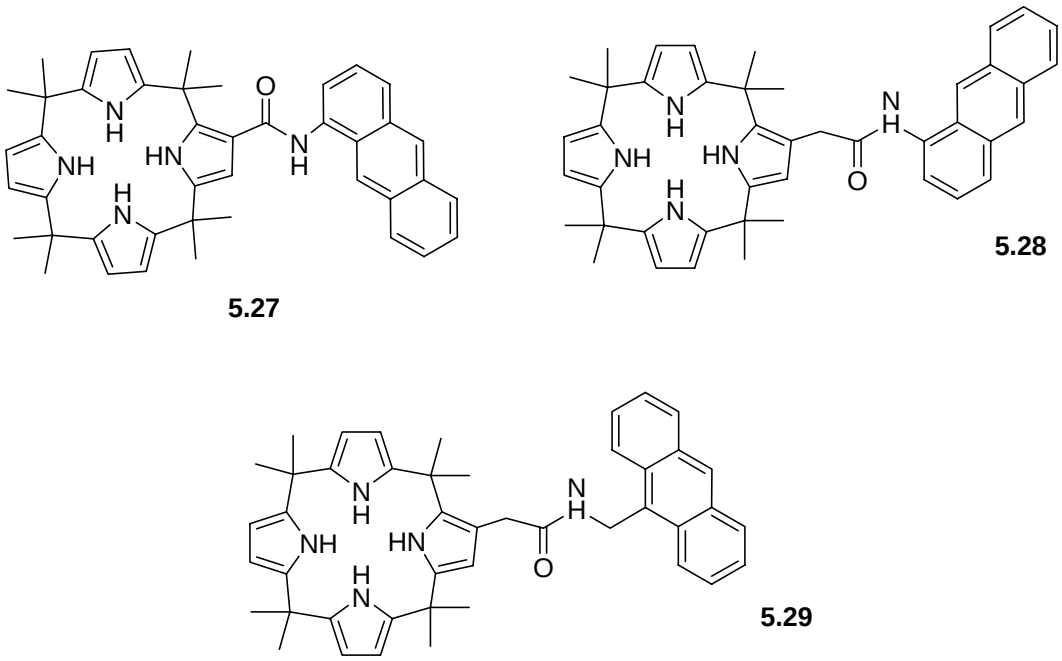

Figure 5.21. Structures of calix[4]pyrrole based optical sensors.

A year later, the same group produced compound 5.30 and 5.31 and showed significant red-shifts in the λ_{max} values and broadenings of the absorption peaks in the UV–vis spectra upon addition of anions (e.g., F^-, Cl^-, $H_2PO_4^-$) (Figure 5.22).

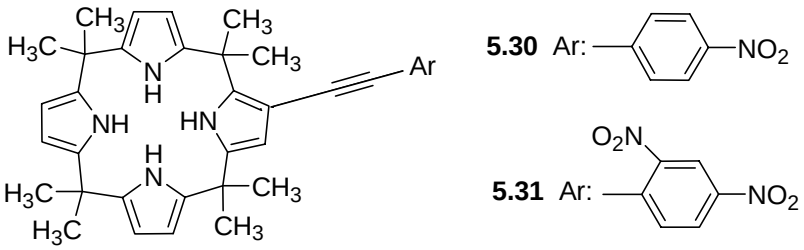

Figure 5.22. Calix[4]pyrrole derivative complexes**.**

Gale et al (1999) used the displacement-assay approach to the *meso*-octamethylcalix[4]pyrrole-4-nitrophenolate complex which is a colorimetric halide sensor system shown in Scheme 5.4. They discovered that when bound to *meso*-octamethylcalix[4]pyrrole, the 4-nitrophenolate anion loses its intense yellow colour in which the decrease in intensity was visible to the naked eye. Anions, such as fluoride, displace the 4-nitrophenolate anion from the complex thereby restoring the native absorbance of the 4-nitrophenolate anion. This was observed as a colorless to yellow colour change, with the intensity of the recovered yellow colour being dependent upon the affinity of the calixpyrrole for the added anion and the anion concentration.

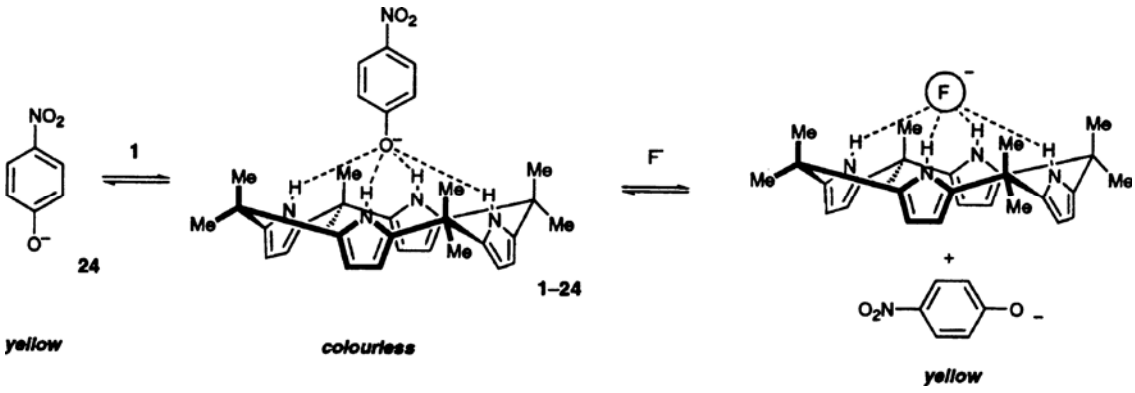

Scheme 5.4. F^- dependent equilibrium between the *meso*-octamethylcalixpyrrole-4-nitrophenolate and *meso*-octamethylcalixpyrrole-fluoride.

5.8. Aim of the Study

Anions play essential roles in biological processes, and it is believed that they participate in 70 % of all enzymatic reactions. Thus, the development of new receptors and sensors for anionic species provides a continuing challenge to the supramolecular community. One of the more attractive approaches in this field involves the construction of optical sensors and among various strategies followed, the displacement assay has proved to be highly productive. Both chromogenic and fluoregenic anion sensors were obtained by this approach. Chemical systems that respond to the presence of anions by a colour change detectable by eye are extremely rare. Colorimetric sensors do not require the use of a potentiostat or spectrometer to detect redox or optical perturbations and therefore have considerable advantages over other molecular sensors.

On the other hand, calix[4]pyrroles, being an easy-to-make class of uncharged anion receptors have shown considerable promise in the area of anion sensing and as a follow-up, novel chromogenic anion sensors based on calixpyrroles were introduced. In previous work, the formation of parent calixpyrrole-anion complex with the colored species, p-nitrophenolate anion, has been reported. That work has shown that the complex perturb the electronic properties of the anion sufficiently and produces a color change.

As part of our ongoing effort in developing novel chemosensor for anions and in attempt to apply the indicator displacement strategy in a homoditopic receptor our goal was to design the calixpyrrole dimer **6.7**. and demonstrate the chromogenic response by displacing the bound p-nitrophenolate anion by varios anions. To achieve that, we studied six different anions; the halide series, acetate and bisulfate because these anions are responsible for the regulation of a large number of biochemical processes

CHAPTER VI

MATERIALS AND METHODS

6.1. Materials

^{1}H and ^{13}C NMR spectra were recorded on a Bruker Instruments Avance Series-Spectrospin DPX-400 Ultra shield (400 MHz) High Performance digital FT-NMR spectrometer (METU NMR Laboratory). All chemical shifts are referenced to residual solvent signals previously referenced to TMS (tetramethylsilane) and splitting patterns are designated as s (singlet), d (dublet), t (triplet), q (quartet), m (multiplet), and br (broad).

Absorption spectrometry was performed using Shimadzu UV-1600PC spectrophotometer. Tetrabutylammonium p-nitrophenolate salt was prepared by the titration of methanolic solution p-nitrophenol with tetrabutylammonium hydroxide.

Chemical and solvents were purchased from Aldrich and used without further purification. Column chromatography of all the products were performed using Merck Silica Gel 60 (particle size: 0.040-0.063 mm, 230-400 mesh ASTM) pretreated with the eluent. Reactions were monitored by thin layer chromatography using fluorescent coated aluminum sheets (20x20 cm).

6.2. Synthesis of *m*-nitroacetophenone (6.2)

Concentrated H_2SO_4 (25 ml) and fuming HNO_3 (2 ml) are stirred together and cooled to 0 ^oC in an ice bath. Acetophenone (59 mmol, 6.8 ml,) is added dropwise from a dropping funnel. The stirring solution is warmed to 40 ^oC and then cooled to room temperature. Afterwards, it is poured on to finely crushed ice. At this point, the reaction mixture is filtered and washed with water. 10 % Na_2CO_3 is added to the bulky residue and the melted solid is stirred, cooled and filtered. The solid is dissolved in hot toluene (12 ml) and any solid present is decanted. Petroleum ether is added to the solution until slight turbidity is resulted. It is kept in the refrigerator overnight and the solvent is evaporated under reduced pressure.

Yield:for **(6.2)** 1.65 g (17 %).

^1H NMR (400 MHz, $CDCl_3$,) δ(ppm) 2.81 (3H, s, CH_3), 7.80 (1H, dd, Ar-H), 8.40 (1H, dd, Ar-H), 8.54 (1H, dd, Ar-H), 8.87 (1H, s, Ar-H).

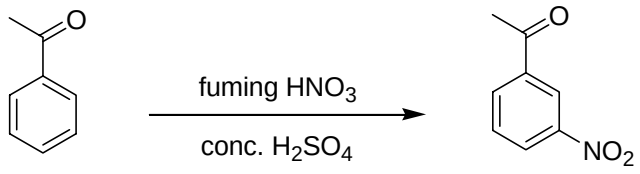

6.1 **6.2**

Figure 6.1. Synthesis of *m*-nitroacetophenone (6.2).

6.3. Synthesis of m-aminoacetophenone (6.3)

m-nitroacetophenone **(6.2)** (10 mmol, 1.65 g) is dissolved in ethanol (80 ml). $SnCl_2$ (71 mmol, 13.5 g) is added into this solution. It is heated to 70 ^oC and stirred at this temperature for 1 hour. The solution is made basic with 1 M NaOH and then extracted with diethylether. The organic phase is collected and the solvent is evaporated under reduced pressure.
Yield:for **(6.3)** 1.02 g (74 %).

^1H NMR (400 MHz, $CDCl_3$) δ(ppm) 1.65 (3H, s, CH_3), 2.82 (2H, s, NH), 5.93 (1H, d, CH), 6.35 (3H, m, CH).

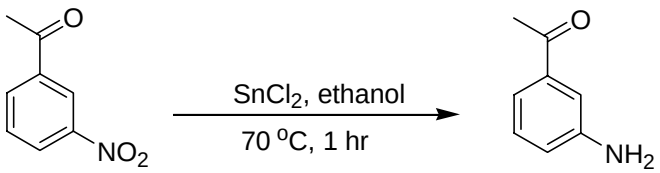

6.2 **6.3**

Figure 6.2. Synthesis of *m*-aminoacetophenone (6.3).

6.4. Synthesis of cbz-protected *m*-aminoacetophenone (6.4)

The synthesis of cbz-protected *m*-aminoacetophenone was carried out as mentioned by Sessler et al. (2000). A solution of *m*-aminoacetophenone **(6.3)** (11.1 mmol, 1.5 g) was dissolved in a mixture of CH_2Cl_2 (52.5 ml) and pyridine (1.5 ml) and was treated with 95% Cbz-chloride (benzyl chloroformate) (1.8 ml).

Then the solution was stirred at room temperature overnight. Later, the reaction mixture was first washed with water, then three times with 0.1 M HCl solution and finally with saturated $NaHCO_3$ solution. After these washings were complete, the organic solvents were removed under reduced pressure. The product was obtained by recrystallization from ethanol.

Yield for **(6.4)** 850 mg (28.3 %).

^{1}H NMR (400 MHz, $CDCl_3$) δ(ppm) 2.40 (3H, s, CH_3), 4.37 (1H, s, NH), 5.0 (2H, s, CH_2), 6.72 (1H, s, Ar-H), 7.12-7.35 (7H, m, Ar-H), 7.47 (1H, d, Ar-H).

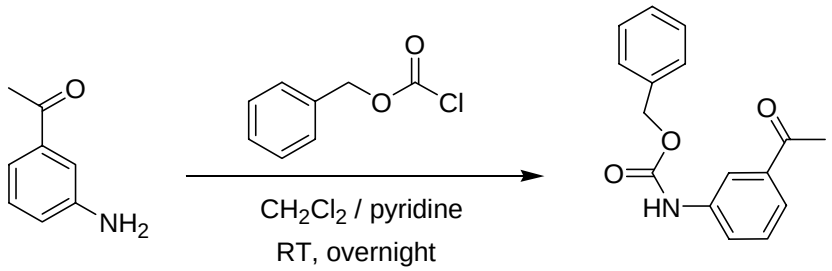

6.3 **6.4**

Figure 6.3. Synthesis of cbz-protected *m*-aminoacetophenone (6.4).

6.5. Synthesis of Calix[4]pyrrole derivative (6.5)

Calix[4]pyrrole derivative **(6.5**) was also synthesized by the procedure published by Sessler et al. (2000). A solution of Cbz-protected *m*-aminoacetophenone **(6.4)** (11.4 mmol, 3.0 g), pyrrole (43.2 mmol, 3 ml), and 3-pentanone (45.6 mmol, 4.8 ml) were dissolved in a 1:1 (v/v) mixture of CH_3OH and CH_2Cl_2 (240 ml). The solution was treated with borontrifluoride-etherate,

(BF_3: Et_2O) (28.6 mmol, 3.6 ml) and then stirred at room temperature for two days. The volume of the solution was reduced to 50 % under reduced pressure and the remaining solution was extracted with a 1:1 solvent mixture of $CHCl_3$ and saturated $NaHCO_3$. The organic layer was collected and washed with brine, dried over Na_2SO_4. The solvent, then removed using rotary evaporator. The product **(6.5)** was obtained by column chromatography (silica gel, 25 % ethylacetate in hexane, eluent).

Yield: for **(6.5)** 1.8 g (21.7 %).

^{1}H NMR (400 MHz, $CDCl_3$) δ(ppm) 0.55 (18H, m, CH_3), 1.70 (15H, m, 6xCH_2 + CH_3), 5.05 (2H, s, CH_2), 5.55-5.90 (8H, m, CH), 6.35 (1H, bs, NH), 6.45-6.65 (1H, m, CH), 6.75 (1H, m, CH), 6.90 (2H, bs, Pyr-H), 7.15-7.40 (9H, m, 7xCH + 2Pyr-H).

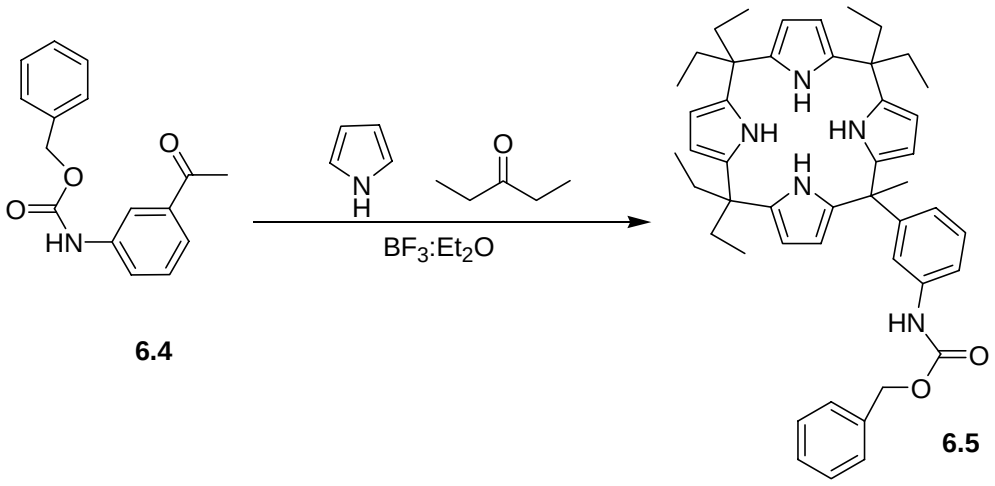

Figure 6.4. Synthesis of Calix[4]pyrrole derivative (6.5).

6.6. Synthesis of deprotected Calix[4]pyrrole (6.6)

The calixpyrrole derivative **(6. 5)** (0.138 mmol, 100 mg) was dissolved in CH_3OH (10 ml). To this solution 40% aqueous KOH solution (10 ml) was added. Then the reaction mixture was put into reflux overnight. After cooling to room temperature, the organic materials were taken up in diethylether (50 ml) and washed with water (3x50 ml). The organic phase was concentrated under reduced pressure and the residue was subjected to silica-gel column chromatography (25% ethyl acetate in hexane, eluent).. The major band corresponded to the desired product.

Yield: for **(6.6)** 65 mg (79.7 %).

^{1}H NMR (400 MHz, $CDCl_3$) δ(ppm) 0.55 (18H, t, CH_3), 1.75 (12H, q, CH_2), 3.40 (2H, bs, NH_2), 5.50-5.85 (8H, m, CH), 6.17 (1H, s, NH), 6.35 (2H, m, CH), 6.85 (3H, m, CH), 7.20 (2H, bs, NH).

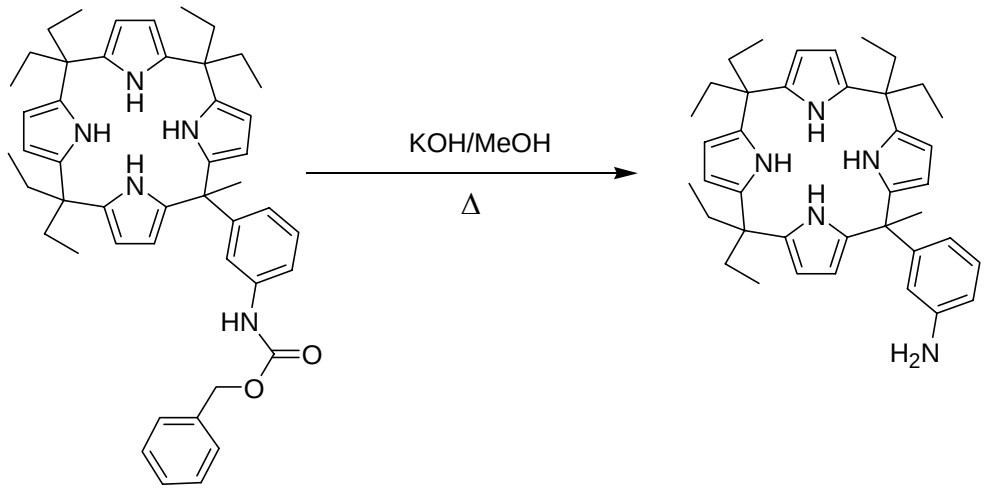

6.5 **6.6**

Figure 6.5. Synthesis of deprotected Calix[4]pyrrole (6.6).

6.7. Synthesis of Calix-dimer derivative (6.7)

Amino-modified calixpyrrole dimer **(6.6)** (0.2 mmol, 114 mg) and *iso*-phthaloyl dichloride (7.74 mmol, 16 mg), CH_2Cl_2 (3 ml) and triethylamine (0.5 ml) were stirred overnight at room temperature. Dichlomethane was added to the reaction mixture and the solution was washed with saturated $NaHCO_3$ (3x15 ml). The organic phase was collected, dried with Na_2SO4 and the solvent was removed under reduced pressure. The product was purified by silica-gel column chromatography (3 % MeOH in $CHCl_3$, eluent).
Yield: for **(6.7)** 155 mg (59 %).

^{1}H NMR (400 MHz, $CDCl_3$) δ(ppm) 1.40 (9H, s, $C(CH_3)_3$), 1.46 (9H, s, $C(CH_3)_3$), 1.75 (6H, s, CH_3), 2.63-2.97 (16H, m, CH_2), 3.81 (2H, s, CH_2), 5.44 (2H, s, CH_2), 6.93 (1H, s, Ar-H), 7.04 (1H, s, Ar-H), 7.17 (1H, s, Ar-H), 7.40 (1H, s, Ar-H), 7.49 (1H, s, Ar-H), 7.54 (1H, s, Ar-H), 7.68 (1H, s, Ar-H).

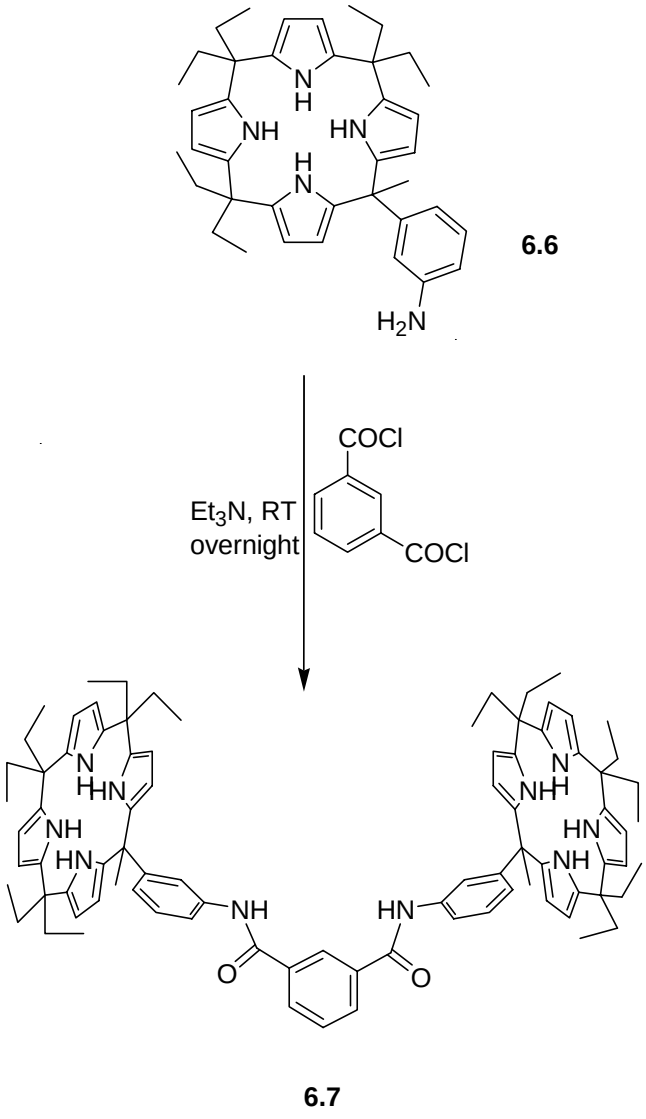

Figure 6.6. Synthesis of calix-dimer derivative (6.7).

6.8. UV-Vis Measurements

Tetrabutylammonium 4-nitrophenolate was prepared by titrating 1 equivalent of *p*-nitrophenol with 1 M solution of tetrabutylammonium hydroxide in MeOH. The solvent was then removed in vacuo and the residue triturated with

diethylether affording the nitrophenolate salt as a yellow powder. The concentrations of stock solutions of *p*-nitrophenolate anion and calixpyrrole dimer derivative **(6.7)** were $3.65x10^{-5}$ M and $7.64x10^{-4}$ M, respectively. For UV/vis measurement, dichloromethane was used as the solvent and scan range was from 350 to 550 nm. Then, increasing amounts of the calix-dimer from stock solution was added to the solution of *p*-nitrophenolate ($3.65x10^{-5}$ M). Upon addition of calix-dimer derivative, final anion concentrations were varied as $3.8x10^{-5}$, $7.6x10^{-5}$, $1.1x10^{-4}$, $1.5x10^{-4}$, $1.9\ x10^{-4}$, $2.3x10^{-4}$, $2.6x10^{-4}$, $3.0x10^{-4}$, $3.4\ x10^{-4}$, $3.8\ x10^{-4}$, $4.2\ x10^{-4}$, $4.5\ x10^{-4}$, $4.9\ x10^{-4}$, $5.3\ x10^{-4}$, $5.7\ x10^{-4}$ M.

Finally, $5x10^{-3}$ M calix-dimer derivative **(6.7)**, and $6x10^{-5}$ M nitrophenolate stock solutions were prepared for the titration experiments with different anions. The anions used were F^-, Cl^-, Br^-, I^-, AcO^- and HSO_4^-. The concentration of stock solution of tetrabutylammonium salts of these anions were $4x10^{-3}$ M. In all measurements, dimer **(6.7)** (200 µl, 0.5 mM in CH_3CN) and p-nitrophenolate (200 µl, $6x10^{-3}$ mM in CH_3CN) were kept constant and the anion concentrations varied as follows: 0, $2x10^{-4}$, $4x10^{-4}$, $8x10^{-4}$, $1.4x10^{-3}$, $2.4\ x10^{-3}$, $3.2x10^{-3}$ M.

CHAPTER VII

RESULTS AND DISCUSSION

The development of receptors for biologically important anions has emerged as a research area of great importance. One of the more attractive approaches in this field involves the construction of chemosensors. In previous work, it was discovered that the parent calix[4]pyrrole structure forms an anion complex with the colored species, *p*-nitrophenolate anion, and produces a color change that can be used as the bais for a colorimetric displacement assay. The basis of anion detection by the displacement assay involves a host-anion complex which dissociates in the presence of other anions, triggering a change in the properties of the system.

With that in mind we first,synthesized and characterized the calix[4]pyrrole complex using the combination of several literature procedures. The ^{1}H NMR results confirmed the structural identity of the compounds that are shown in appendix A.20-A.25. Then, this complex was reacted with *iso*-phthaloyl dichloride to give the desired calixpyrrole-dimer. To prove the structure of this dimer we took advantage of 2D NMR technique, specifically HMBC (Heteronuclear Multiple Bond Correlation) spectrum. This NMR is given in Appendix A.25 and shows correlations which support the proposed structure. The ^{13}C peak at 163 ppm refers to the amide carbonyl carbon and shows the different correlations at 8.23 with the singlet proton which is the aromatic one between the

two carbonyls on the iso-phthaloyl ring. The broadened peak at 7.74 most likely belongs to the amide hydrogens on the complex. Other correlations are also in accordance with the expected structure.

Later on, we studied the colorimetric properties of calix-dimer complex by using UV/vis spectroscopic techniques. In order to do that we prepared 7.64×10^{-3} M calix-dimer and 3.65×10^{-5} M tetrabutylammonium p-nitrophenolate stock solutions in dichloromethane. Addition of increasing amount calix-dimer to the stock solution of tetrabutylammonium *p*-nitrophenolate at 25 ^{o}C resulted the concentration of solution change from 3.8×10^{-5} to 5.7 $\times 10^{-4}$ and caused a significant decrease in intensity at 430 nm. This decrease in intensity was visible to the naked eye as a yellow-to-colorless color change and was attributed to the formation of the dimeric calixpyrrole-phenolate complex which is shown in Figure 7.1.

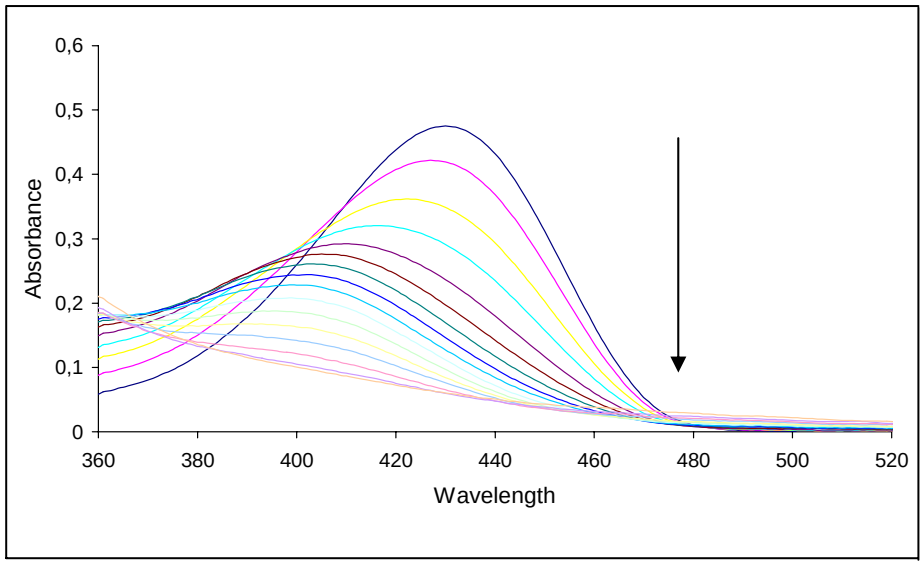

Figure 7.1. Decreasing absorbance of the p-nitrophenolate anion (3.65×10^{-5} M) upon addition of calix[4]pyrrole dimer (0, 3.8×10^{-5}, 7.6×10^{-5}, 1.1×10^{-4}, 1.5×10^{-4}, 1.9×10^{-4}, 2.3×10^{-4}, 2.6×10^{-4}, 3.0×10^{-4}, 3.4×10^{-4}, 3.8×10^{-4}, 4.2×10^{-4}, 4.5×10^{-4}, 4.9×10^{-4}, 5.3×10^{-4}, 5.7×10^{-4} M) in CH_2Cl_2.

Benesi-Hildebrand plot 1/Δ(Absorbance) versus 1/[dimer] in Figure 7.2. yields for both binding sites an avarage macroscopic dissociation constant of $4x10^{-4}$ M for 1:2 binding.

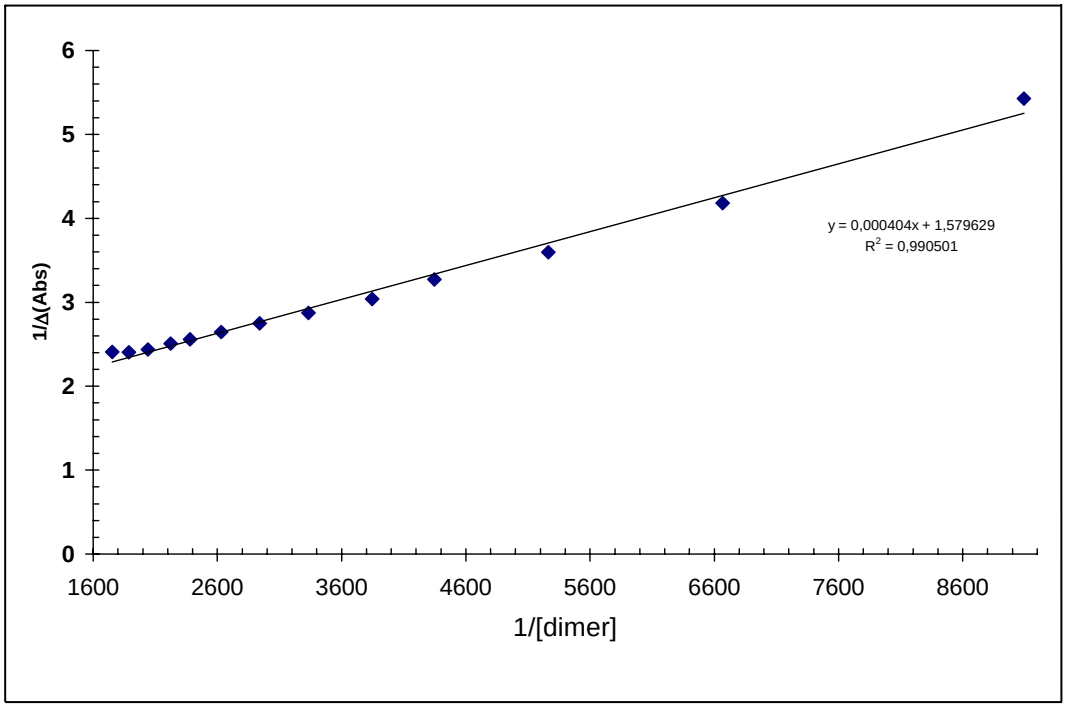

Figure 7.2. Benesi-Hildebrand plot for binding constant determination. The slope yields K_a of $2.98x10^{-3}$ M^{-1} for 1:2 complexation

We then targeted to demonstrate that a chromogenic response is obtained by displacing the bound *p*-nitrophenolate anion by various anions. We used the fluoride, chloride, bromide, iodide, bisulfate and acetate anions for this study, and prepared the solutions of tetrabutylammonium salts of each anion. In all cases the concentration was $4x10^{-3}$ M for each one. Calix-dimer and nitrophenolate stock solutions used in this part were, $5x10^{-3}$ M and $6x10^{-5}$ M, respectively. Each time of the measurement, the concentration was kept $5x10^{-4}$ M for dimeric calixpyrrole and $6x10^{-6}$ M for p-nitrophenolate in the cuvette. Addition of chloride, bromide, iodide, and bisulfate anions to dimer**:**nitrophenolate solution did not show much effect as seen in Figure 7.3-7.6 and almost no change over the background absorbance at 430 nm is detected. However; the addition of fluoride anion displaced the p-nitrophenolate anion from the complex most effectively, thereby restoring the native absorbance of the p-nitrophenolate anion. We observed this as a colorless to yellow color change. In Figure 7.7., free p-nitrophenolate peak is clearly identifiable at 0.8 mM of fluoride ion addition. As shown in Figure 7.8. the acetate was also somewhat effective in displacing p-nitrophenolate.

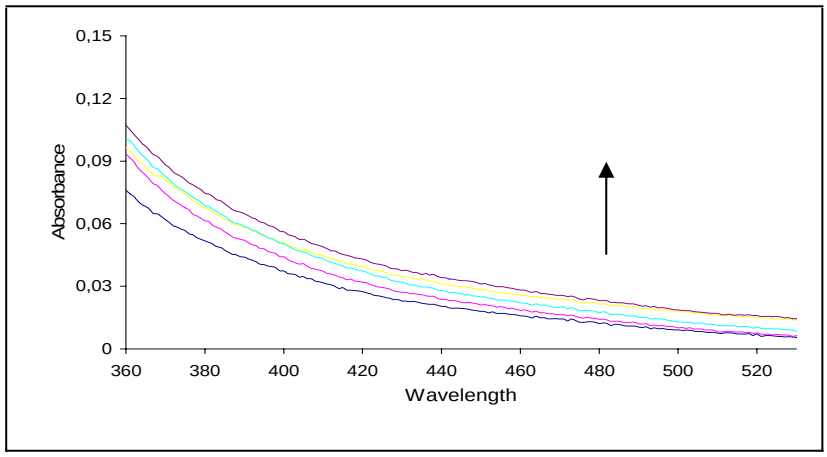

Figure 7.3. Absorption spectra of the calix[4]pyrrole dimer ($5x10^{-4}$ M) and p-nitrophenolate anion ($6x10^{-6}$ M) with $\mathbf{Cl^-}$ (0, $2x10^{-4}$, $4x10^{-4}$, $8x10^{-4}$, $3.2x10^{-3}$ M) in CH_3CN.

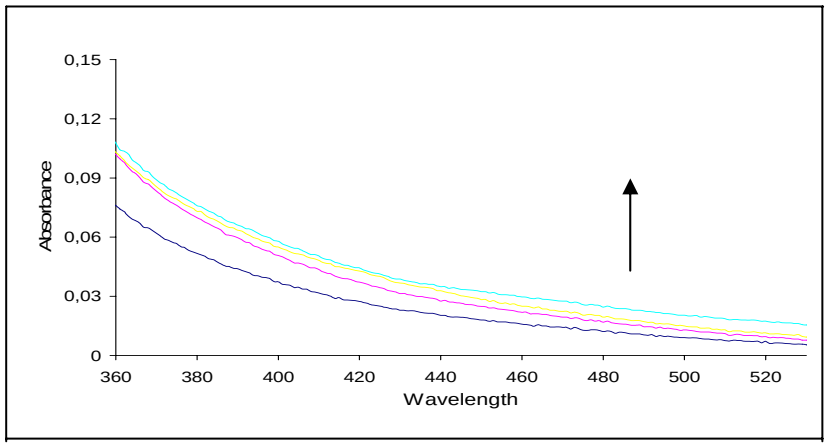

Figure 7.4. Absorption spectra of the calix[4]pyrrole dimer ($5x10^{-4}$ M) and p-nitrophenolate anion ($6x10^{-6}$ M) with $\mathbf{Br^-}$ (0, $4x10^{-4}$, $8x10^{-4}$, $3.2x10^{-3}$ M) in CH_3CN.

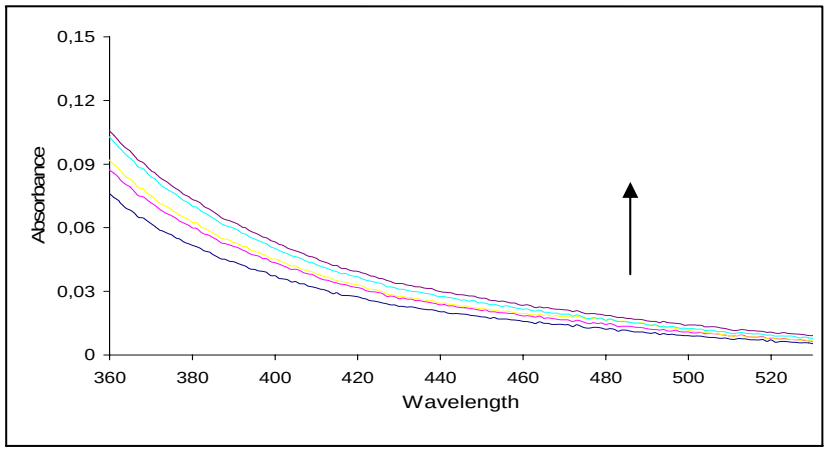

Figure 7.5. Absorption spectra of the calix[4]pyrrole dimer ($5x10^{-4}$ M) and p-nitrophenolate anion ($6x10^{-6}$ M) with $\mathbf{I^-}$ (0, $4x10^{-4}$, $8x10^{-4}$, $2.4\ x10^{-3}$, $3.2x10^{-3}$ M) in CH_3CN.

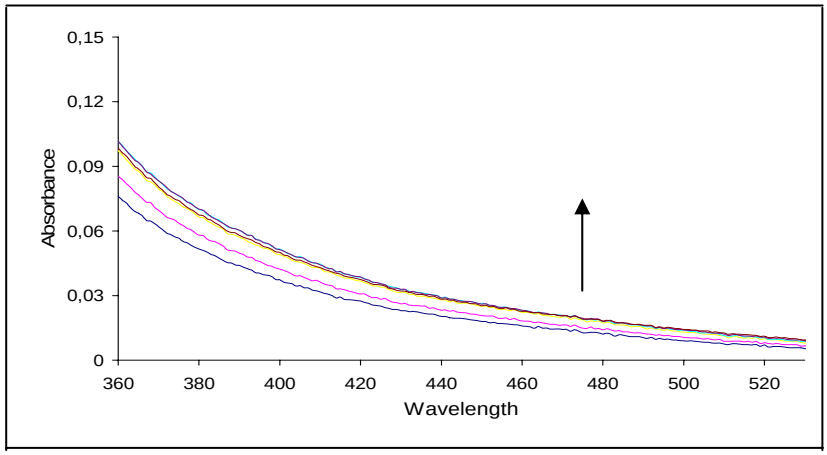

Figure 7.6. Absorption spectra of the calix[4]pyrrole dimer ($5x10^{-4}$ M) and p-nitrophenolate anion ($6x10^{-6}$ M) with $\mathbf{HSO_4^-}$ (0, $2x10^{-4}$, $4x10^{-4}$, $8x10^{-4}$, $1.4x10^{-3}$, $3.2x10^{-3}$ M) in CH_3CN.

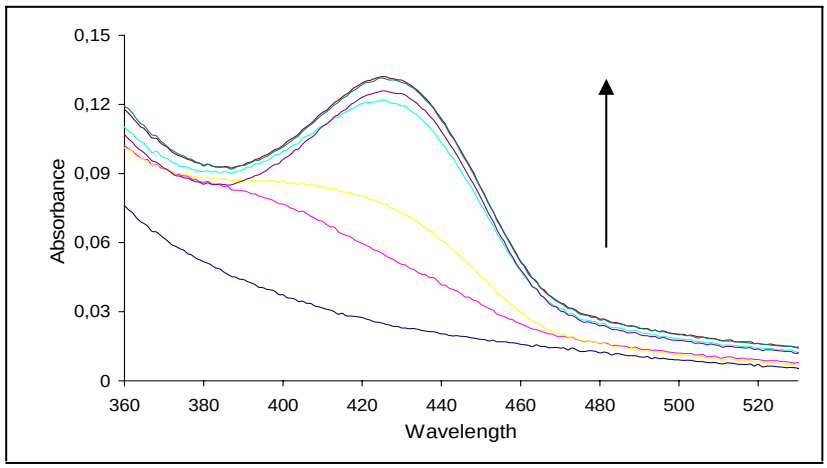

Figure 7.7. Absorption spectra of the calix[4]pyrrole dimer ($5x10^{-4}$ M) and p-nitrophenolate anion ($6x10^{-6}$ M) with $\mathbf{F^-}$ (0, $2x10^{-4}$, $4x10^{-4}$, $8x10^{-4}$, $1.4x10^{-3}$, $2.4\ x10^{-3}$, $3.2x10^{-3}$ M) in CH_3CN.

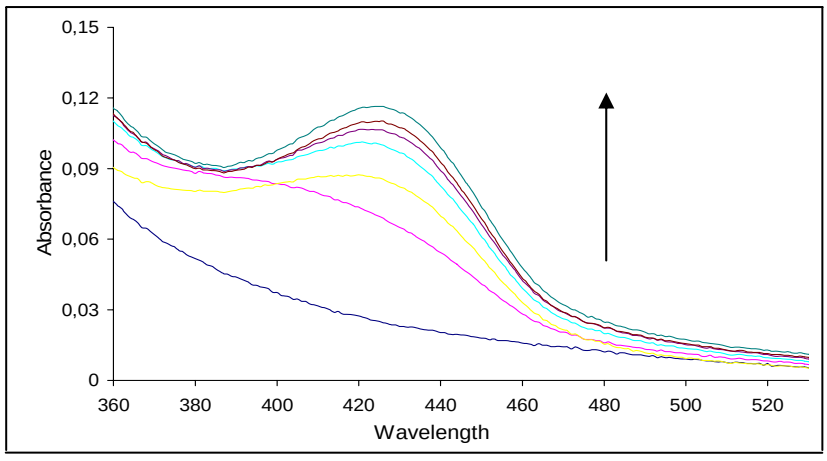

Figure 7.8. Absorption spectra of the calix[4]pyrrole dimer ($5x10^{-4}$ M) and p-nitrophenolate anion ($6x10^{-6}$ M) with $\mathbf{AcO^-}$ (0, $2x10^{-4}$, $4x10^{-4}$, $8x10^{-4}$, $1.4x10^{-3}$, $2.4\ x10^{-3}$, $3.2x10^{-3}$ M) in CH_3CN.

The Figure 7.9 illustrates the effectivity, with the intensity of the recovered yellow color, being both a relative and absolute measure of the affinity of calix-dimer for each of the analyte anion.

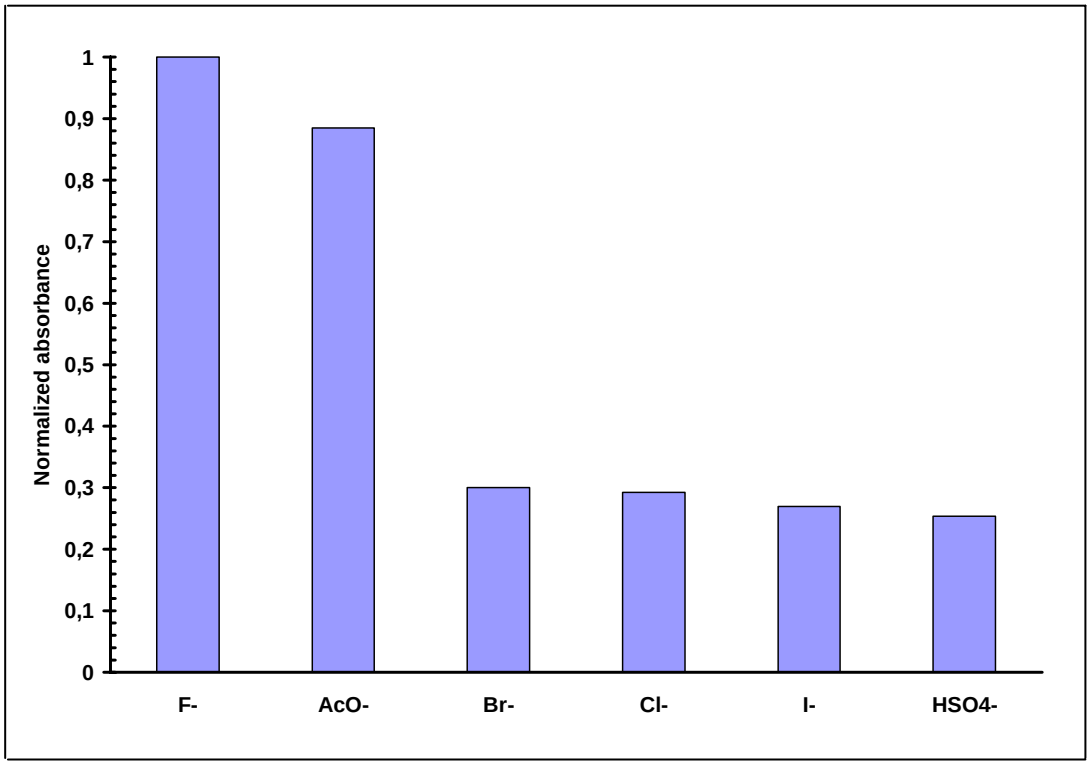

Figure 7.9. Normalized absorbance values for p-nitrophenolate displaced by the anions indicated at 3.2 mM concentration. Dimer concentration was 0.5 mM and p-nitrophenolate concentration was 6.0 μM.

CHAPTER VIII

CONCLUSION

With the aim of advancing chemical sensor technology, considerable recent attention was focused on the design of receptors that have the ability to selectively bind and sense the anion recognition event through an optical response. Colorimetric studies are essential to elucidate the specific contributions such as electrostatics, hydrogen bonding, hydrophobicity, etc.

Calix[4]pyrroles act as such effective receptors for neutral and anionic substrates and their derivatives are among the most promising molecules currently being explored for the purpose of anion binding. Our study covers the synthesis and characterization of a novel dimeric calixpyrrole anion sensor (6.7) which recognizes effectively and selectively the fluoride anion over other anions. In addition, this dimer shows reasonably high affinity toward the biologically important acetate anion.

In the first part of the study, a calix[4]pyrrole derivative was synthesized. By using an appropriate coupling procedure, we succeeded in synthesizing the dimeric calixpyrrole.

In the second part, we first studied the colorimetric properties of this dimer and demonstrated the formation of the calix-dimer:p-nitrophenol complex, then

showed that a chromogenic response is obtained by displacing the bound p-nitrophenolate anion by various anions.

The present finding serves to illustrate that calixpyrrole dimer may be used as an anion sensor that can report the presence of anions by means of a colour change.

While fluoride and chloride ions themselves are have significant biochemical implications, selective binding of biologically important anions such as ATP and glutamate might be expected using appropriately designed calixpyrrole dimers as the anion recognition elements.

As a result, new and more application oriented chemosensors are sure to follow this pioneering work.

REFERENCES

Adrian, J. C. Jr.; Wilcox, C. S. *J. Am. Chem. Soc*. **1989,** 111, 8055.

Alcalde, E.; Alvarez-Rua, C.; Garcia-Granda, S.; Mesquida, N.; Perez-Garcia, L. *Chem. Commun.*, **1999,** 295.

Allen, W. E.; Gale, P. A.; Brown, C. T.; Lynch, V ; Sessler, J. L.; *J. Am. Chem. Soc.*, **1996,** 118, 12471.

Anzenbacher, P.; Jursikova, K.; Sessler, J. L. *J. Am. Chem. Soc.*, **2000,** 122, 935.

Aoyagi, S.; Tanaka, K.; Takeuchi, Y. *J. Chem. Soc.Perkin Trans. 2* **1994,** 1549.

Azuma, Y.; Newcomb, M. *Organometallicsic*, **1984,** 3, 9.

Baeyer, A. *Ber. Dtsch. Chem. Ges*., 1**886**, 19, 2184.

Barrett, G.; Fanni, S.; Marrs, D.; Vetrogon, V.; Wechsler, S. *J. Chem. Soc. Perkin Trans 2* **1995**, 453.

Beer, P. D.; Bernhardt, P. V. *J. Chem. Soc. Dalton Trans.*, **2001,** 1428.

Bell, T. W.; Liu, J. *J. Am. Chem. Soc.* **1988,** 110, 3673.

Boger, J.; Knowles, J. R. *Ciba. Found. Symp. Mol. Interact. Act. Proteins* **1978**, 60, 225.

Boseggia, E.; Gatos, M.; Palumbo, M.; Zagotto, G.; Sissi, C.; Tecilla, P.; Moro, S., Tonellato, U.; Lucatello, L.; Mancin, F. *J. Am. Chem. Soc.* **2004.**

Brerslow, D.; Canary, J. W.; Lajmi, A. R. *J. Am. Chem. Soc.* **1980**, 102, 421.

Breslow, R. *Acc. Chem. Res*. **1995**, 28, 146.

Breslow, R. *Science* **1982**, 218, 532.

Breslow, R.; Overman, L. E. *J. Am. Chem. Soc.* **1970**, 92, 1075.

Breslow, R.; Singh, S. *Bioorg. Chem*. **1998**, 16, 408.

Breslow, R.; Zhang, B. *J. Am. Chem. Soc.* **1992**, 114, 5882.

Brown, C. H.; Weissman, P. M .; Yoon, N. M. *J. Am. Chem. Soc*. **1966,** 87, 1458.

Brown, W. H.; Hutchinson, B. J.; MacKinnon, M. H. *Can.J. Chem.*, **1971**, 49, 4017.

Bugg, T. *An introduction to enzyme and co-enzyme chemistry* **1997**, Blackwell Science Ltd.

Chapman, W. H.; Breslow, R. *J. Am. Chem. Soc.* **1995**, 117, 5851.

Chelintzev, V. V.; Tronov, B. V. *J. Russ. Phyys. Chem. Soc*., 1**955**, 77, 3340.

Chin, J. *Acc. Chem. Res*. **1991**, 24, 145.

Chin, J. *Current Opinion in Chem. Biol.* **1997**, 1, 514.

Chin, J.; Wall, M.; Hynes, R. C. *Angew. Chem. Int. Ed. Engl*. **1993**, 32, 1633.

Choi, K. H.; Hamilton, A. D. *J. Am. Chem. Soc.* **2001,** 123, 2456.

Czarnik, A. W. ACS Symposium Series 538, American Chemical Society, **1993**, 104.

D'Souza, V. T.; Bender, M. L. *Acc. Chem. Res*. **1987**, 20, 146.

Dennstedt, M. *Ber. Dtsch. Chem. Ges*., 1**890**, 23, 1370.

Dennstedt, M.; Zimmermann, J. *Ber. Dtsch. Chem. Ges*., 1**886**, 19, 2189.

Dennstedt, M.; Zimmermann, J. *Chem. Ber.*, 1**887**, 20, 850.

Dugas, H. *Bioorganic Chemistry-A Chemical Approach to Enzyme Action* **1980**, 3 rd edition.

Fersht, A. *Enzyme Structure and Mechanism* **1985**, New York

Galan, A.; Andreu, D.; Echavarren, A. M.; Prados, P.; Mendoza, J. *J. Am. Chem. Soc.* **1992,** 114, 1511.

Gale, P. A.; Anzenbacher, P.; Sessler, J. L. *Coord. Chem. Rev.*, **2001,** 222, 57.

Gale, P. A.; Hursthouse, M. B.; Light, M. E.; Sessler, J. L.; Zimmerman, R. S.; Warriner, C. N. *Tetrahedron Letters*, **2001,** 42, 6759.

Gale, P. A.; Sessler, J. L.; Allen, W. E.; Tvermoes, N. A.; Lynch, V. *Chem. Commun.*, **1997,** 667.

Gale, P. A.; Sessler, J. L.; Kral, V. *Chem. Commun.*, **1998,** 1.

Gale, P. A.; Sessler, J. L.; Kral, V.; Lynch, V. .*J. Am. Chem. Soc.*, **1996,** 118, 5140.

Gale, P. A.; Twyman, L. J.; Handlin, C. I.; Sessler, J. L. *Chem. Commun.*, **1999,** 1851.

Garrett, R. H.; Grisham, C. M. *Biochemistry* **1995**, Saunders Coll.

Gokel, G. W. *Advances in Supramolecular Chemistry* **1999**, JAI Press Ltd.

Göbel, M. W. *Angew. Chem. Int. Ed. Engl*. **1994**, 33, 1141.

Grummit, O.; Buck, A. *Organic Syntheses*, CV 3, 195.

Gunnlaugsson, T.; Davis, A. P.; O'Brien, J. E.; Glynn, M. *Organic Letters*, **2002**, 2449.

Ihm, H.; Yun, S.; Kim, H. G.; Kim, J. K.; Kim, K. S. *Organic Letters*, **2002,** 295

Inoue, Y.; Hakushi, T.; Liu, Y. *J. Am. Chem. Soc.* **1993,** 115, 475.

Kelley, T. R.; Kim, M. H. *J. Am. Chem. Soc.* **1994,** 116, 7072.

Kelly, T. R.; Maguire, M. P. *J. Am. Chem. Soc.* **1987,** 109, 6549.

Kimura, E.; Aoki, S.; Koike, T.; Shiro, M. *J. Am. Chem. Soc*. **1997,** 119, 3068.

Kimura, E.; Aoki, S.; Shiro, M. *J. Am. Chem. Soc.* **1997,** 119, 3068.

Koçak, M.; Gürek, A.; Gül, A.; Bekaroğlu, Ö. *Chem. Ber.* **1994**, 127, 355.

Koike, T.; Inoue, M.; Kimura, E.; Shiro, M. *J. Am. Chem. Soc.* **1996**, 118, 3091.

Komiyama, M.; Matsumara, K.; Matsumoto, Y. *Chem. Commun*. **1992**, 640.

Laidler, K. J. *The Chemical Kinetics of Enzyme Action* **1958**, Oxford.

Lakowicz, J. R.; Szmacinski, H.; Nowaczyk, K.; Johnson, M. L. *Cell Calcium*, **1992**, 13, 131.

Lee, D. H.; Lee, H. Y.; Lee, K. H.; Hong, J. *Chem. Commun.*, **2001,** 1188.

Lee, D. H.; Lee, K. H.; Hong, J. *Organic Letters*, **2001,** 1, 5.

Lehn J.M. *Supramolecular Chemistry: Concepts and Perspectives* **1995,** VCH.

Lehn, J. M. *Angew. Chem. Int. Ed. Engl*. **1988**, 27, 89.

Marquez, C.; Hudgins, R. R. ; Nau, W. M. *J. Am. Chem. Soc.* **2004.**

Matthews, J. C. *Fundamentals of Receptor, Enzyme, and Transport Kinetics* **1993**, CRC Press.

Minta, A.; Tsien, R. Y. *J. Biol. Chem*. **1989**, 264, 19449.

Miyaji, H.; Anzenbacher, P.; Sessler, J. L.; Bleasdale, E. R.; Gale, P. A. *Chem. Commun.*, **1999,** 1723.

Miyaji, H.; Sato, W.; Sessler, J. L. *Angew. Chem. Int. Ed. Engl.* **2000,** 39, 1777.

Miyaji, H.; Sato, W.; Sessler, J. L. *Tetrahedron Letters*, **2000,** 41, 1369.

Molenveld, P.; Kapsabelis, S.; Engbersen, J. F. J.; Reinhoudt, D. N. *J. Am. Chem. Soc.* **1997**, 119, 2948.

Molenveld, P.; Kooijman, H.; Engbersen, J. F. J.; Spek, A. L. *J. Am. Chem. Soc.* **1998**, 120, 6726.

Moss, B. *Chem. Ind.*, **1996,** 407.

Murakami, Y.; Kikuchi, J.; Hisaeda, Y.; Hayashida, O. *Chem. Rev.* **1996,** 96, 721.

Noodleman, L.; Lovell, T.; Han, W.; Li, J.; Himo, F. *J. Am. Chem. Soc.* **2003.**

Northrup, J. H.; Kunitz, M. *J. Gen. Physiol*. **1932,** 16, 267.

Nowick, J. S.; Ballester, P.; Ebmeyer, F.; Rebek, J. Jr. *J. Am. Chem. Soc*. **1990,** 112, 8902.

Park, C. H.; Simmons, H. E. *J. Am. Chem. Soc.* **1968,** 90, 2431.

Park, T. K.; Feng, Q.; Rebek, J. Jr. *J. Am. Chem. Soc.* **1992,** 114, 4529.

Parkin, G. *Chemical Reviews*. **2004**.

Pascal, R. A.; Spergel, J.; Engbersen, D. V. *Tetrahedron Letters*, **1986,** 27, 4099.

Price, N. C.; Stevens, L. *Fundamentals of Enzymology* **1982**, New York.

Ragunathan, K. G.; Schneider, H. *Angew. Chem. Int. Ed. Engl.* **1996,** 35, 1219.

Rebek, J. Jr. *Angew. Chem. Int. Ed. Engl.* **1990,** 29, 245.

Rebek, J. Jr**.** *J. Am. Chem. Soc.* **1984,** 17, 258.

Rebek, J. Jr. *Science* **1987**, 235, 1478.

Robyt, J. F.; White, B. J. *Biochemical Techniques: Theory and Practice* **1987**, Waveland Press, Inc.

Rojas, C. M.; Rebek, J. Jr. *J. Am. Chem. Soc.* **1998,** 120, 5120.

Sato, K.; Arai, S.; Yamagishi, T. *Tetrahedron Letters*, **1999,** 40, 5219.

Sato, W.; Miyaji, H.; Sessler, J. L. *Tetrahedron Letters*, **2000,** 41, 6731.

Schmidtchen, F. P. *Chem. Ber.* **1980,** 113, 864.

Sessler, J. L.; Anzenbacher, P.; Shriver, J. A.; Jursikova, K.; Lynch, V. M.; Marquez, M. *J. Am. Chem. Soc.*, **2000,** 122, 12061.

Shimizu, K. D.; Dewey, T. M.; Rebek, J. Jr. *J. Am. Chem. Soc.* **1994,** 116, 5145.

Shipps, ; Rebek, J. Jr. *Tetrahedron Letters.* **1994,** 35, 6823.

Spiro, T.G. *Zinc Enzymes* **1991**, Krieger.

Steed, J. W.; Atwood, J. L. *Supramolecular Chemistry* **2000**, Wiley.

Takasaki, B. K.; Chin, J. *J. Am. Chem. Soc.* **1993,** 115, 9337.

Tamao, K.; Hayashi, Y.; Ito, Y. *Organomet. Chem.*, **1996,** 506, 85.

Tecilla, P.; Chang, S. K.; Hamilton, A. D. *J. Am. Chem. Soc*. **1990,** 112, 9586.

Thompson, R. B.; Peterson, D.; Mahoney, W.; Cramer, M.; Herman, P.; Fierke, C. *J. of Neuroscience Methods*. **2002**, 63.

Tomapatanaget, B.; Tuntulani, T. *Tetrahedron Letters*, **2001,** 42, 8105.

Turner, B.; Botoshansky, Y.; Eichen, Y. *Angew. Chem. Int. Ed. Engl.* **1998,** 37, 2475.

Valeur, B. *Molecular Luminescence Spectroscopy, Methods and Applications* **1993**, Wiley.

Valiyaveettil, S.; Engbersen, J. F. J.; Verboom, W.; Reinhoudt, D. N. *Angew. Chem. Int. Ed. Engl.* **1993,** 105, 942.

Volbeda, A.; Lahm, A.; Sakiyama, F.; Suck, D. *EMBO J.* **1991,** 10, 1607.

Vögtle, F. *Supramolecular Chemistry* **1991**, Wiley.

Walkup, G. K.; Burdette, S. C.; Lippard, S. P.; Tsien, R. Y. *J. Am. Chem. Soc.* **2000,** 122, 5644.

Whitesides, G. M. *Angew. Chem. Int. Ed. Engl*. **1990**, 29, 1209.

Wolfe, J. ; Nemeth, D. ; Costero, A. ; Rebek Jr., J. *J. Am. Chem. Soc*. **1988,** 110, 983.

Wolfe, J.; Nemeth, D.; Costero, A.; Rebek, J. Jr. *J. Am. Chem. Soc.* **1988,** 110, 983.

Wolfe, J.; Nemeth, D.; Costero, A.; Rebek, J. Jr**.** *J. Am. Chem. Soc.* **1988,** 110, 983.

Worm, K.; Schmidtchen, F. P.; Schier, A.; Schafer, A.; Hesse, M. *Angew. Chem. Int. Ed. Engl.* **1994,** 33, 327.

Wu, F.; Li, Z.; Wen, Z.; Jiang, Y. *Organic Letters*, **2002**, 1109.

Yashiro, M.; Ishikubo, A.; Komiyama, M. *Chem. Commun*. **1997**, 83.

Zimmerman, S. C.; Wu, W. *J. Am. Chem. Soc.* **1989,** 111, 8054.

APPENDIX

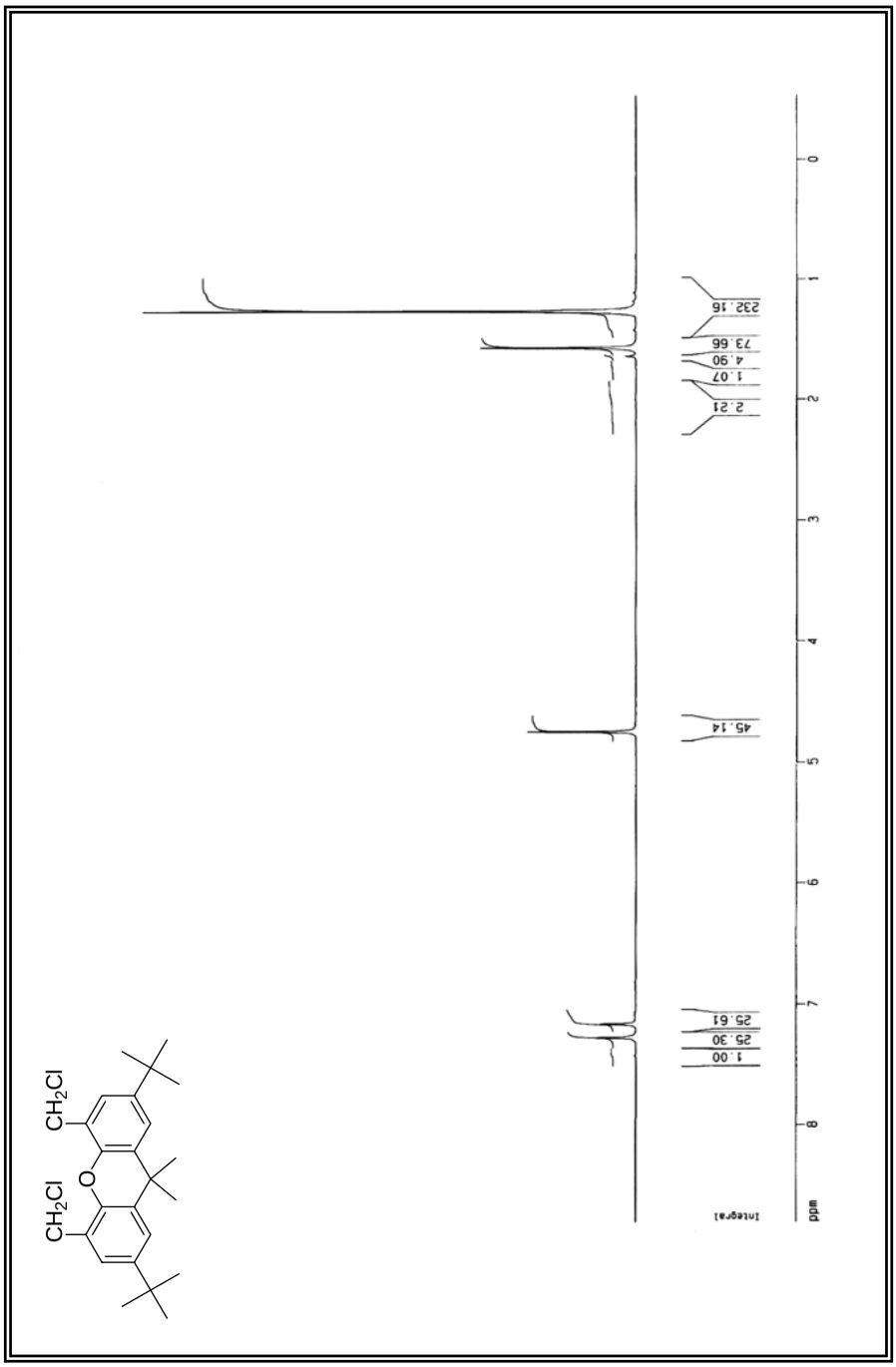

Figure A.1. ^{1}H-NMR spectrum of (2.1).

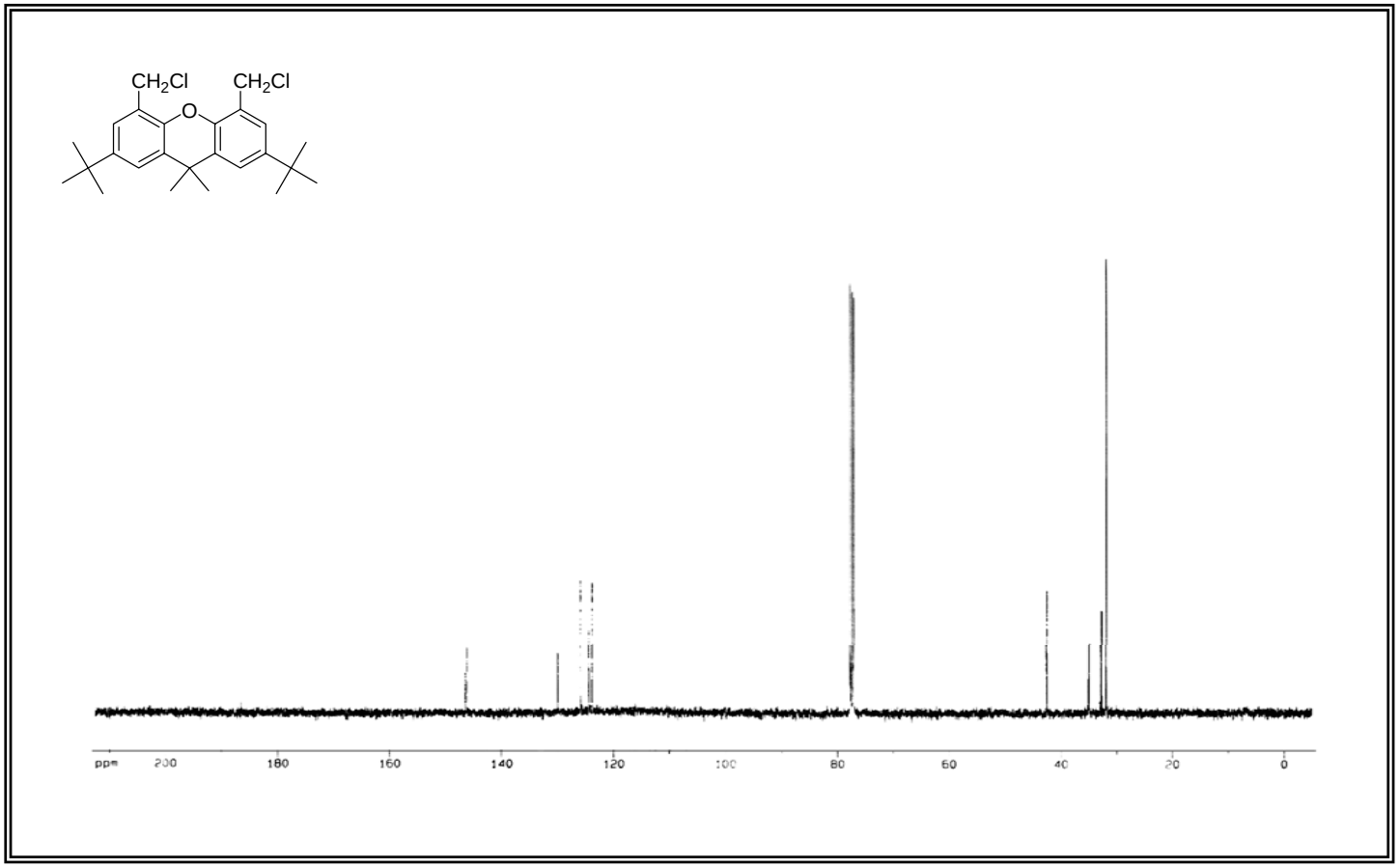

Figure A.2. ^{13}C-NMR spectrum of (2.1).

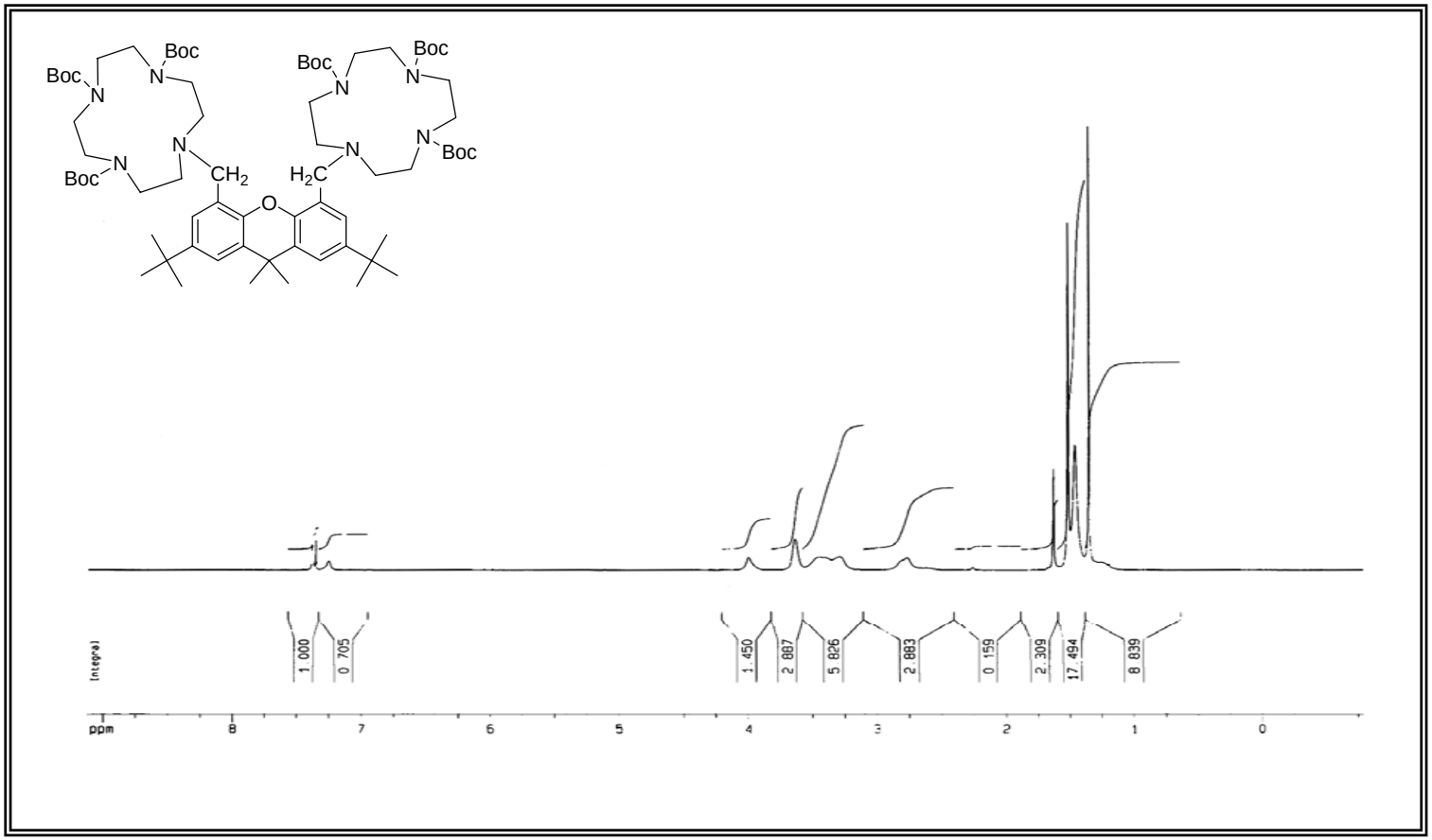

Figure A.3. ^{1}H-NMR spectrum of (2.5).

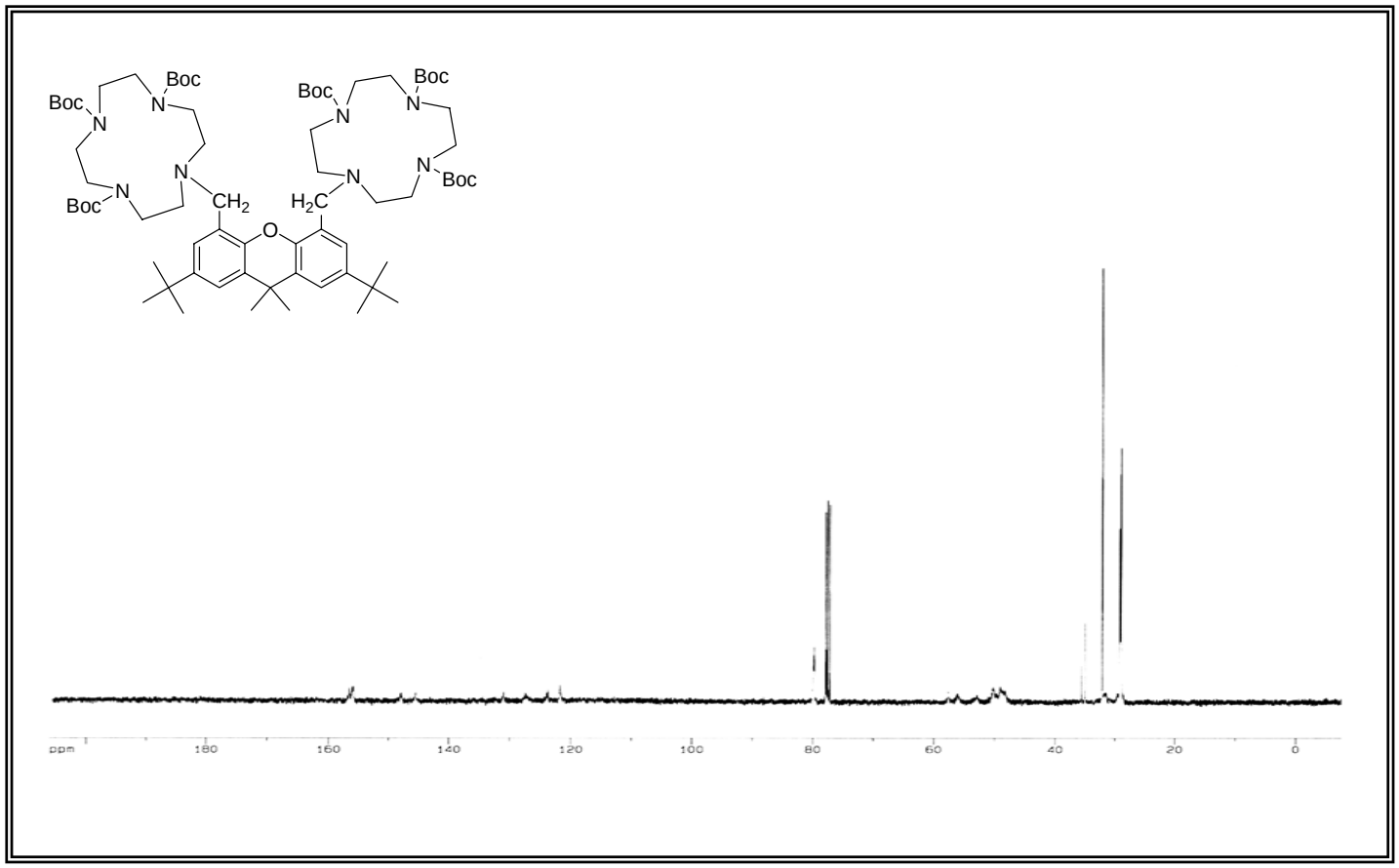

Figure A.4. ^{13}C-NMR spectrum of (2.5).

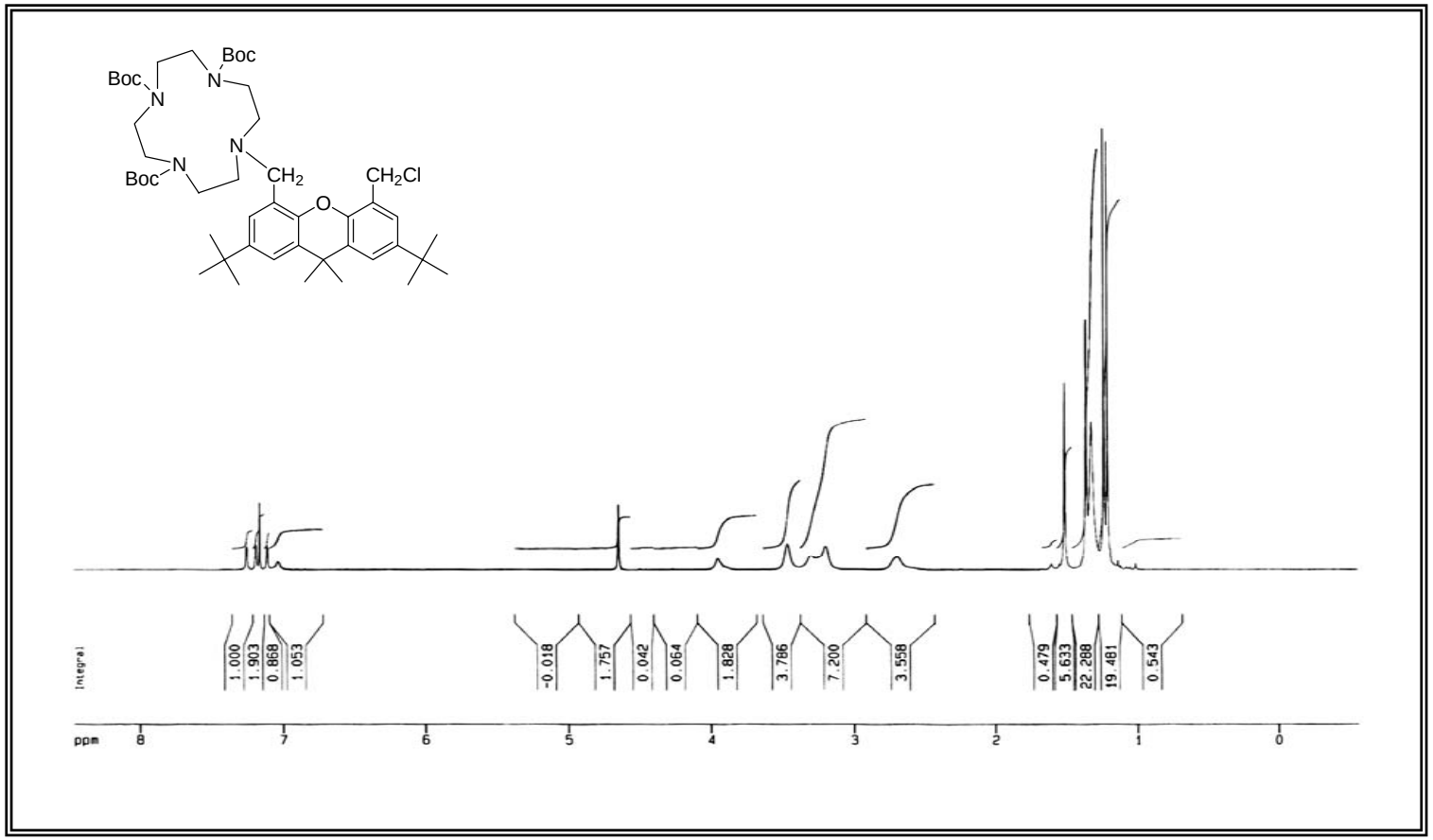

Figure A.5. ^{1}H-NMR spectrum of (2.6).

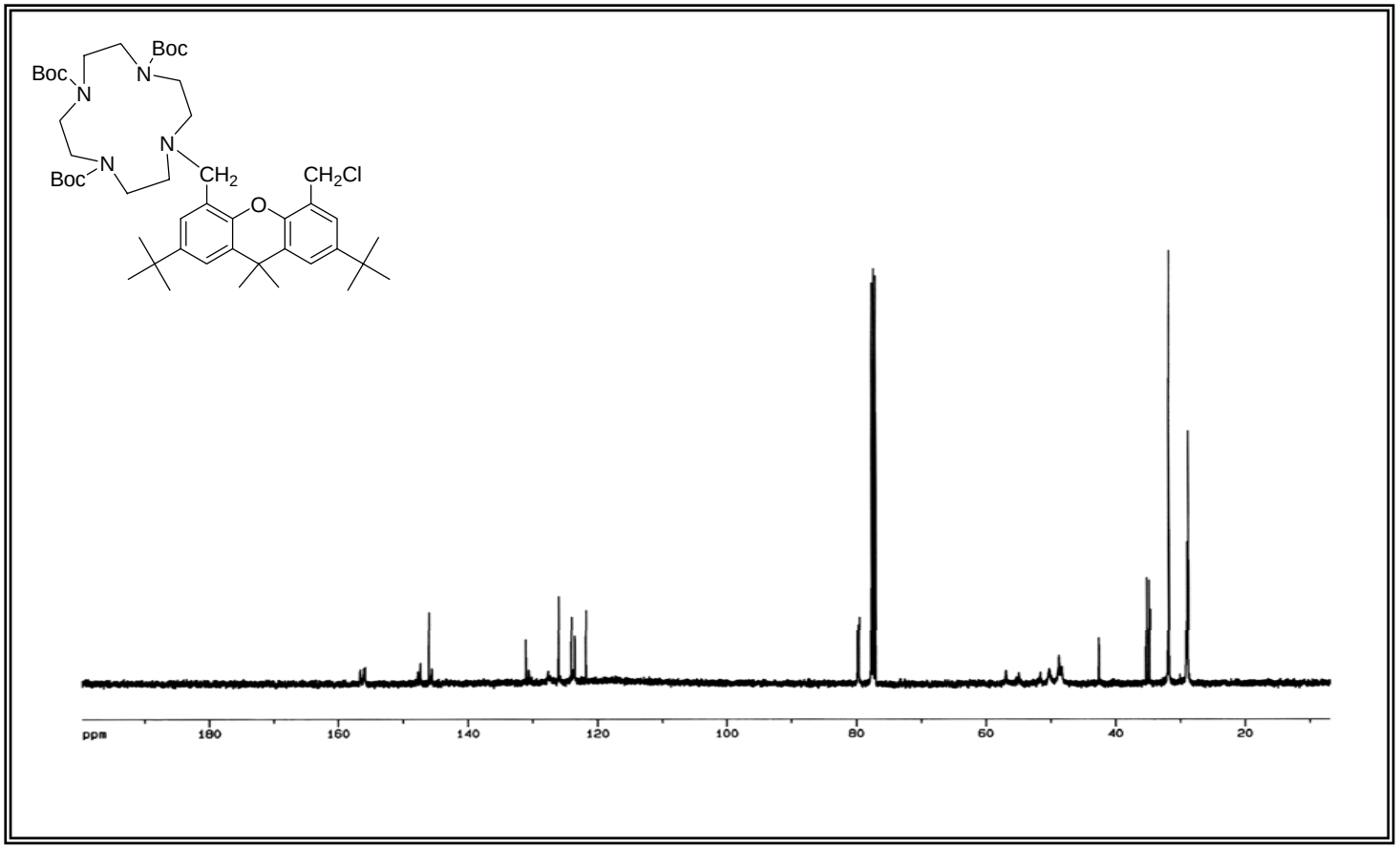

Figure A.6. ^{13}C-NMR spectrum of (2.6).

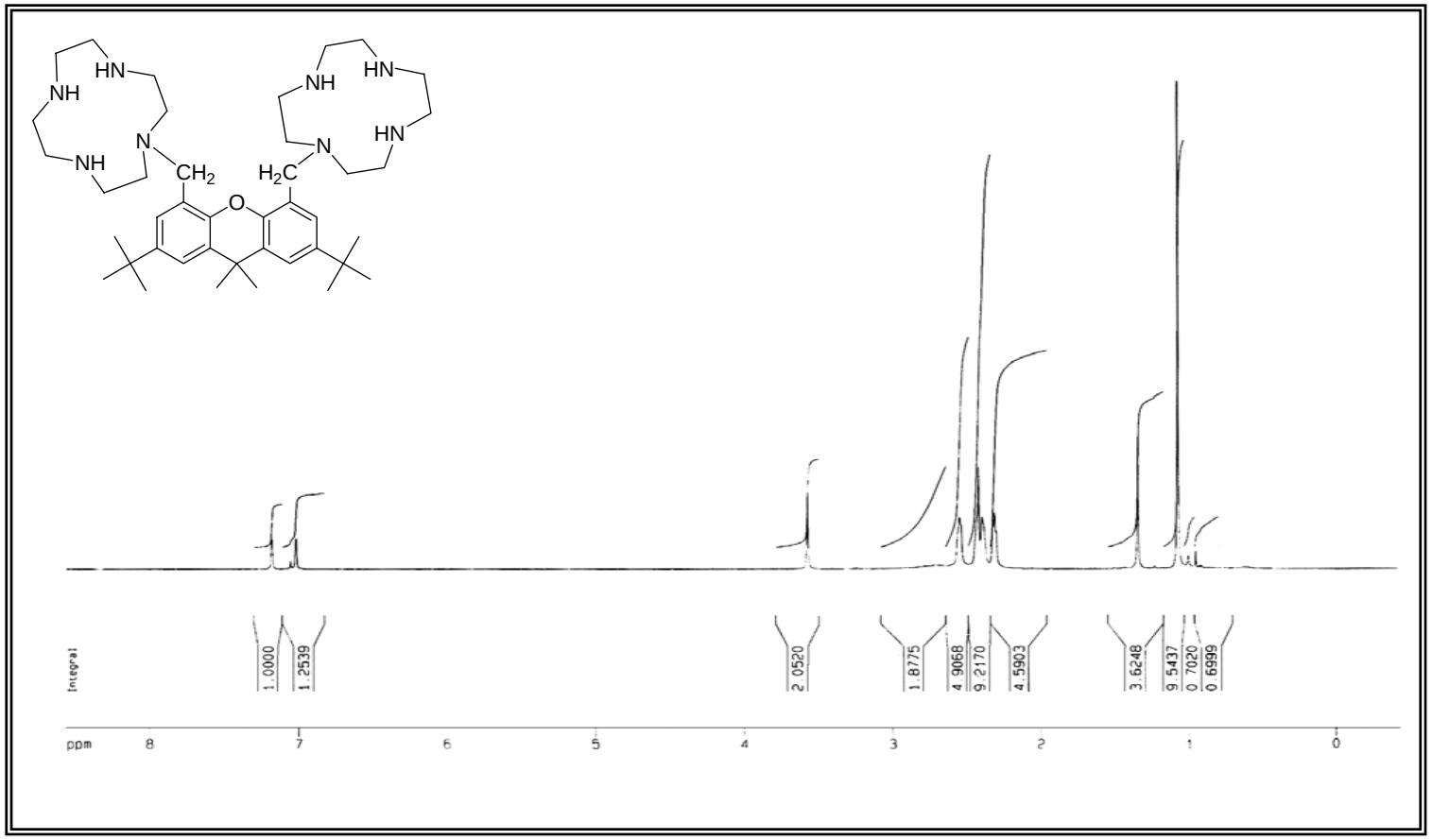

Figure A.7. ^{1}H-NMR spectrum of (2.7).

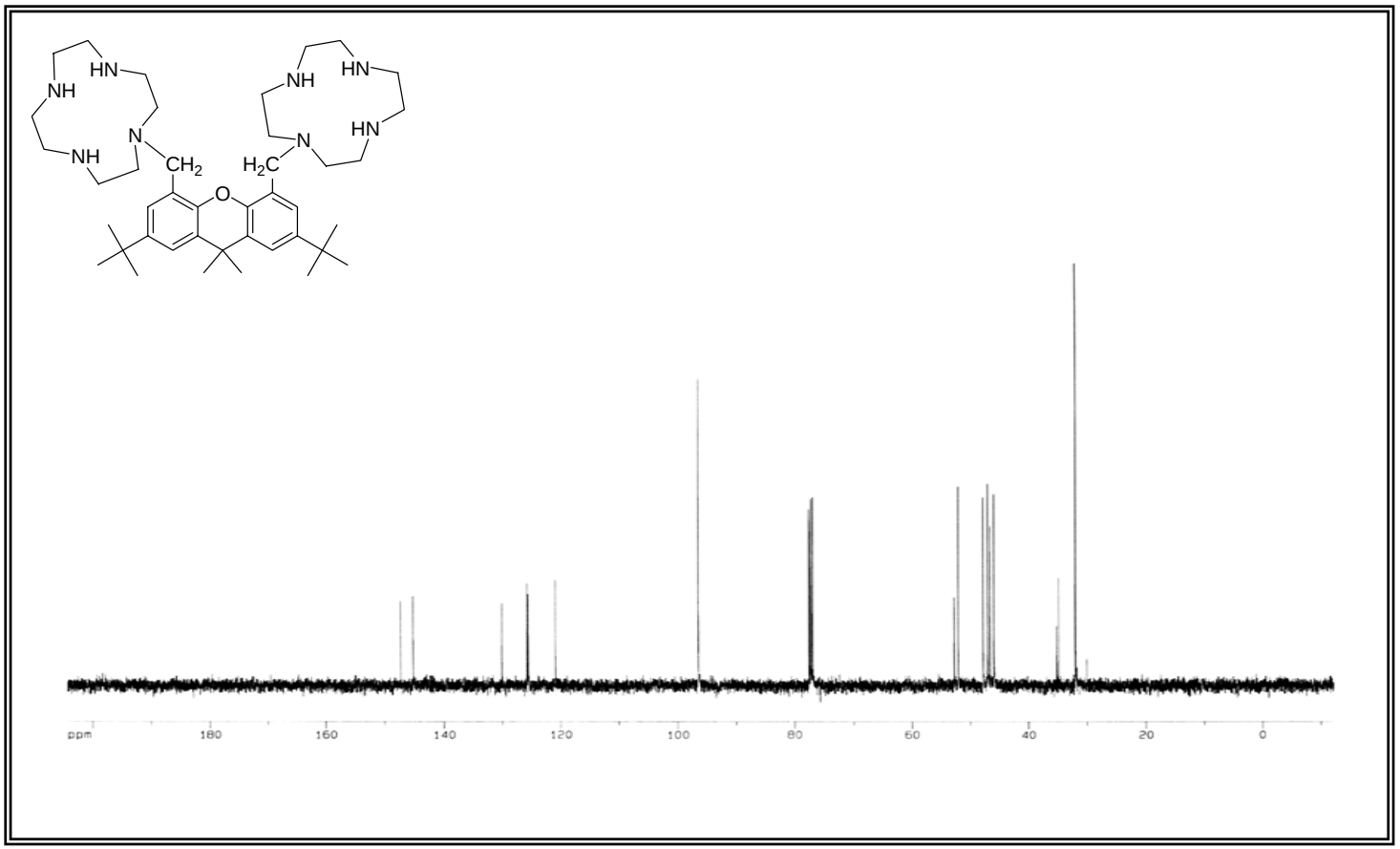

Figure A.8. ^{13}C-NMR spectrum of (2.7).

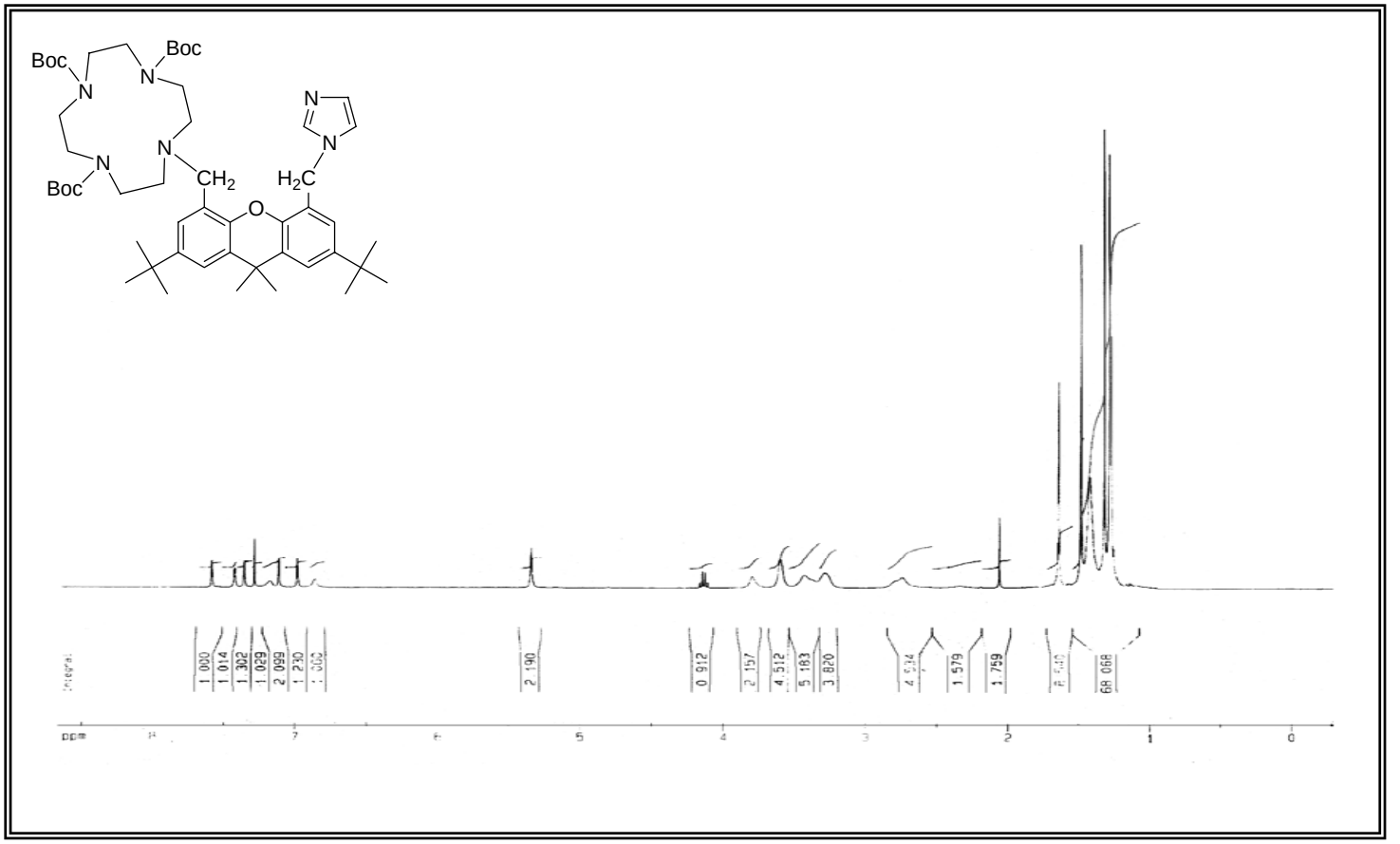

Figure A.9. ^{1}H-NMR spectrum of (2.8).

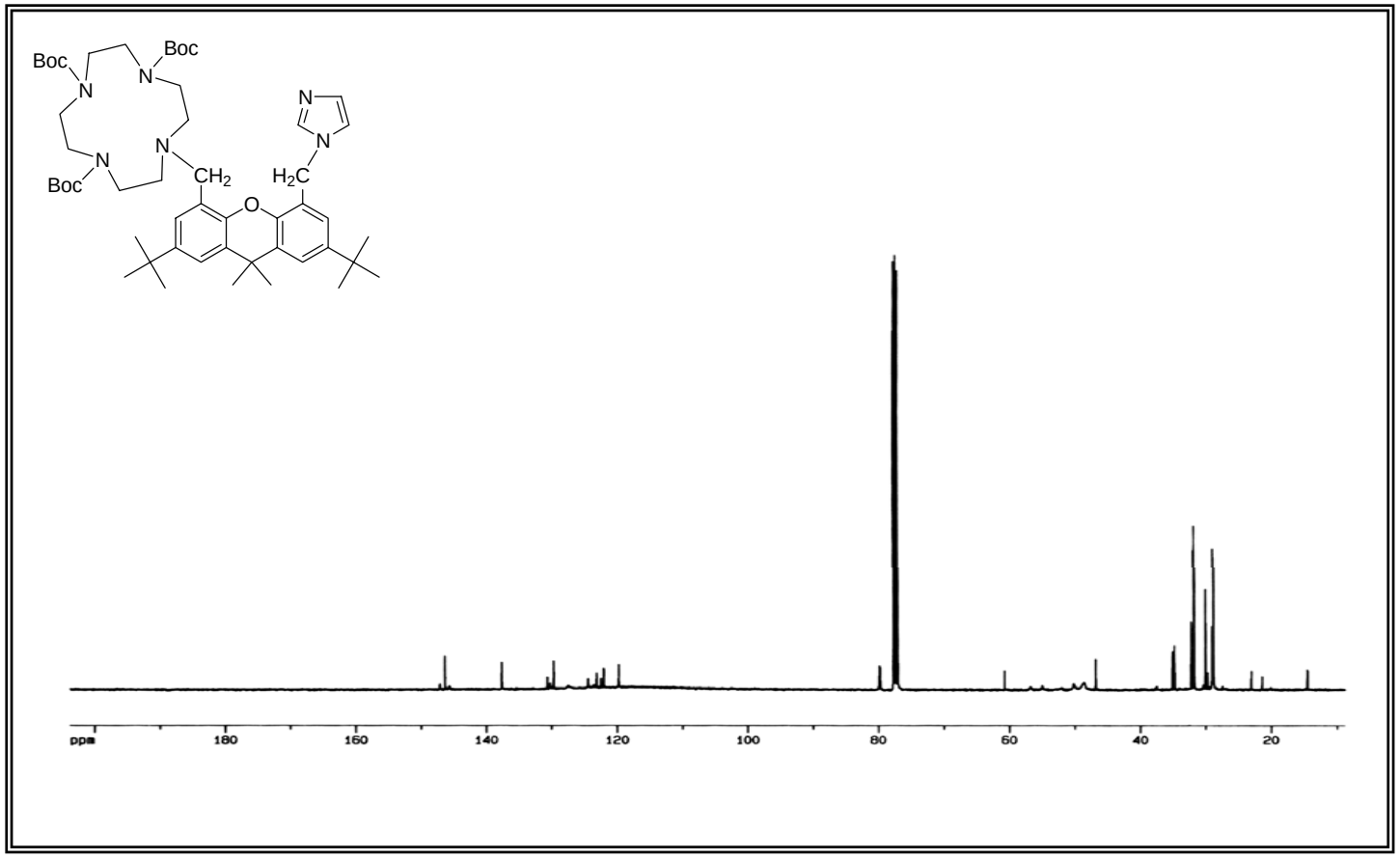

Figure A.10. ^{13}C-NMR spectrum of (2.8).

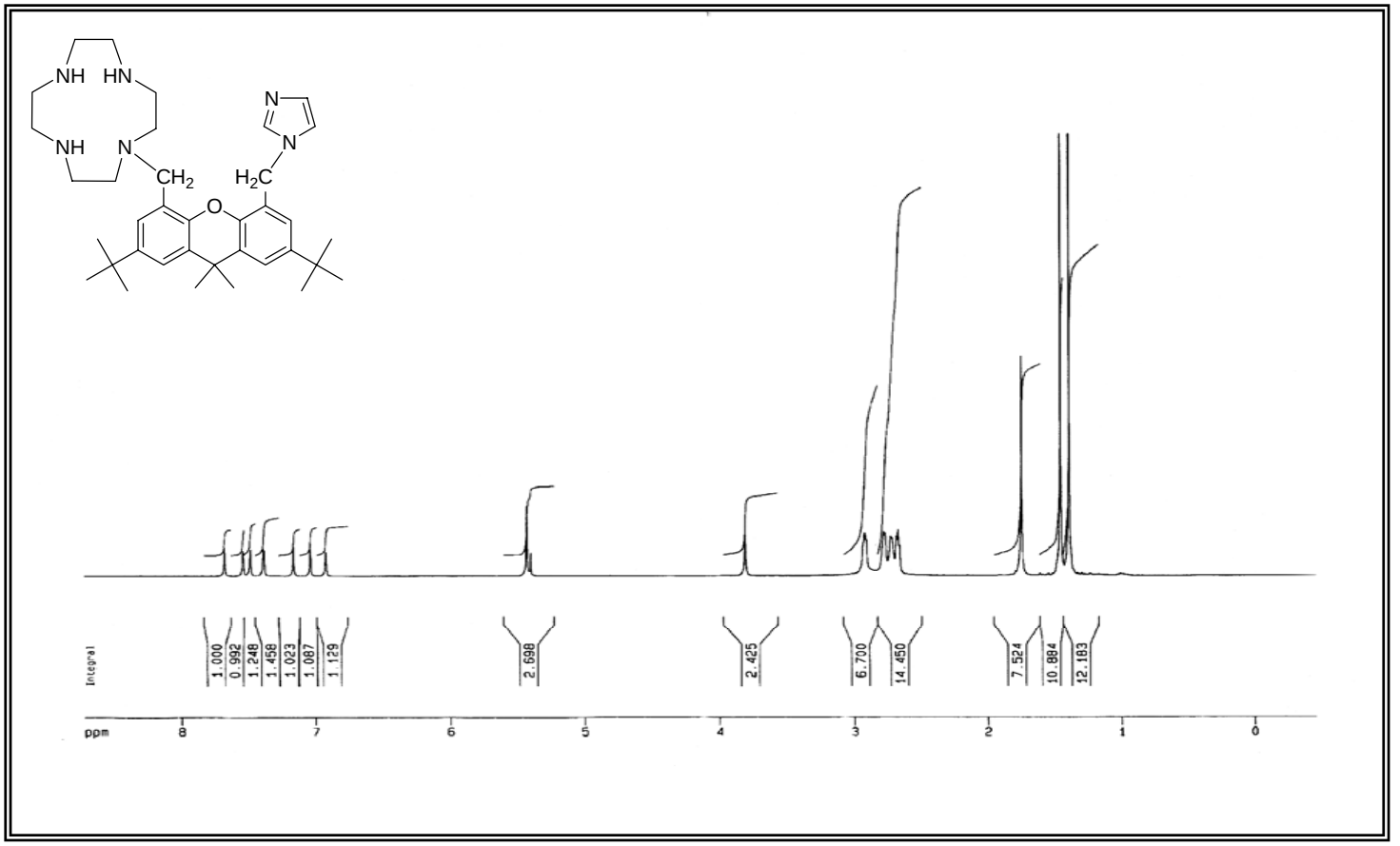

Figure A.11. ^{1}H-NMR spectrum of (2.9).

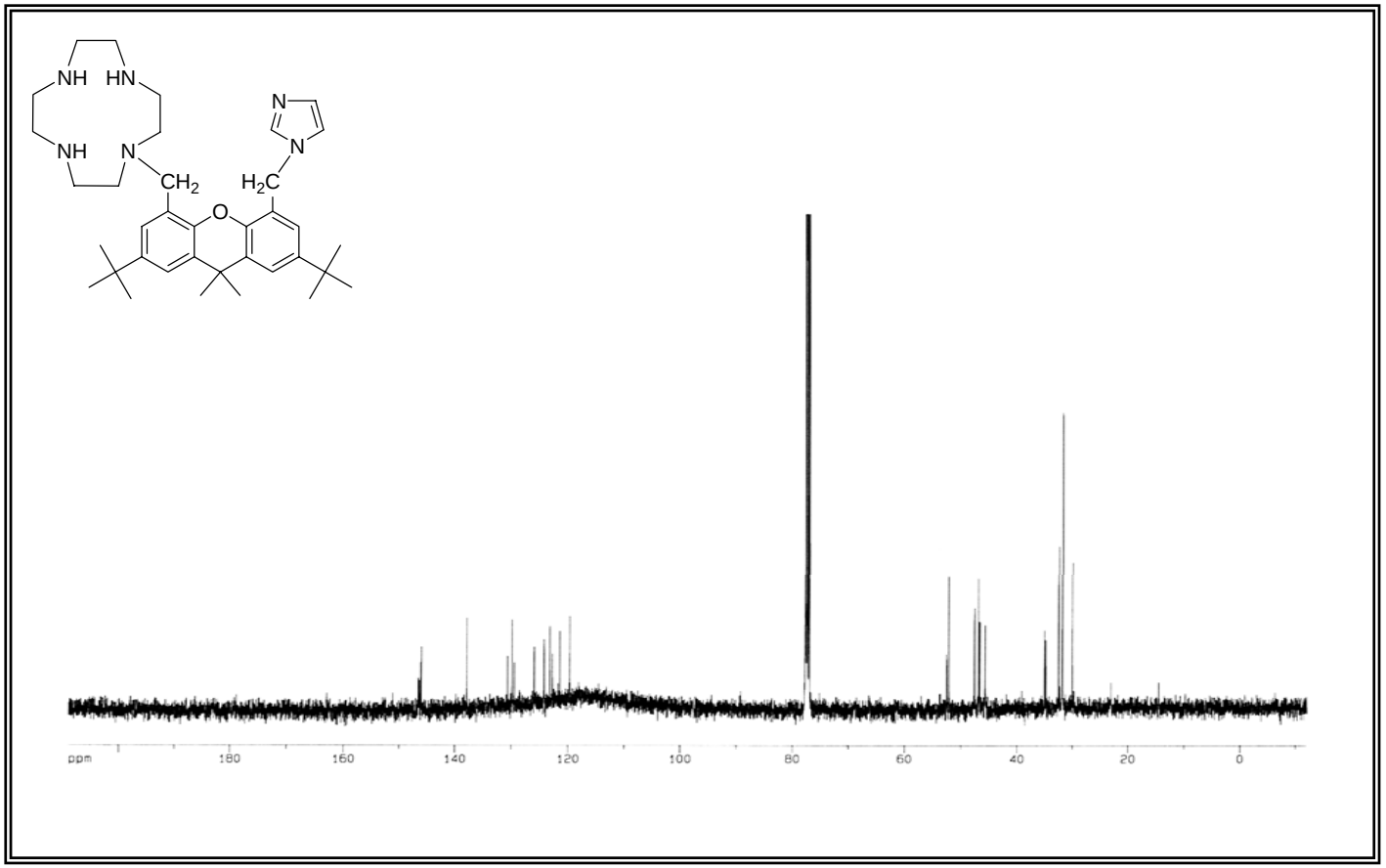

Figure A.12. ^{13}C-NMR spectrum of (2.9).

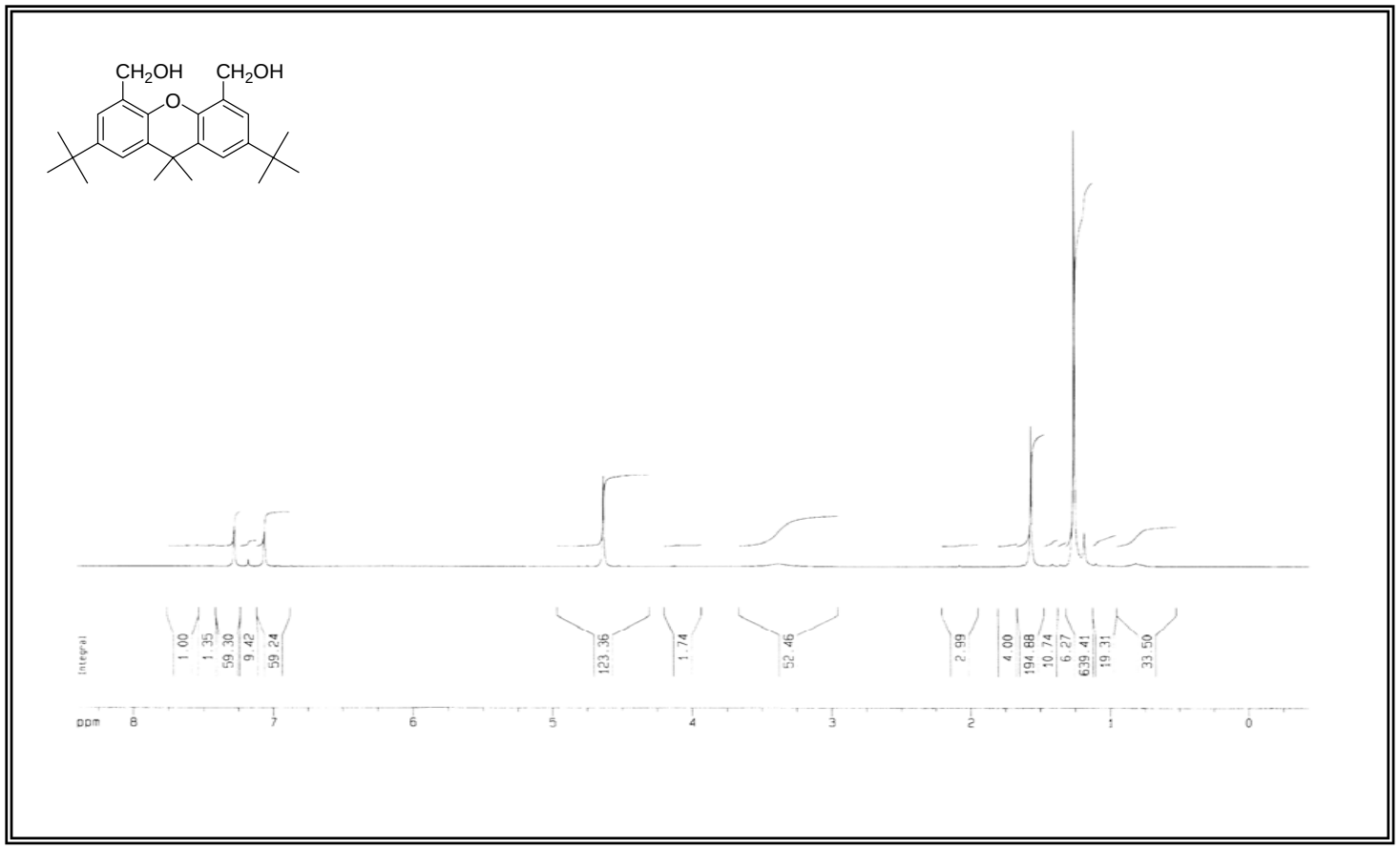

Figure A.13. ^{1}H-NMR spectrum of (2.11).

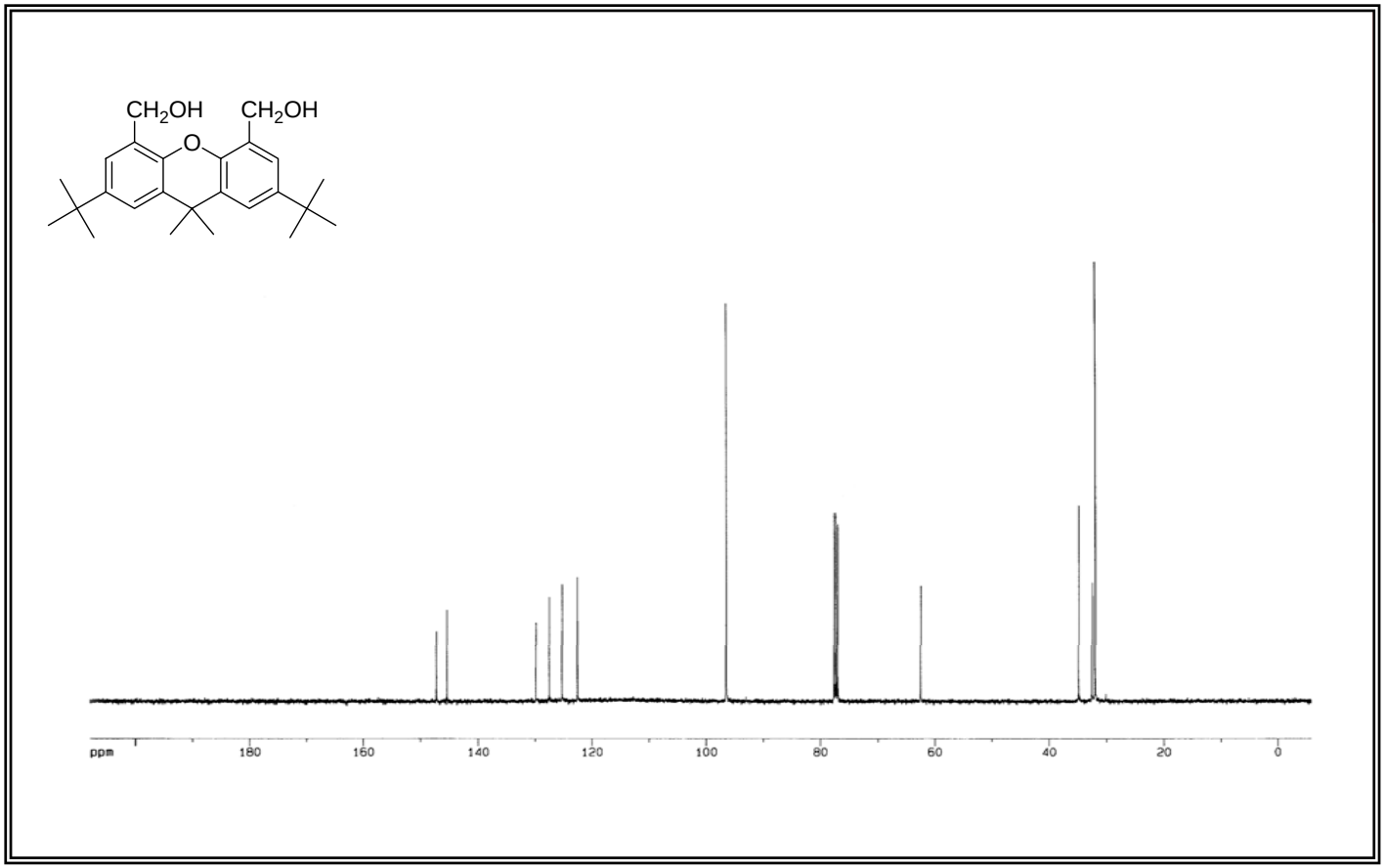

Figure A.14. ^{13}C-NMR spectrum of (2.11).

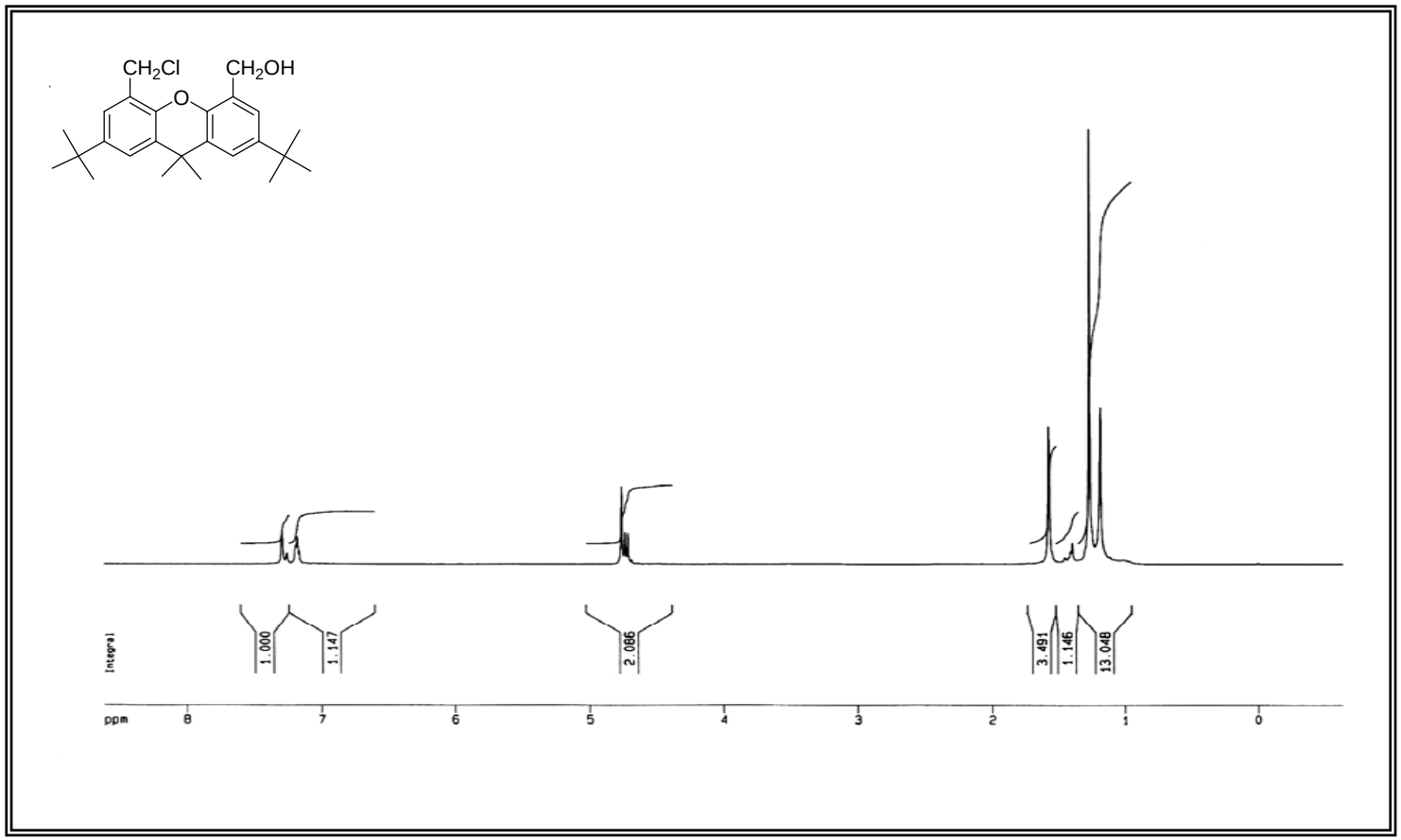

Figure A.15. ^{1}H-NMR spectrum of (2.12).

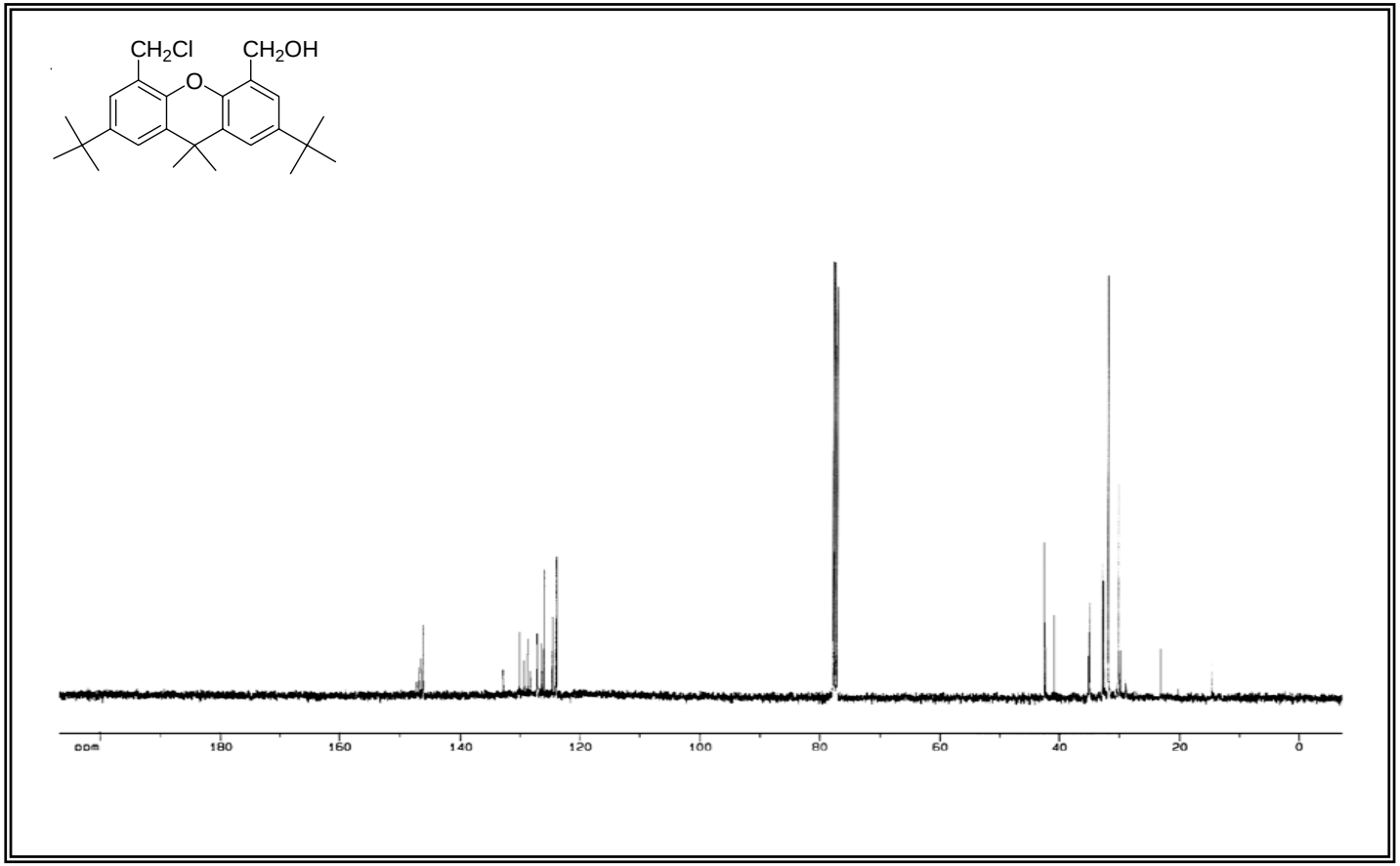

Figure A.16. ^{13}C-NMR spectrum of (2.12).

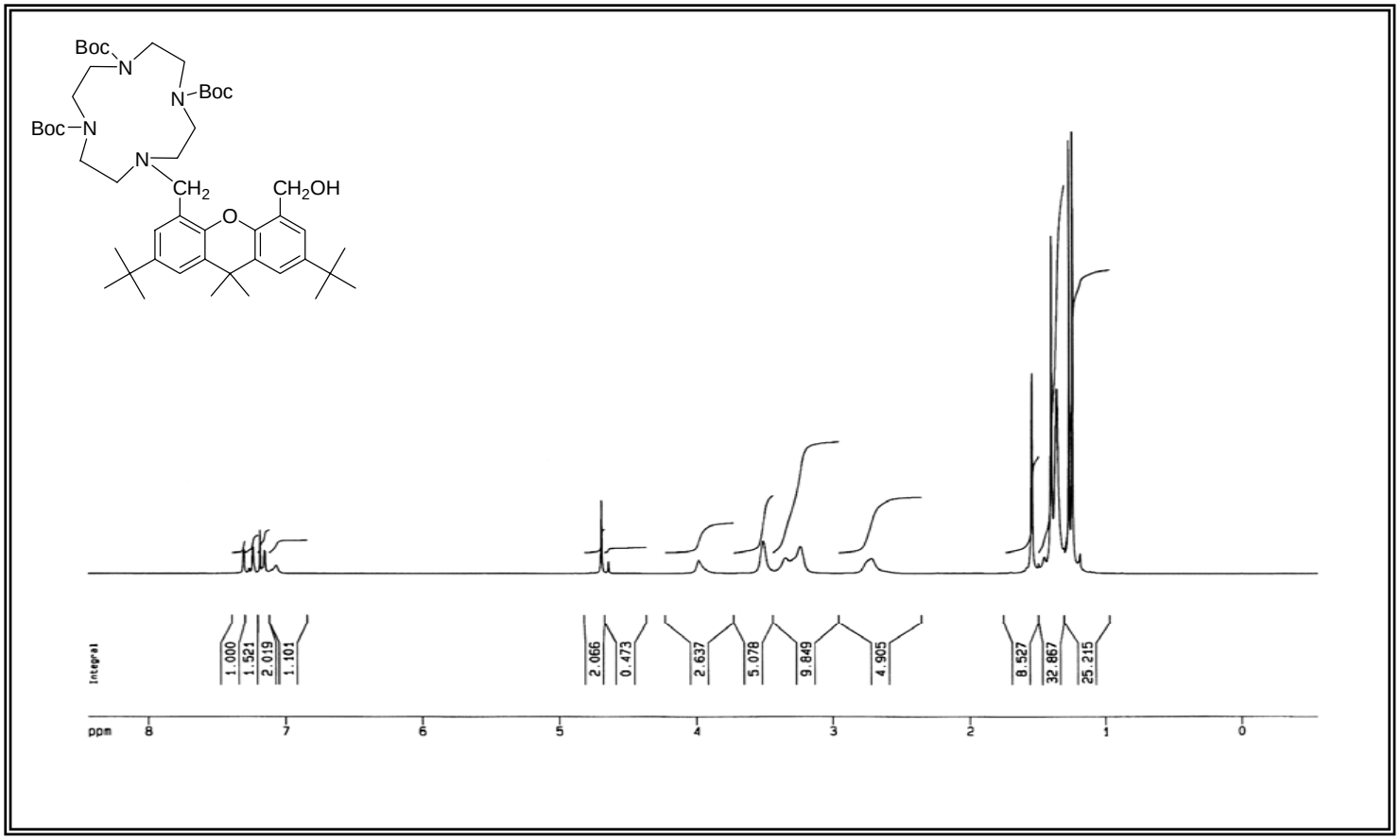

Figure A.17. ^{1}H-NMR spectrum of (2.13).

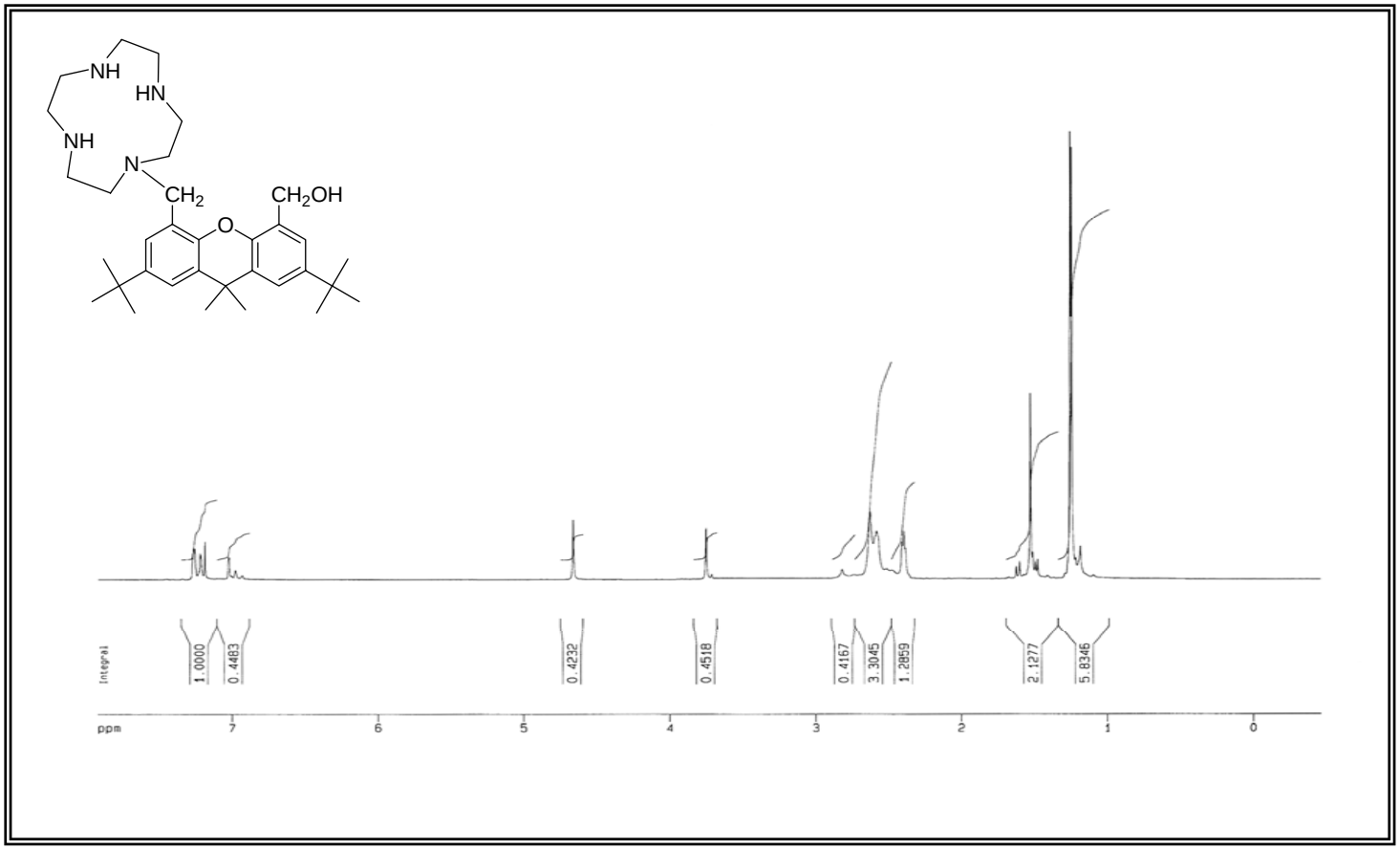

Figure A.18. ^{1}H-NMR spectrum of (2.14).

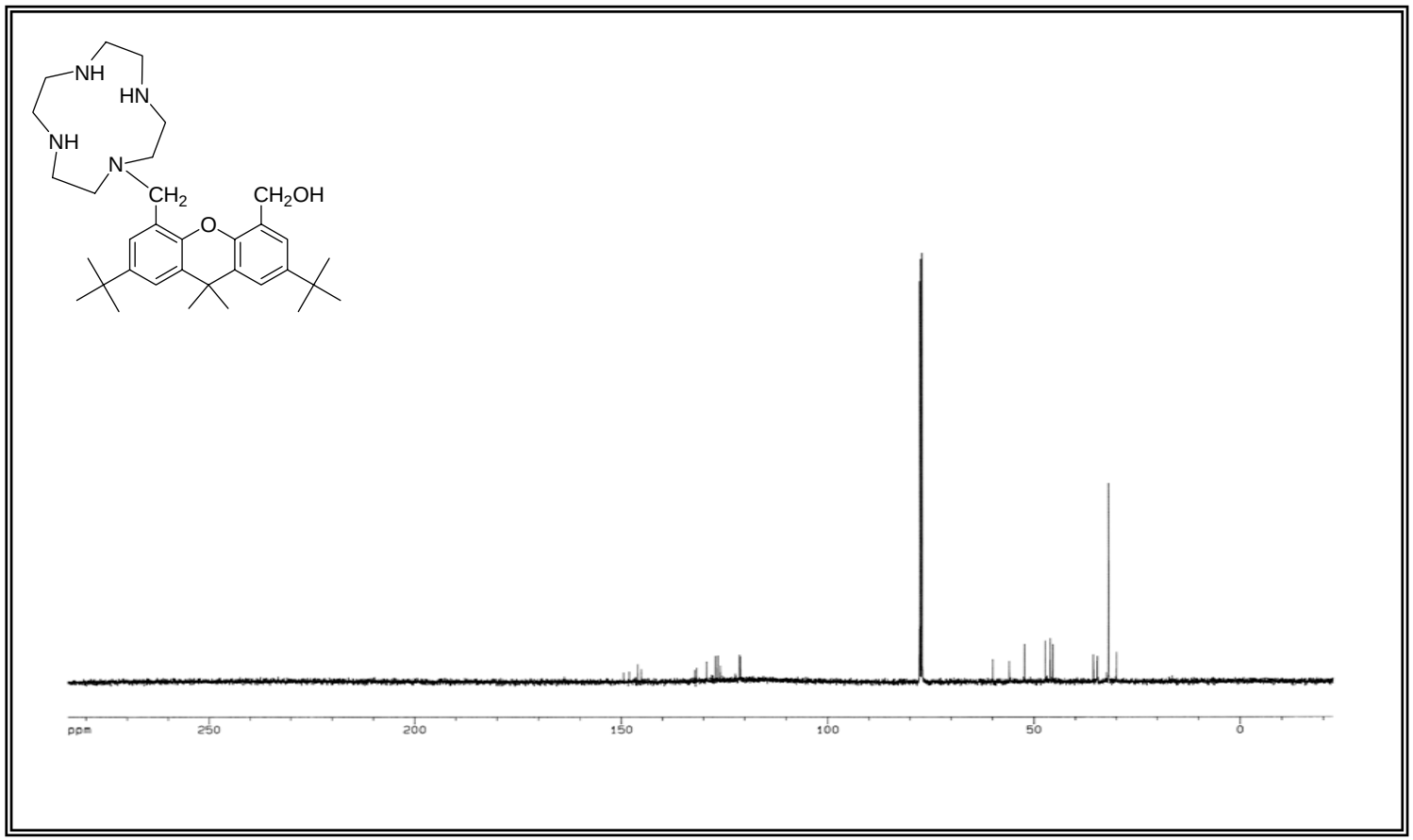

Figure A.19. ^{13}C-NMR spectrum of (2.14).

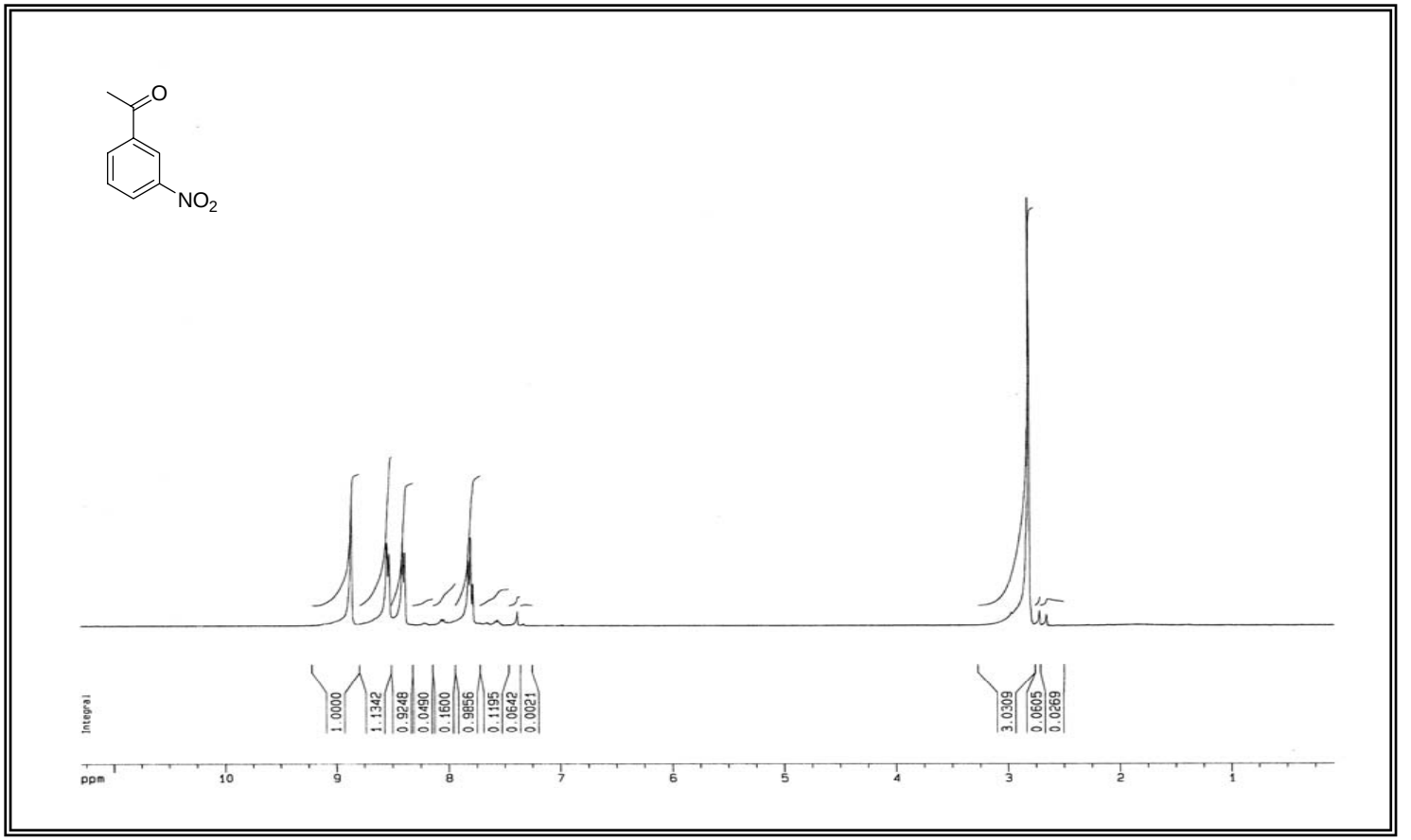

Figure A.20. ^{1}H-NMR spectrum of (6.2).

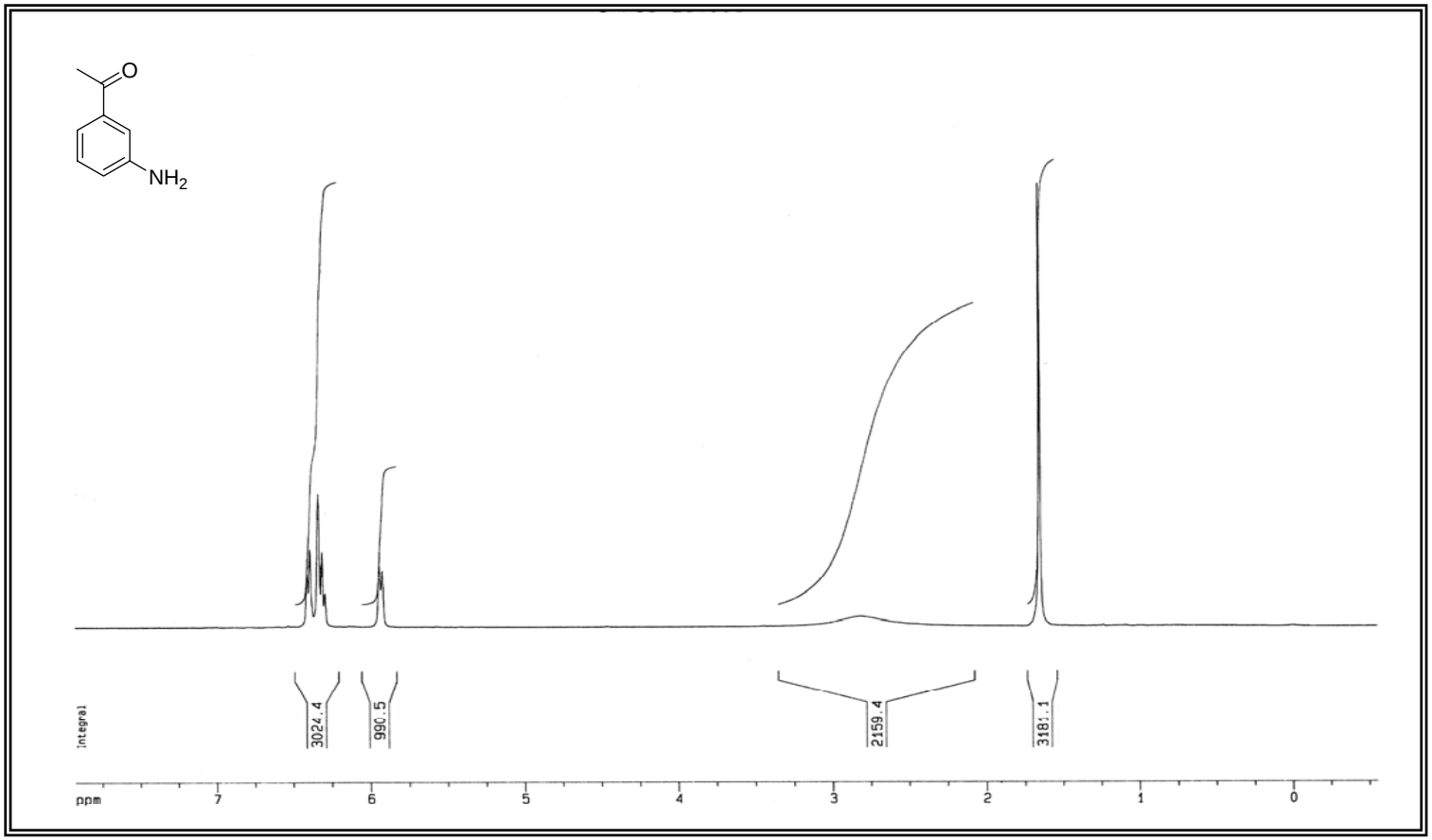

Figure A.21. ^{1}H-NMR spectrum of (6.3).

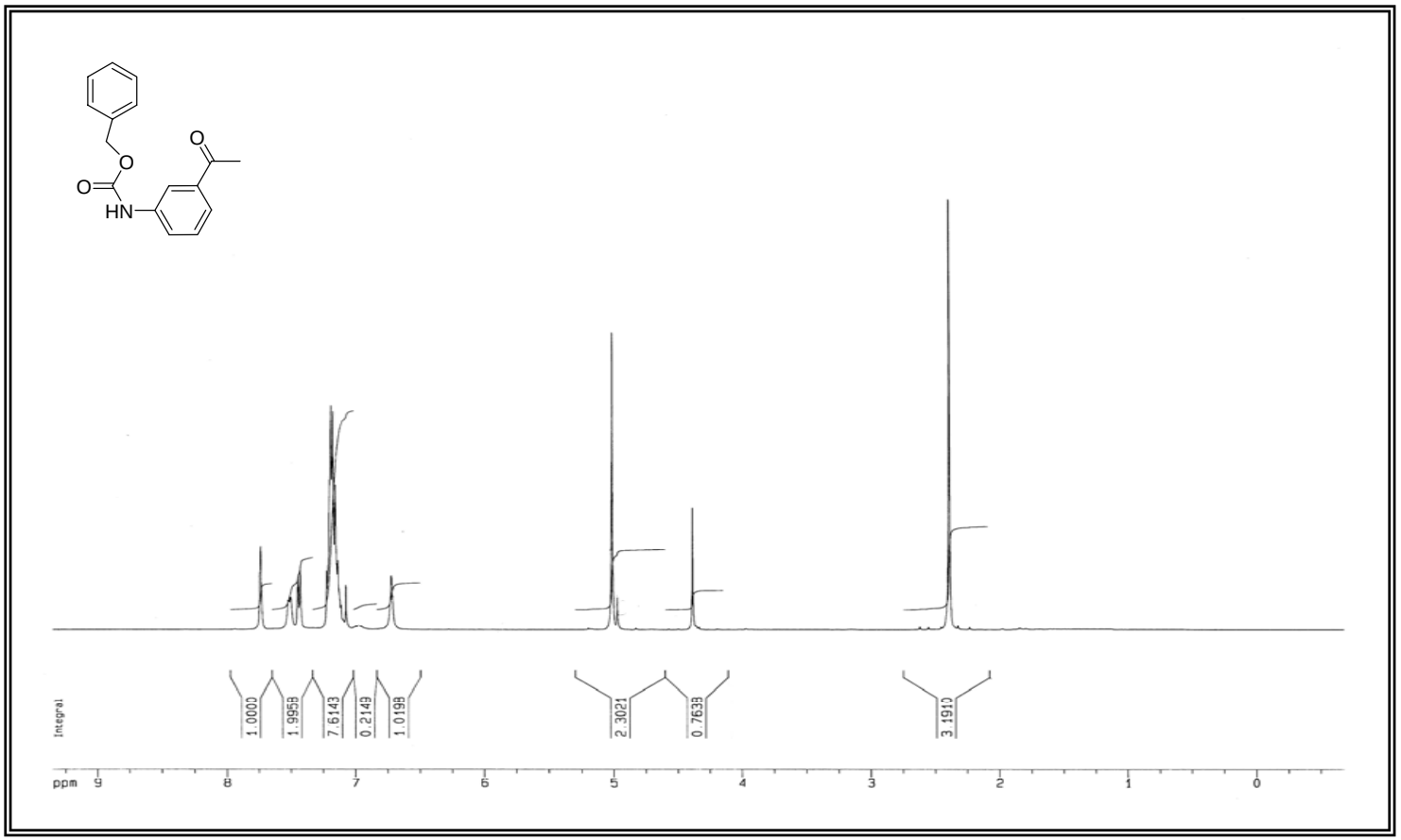

Figure A.22. ^{1}H-NMR spectrum of (6.4).

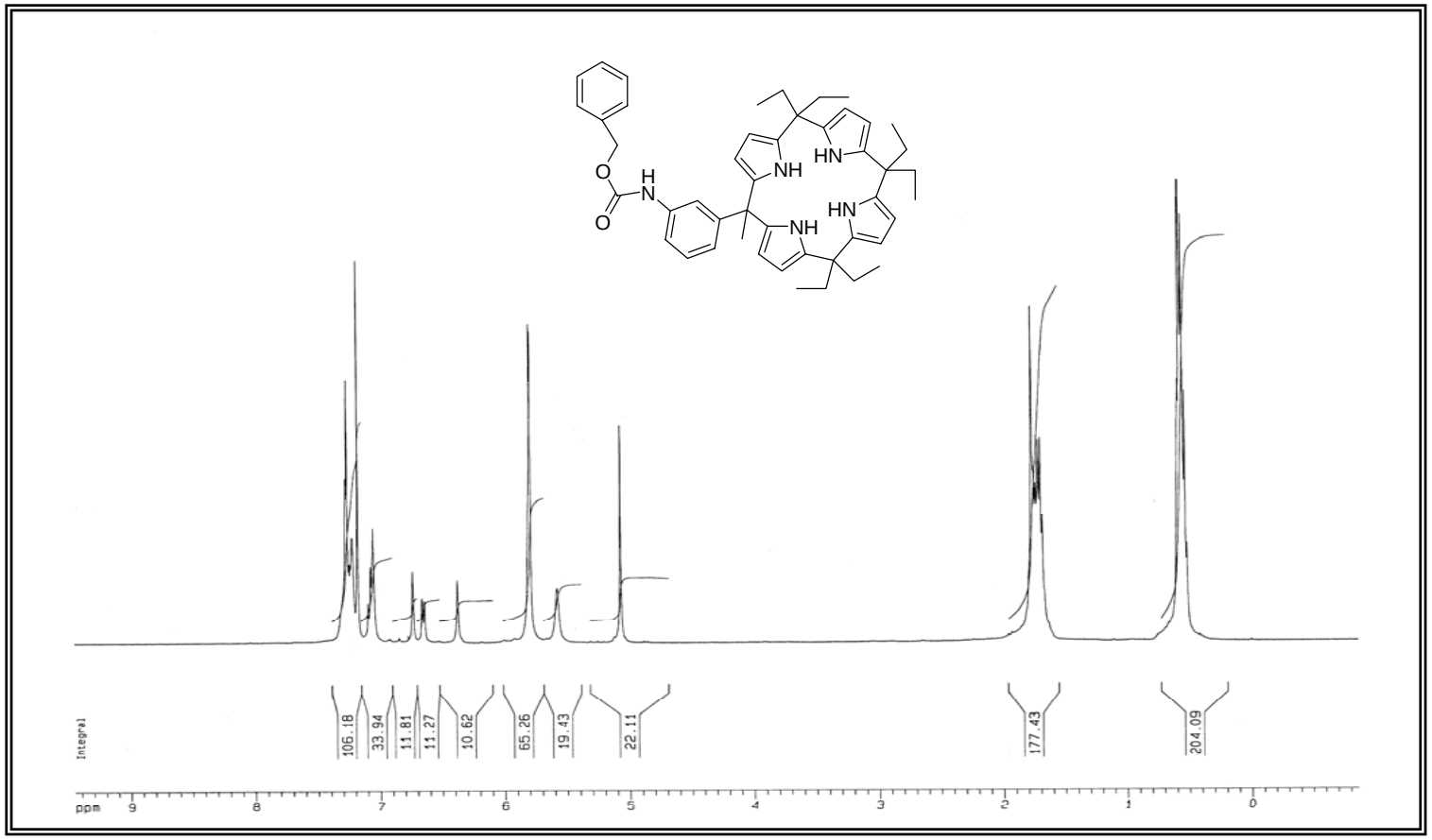

Figure A.23. ^{1}H-NMR spectrum of (6.5).

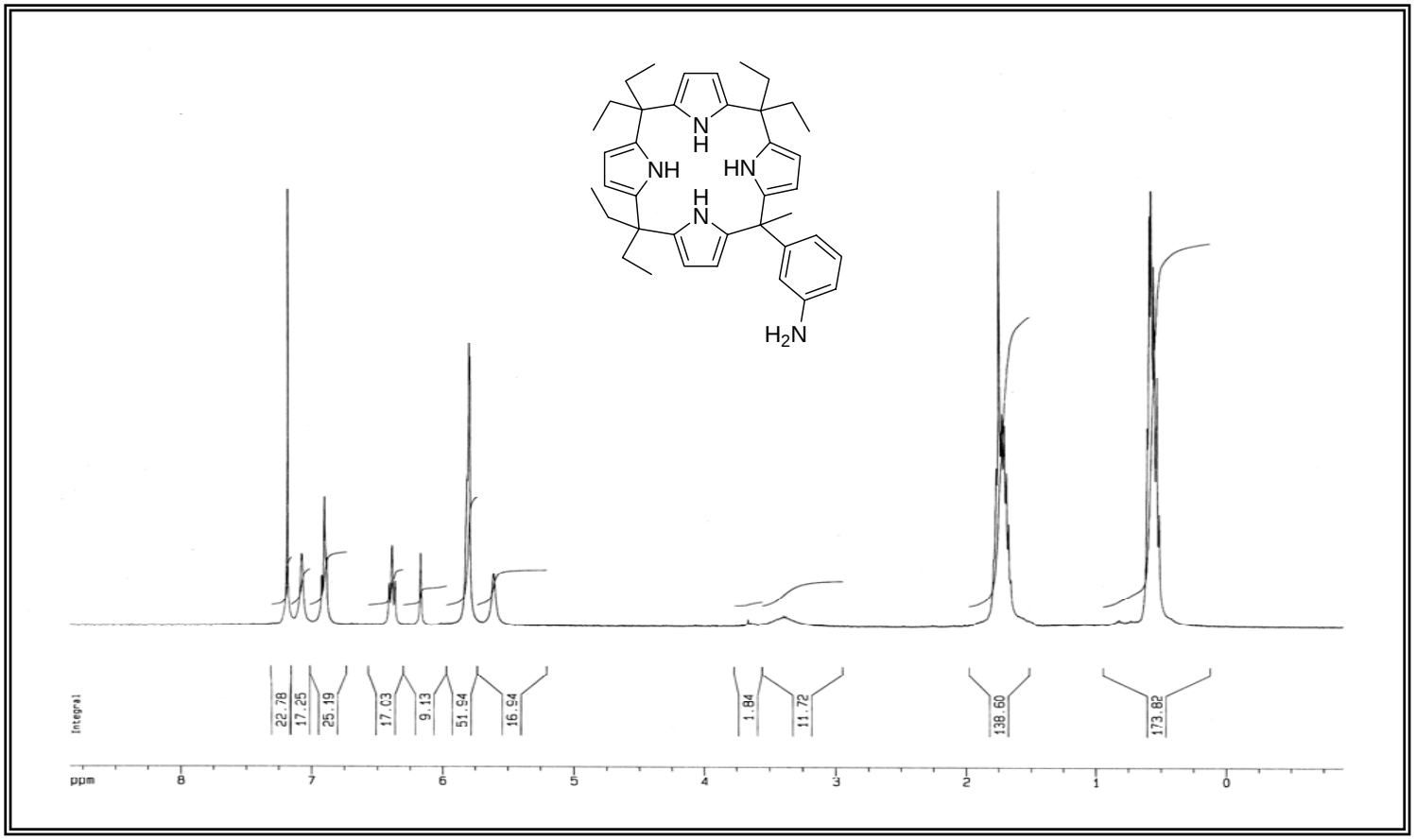

Figure A.24. ^{1}H-NMR spectrum of (6.6).

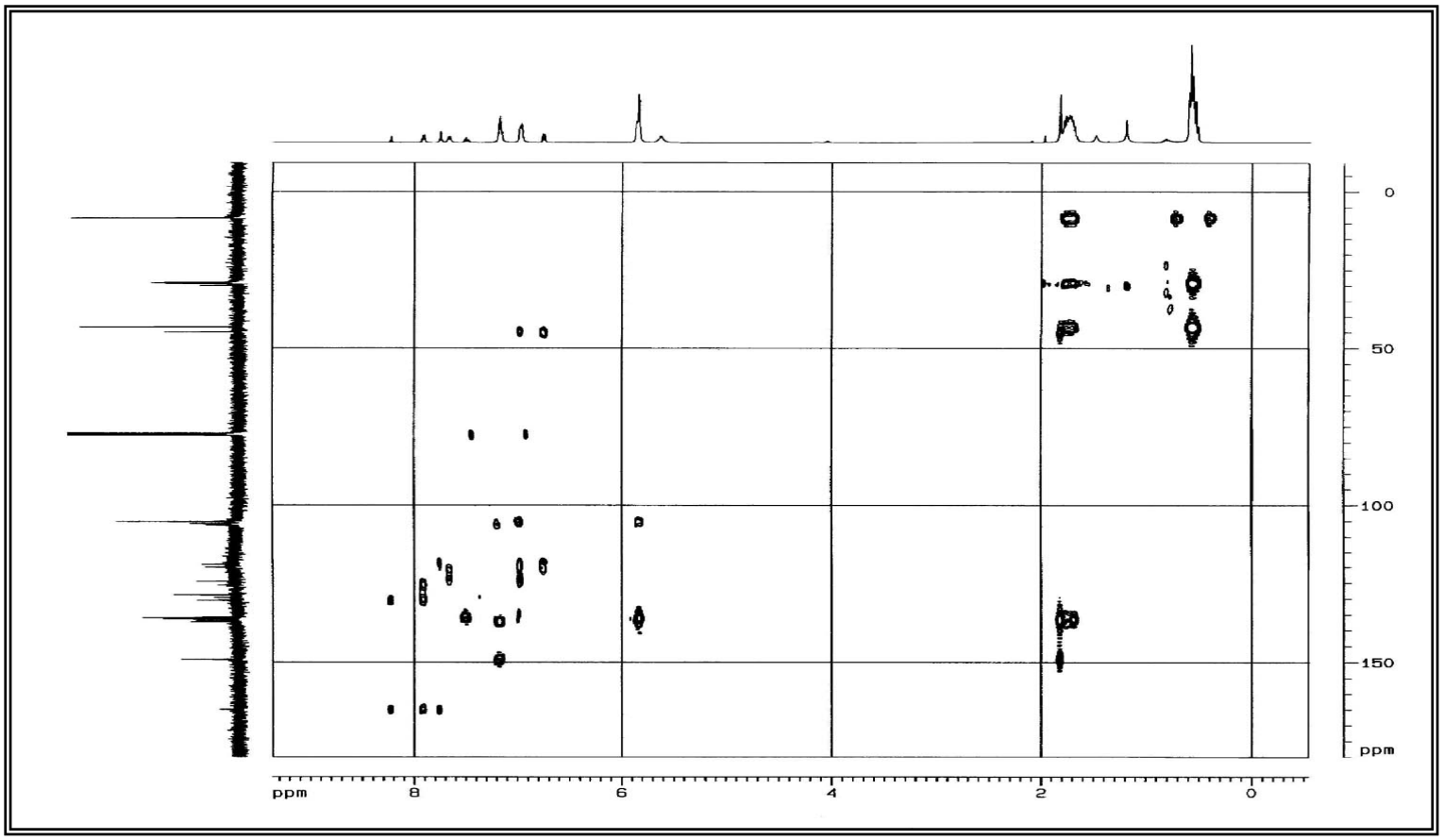

Figure A.25. ^{1}H-NMR spectrum of (6.7).

VİTA

Research Assistant, Middle East University, 1999-2004.

Education:

Erenköy Girl High School, 1984-1987.

Istanbul Technical University, Department of Chemistry; 1987-1992.

University of Cincinnati, Department of Chemistry (Biochemistry); 1995-1997.

Middle East Technical University, Department of Biochemistry; 1999- .

Meeting and Posters:

8th Conference on Methods and Applications of Fluorescence, August 24-27, 2003, Praque, Czech Republic; Towards Novel Fluorescent Chemosensors for Anions.

XVII. National Chemistry Congress, September 8-11 2003, Istanbul, Turkey; Dimerik Kalikspirol Sentezi ve Reseptör-Algılayıcı olarak karakterizasyonu.

XVIII. National Chemistry Congress, July 5-9 2004, Kars, Turkey; Boradiazaindasen Türevlerinin Süpramoleküler Kimyası.

XVIII. National Chemistry Congress, July 5-9 2004, Kars, Turkey; Yeni Kükürbitüril Türevleri ve Rotaksanların Sentezi ve Karakterizasyonu.

XVIII. National Chemistry Congress, July 5-9 2004, Kars, Turkey; Ksanten Türevi Fonksiyonel Enzim Modellerinin Sentezi ve Aktiviteleri.

XVIII. National Chemistry Congress, July 5-9 2004, Kars, Turkey; Boradiazaindasen Türevleri; Eksiton Etkileşimleri ve Enerji Transferi.

13 th International Symposium on Supramolecular Chemistry, July 25-29, 2004, Indiana, U.S.A.; Large Pseudo Stokes' Shift Molecular Sensors Through Resonance Energy Transfer.

ICSS&T 2004 Congress, Supramolecules: Design and Funcionality on a Nanomolecular Scale, September 5-9, 2004, Praque, Czech Republic; Artificial hydrolytic metalloenzyme mimics based on a xanthene framework.

Publications:

Bifunctional catalysis of ester hydrolysis: Novel hydrolytic enzyme models based on xanthene framework, **Şaki, N**.; Akkaya, E.U. *Journal of Molecular Catalysis A, Chemical 219, 227-232, (2004).*

Synthesis, *p*-Nitrophenolate Complexation and Competitive Anion Signaling of a Novel Calixpyrrole Dimer, **Şaki, N**.; Akkaya, E.U. submitted for publication in *Journal of Inclusion Phenomena.*